Pseudo-Graphite from the University of Idaho Thermolyzed Asphalt Reaction (GUITAR): Fundamental Characterizations and Its Potential in Electrochemical Applications

A Dissertation

Presented in Partial Fulfillment of the Requirements for the

Degree of Doctorate of Philosophy

with a

Major in Chemistry

in the

College of Graduate Studies

University of Idaho

Haoyu Zhu

Major Professor: I. Francis Cheng, Ph.D.

Committee Members: Peter B. Allen, Ph.D.; D. Eric Aston, Ph.D.; Dean B. Edwards, Ph.D.;

Department Administrator: Ray von Wandruszka, Ph.D.

August 2018

Authorization to submit dissertation

This dissertation of Haoyu Zhu, submitted for the degree of doctorate of philosophy with a Major in Chemistry and titled " Pseudo-Graphite from the University of Idaho Thermolyzed Asphalt Reaction (GUITAR): Fundamental Characterizations and Its Potential in Electrochemical Applications," has been reviewed in final form. Permission, as indicated by the signatures and dates below, is now granted to submit final copies to the College of Graduate Studies for approval.

Major Professor: _____ Date: _____

I. Francis Cheng, Ph.D.

Committee members: _____ Date: _____

Peter B. Allen, Ph.D.

_____ Date: _____

D. Eric Aston, Ph.D.

_____ Date: _____

Dean B. Edwards, Ph.D.

Departmental

Administrator: _____ Date: _____

Ray von Wandruszka, Ph.D.

Abstract

This dissertation describes the identification of a new form of carbon, Graphite from the University of Idaho Thermolyzed Asphalt Reaction (GUITAR) and its potential electrochemical applications in five chapters. Chapter one discusses physical characterizations of GUITAR in detail and how it compares to other carbon materials. According to their carbon sp^2 and sp^3 hybridizations revealed by XPS and H content by atomic percentage by elemental analysis, GUITAR has been placed on ternary diagram in the Graphite like hydrogenated amorphous carbon region. Raman and Thermal Gravimetric Analysis results indicated GUITAR is more graphitized. With both Raman and X-Ray diffraction, the crystal size was in nm range. The following chapters are more focused on the electrochemical application of functionalized GUITAR. Chapter two and three introduced the electrochemically treated GUITAR as competitive pH sensor and micro supercapacitor electrode. The treatment modified GUITAR with quinoid group and formed a 25 nm thick oxide film. The square voltammetric peak potential on the quinoid modified GUITAR (q-GUITAR) shifts by -63.3 mV/pH over the range of pH 0 to 11. The response is robust with up to 20 voltammetric runs between pH 0-9 and 2 runs between pH 10-11. The thin oxide film exhibited a high areal capacitance up to 890 $\mu F/cm^2$ at the current density of 10 $\mu A/cm^2$. With a wide capacitive window of 1.7V, the estimated maximum energy density and power density on q-GUITAR based micro supercapacitor is 35.8 mWh/cm^3 and 8.5 W/cm^3 respectively. The ease of q-GUITAR electrode formation and in-situ formed functional groups made this electrode system very cost effective. In Chapter four, one other modification-amination was applied onto GUITAR. High nitrogen content (8 at. %) was confirmed by XPS on aminated GUITAR (am-GUITAR) basal plane, which is comparable to

that on edge rich carbon materials. The am-GUITAR also demonstrated a superior resistance to air and solution aging effect and presented a competitive performance in sensing hypochlorite ion. A successful dihydroquinone attachment was also demonstrated. Chapter five summarized the important findings as well as the other ongoing and future studies.

Acknowledgements

I would like to express my great appreciation to Dr. I. Francis Cheng for his extensive professional and personal suggestions throughout my Ph.D. study which had huge and positive impact in my academic development. I would like also to thank my committee members: Dr. Peter B. Allen, Dr. D. Eric Aston, and Dr. Dean B. Edwards, for their great academic support, time and invaluable knowledge. To Dr. Peter B. Allen, thank you for being prompt to all my questions and all your academic suggestions. To Dr. Eric Aston, thank you for being critical to my research and willing to spend your own time to help on instrumentations. To Dr. Dean B. Edwards, thank you for introducing me to and being willing to have me involved in so many interesting projects.

To Dr. David McIlroy, Dr. Armando McDonald, Mr. Jacob Turner, Dr. Thomas Williams and Ying Qin, thank you for providing the access to instrumentations and generously sharing your knowledge and time with me. To Dr. Nolan W. Nicholas, thank you for providing the funding to some of my projects and the amazing summer internship. I would like also to thank Dr. and Mrs. Renfrew and Thomas F. Harland for all the scholarships.

I am very grateful for the faculty and staff and all other graduate students in Chemistry Department, University of Idaho who have created such a friendly research environment. Last but not the least, I would like to thank the former and current lab mates in Cheng group: Dr. Yuqun Xie, Dr. Isaiah Gyan, Jeremy Foutch, Charles Nwamba, Humayun Kabir (and his lovely family), Mathew Jones, Hamal Kaliash, Jeremy May, Hailey Smith, Peng Ma, Nicholas Renn, Ricardo Lopez, Ronald Wright, and Thomas Zeliff. I could not appreciate more to have chances to work with such a great group of people.

Dedication

This dissertation is dedicated to my awesome parents (Naiyang Zhu and Hua Ji). And it is also dedicated to all my great friends in US and China. Without your support, I will not be able to make this far.

Table of Contents

List of Figures

List of Tables

Chapter 1 . Introduction- What is GUITAR?

1.1 Introduction

1.1.1 Carbon allotropes

Carbon materials have attracted much attention due to the abundant allotropes adequate for different application areas. Graphite and diamond are two most widely known carbon allotropes. General speaking, graphite is pure sp^2 hybridized carbon while diamond is pure sp^3. Graphite has multilayered structure. Each single layer is known as graphene, which is a basic structural element of other allotropes. The graphene can be rolled up into carbon nanotubes (CNTs), or rounded up into fullerene or bucky balls. The mixture of sp^2 and sp^3 hybridized carbon generates amorphous carbon. The dangling bond in amorphous carbon is sometimes terminated by hydrogen atoms. Such amorphous carbon is named hydrogenated amorphous carbon. Amorphous carbon with more sp^3 behave more like a diamond, thus is known as diamond like carbon. If there is more sp^2 content in the structure, the amorphous carbon is known as graphite like carbon.

1.1.2 Graphene

Among all the carbon allotropes, Graphene is the one that received most attention in the past decade. Though the concept "graphene" has been around for some time,[1] Geim and Novoselov[2] were the first to demonstrate the production of graphene through exfoliation of graphite in 2007. They were awarded by the Nobel Prize in 2010 for this extraction. As the scale and yield of the graphene sheet from this method is limited, other methods have been developed. [3] [4]

1.1.3 What is GUITAR?

GUITAR (pseudo-**G**raphite from **U**nviersity of **I**daho **T**hermalyzed **A**sphalt **R**eaction) was discovered in 2008[5] through a workup for the analysis of Piceance Basin (Colorado) oil shale which required the removal of the organics by heat in a crucible. After cooling down, a thin coating with metallic sheen in the interior of the ceramic crucible was observed. This coating was removed from the crucible and was then named GUITAR. It was initially mistaken for a graphite, as it has some physical and morphological similarities with other

sp^2-hybridized carbon materials. But later on, it was identified as pseudo-graphite, which can better describe its properties.

1.1.4 Similarity to and difference from Pyrolytic carbon/graphite

The synthesis mechanism of GUITAR has been proposed in previous study, with sulfur as a catalyst.[5 12] This thermalized procedure has been recently further developed into a more productive and reproducible procedure with the tube furnace. This new procedure is free of sulfur at a temperature range of 750 °C to 900 °C in an inert atmosphere, where nitrogen was used as the carrier gas. Purer hydrocarbon sources, such as cyclohexanol, were used to replace the asphalt. This synthetic procedure of GUITAR is very similar to that of pyrolytic carbon.[6 7 8 9 10] Optical and scanning electron micrographs also show GUITAR has clearly discernable basal and edge planes with a layered structure, similar to graphites and graphenes.[11 12] Despite these morphological similarities, GUITAR has electrochemical properties that diverge from graphites. One of these properties is a higher resistance to corrosion, as qualitatively confirmed by cyclic voltammetry in aqueous electrolytes.[13 14 15] The anodic limit of GUITAR is 1.9 V vs. Ag/AgCl in 1.0 M H_2SO_4 at 200 $\mu A/cm^2$, which is 300 to 500 mV greater than graphites in various electrolytes. [13,14,15] Taken with the higher H_2 overpotential, GUITAR has a 3 V aqueous electrochemical window as opposed to 2 V for other sp^2 graphitic electrodes. [13,14,15,16,17] Corrosion resistance relative to graphites is attributed to a lack of electrolyte intercalation across its basal plane (BP), and interestingly the edge planes (EP) of GUITAR.[13,14] Graphites exhibit this intercalation behavior, resulting in blisters and pit corrosion.[18,19,20] Another distinguishing property is fast HET(heterogeneous electron transfer rate) across the basal plane (BP) of GUITAR.[13,14,15,21] The $Fe(CN)_6^{4-/3-}$ redox probe is often employed to measure these rates on carbon materials (Reaction 2). [22,23,24]

$$Fe(CN)_6^{3-} + e^- = Fe(CN)_6^{4-} \qquad E^0_{red} = 0.430\ V \qquad (2)$$

The standard rate constant for BP-GUITAR (k^0 = 0.01 cm/s) exceeds the basal planes of other graphites and graphenes by 2-6 orders of magnitude.[13,21] This can be attributed to the low density of electronic states (DOS) at the Fermi-level in crystalline graphites.[22,23] On the other hand, increasing the structural defect density increases DOS and the HET rates. The Raman spectra of GUITAR indicate that it is rich in structural defects, consistent with the observed fast HET rates relative to the BP of highly ordered pyrolytic graphite (HOPG).[13,21]

The contradictory features, a good HET rate while with a good corrosion resistance, make GUITAR unique. Thus, it is hypothesized to be a new form of carbon. In this chapter, more physical characterizations will be introduced. From the results, GUITAR will be compared with other carbon materials in more details. Three main properties on GUITAR will be considered: (1) the morphology by SEM and AFM; (2) sp^2 and sp^3 and elemental content by XPS and elemental analysis; (3) crystalline grain size, interlayer spacing and corresponding decomposition temperature by Raman, XRD and TGA.

1.2 Experimental

Chemicals

The vegetable oil precursors were obtained from local Walmart. The Tube furnace is a Hevi Duty Electric Co. brand, type M-3024. The gas purifier was obtained from Supelco (PA, USA). The peristaltic pump, steel injection needle, tubing, and thermocouple were obtained from McMaster-Carr (IL, USA). Paraffin wax and high vacuum grease were obtained from Royal Oak Enterprises (GA, USA) and Dow Corning (MI, USA) respectively. Graphite rods (6.3 mm diameter, lot # E10P26) were obtained from Alfa Aesar (MA, USA). Graphite felt (KFD 2.5 EA) were obtained as gift from SGL Carbon Company (PA, USA). Sulfuric acid (96.3%) were purchased from J. T. Baker (NJ, USA). Anhydrous sodium sulfate (≥ 99.0 %) was from EMD chemicals (NJ, USA). All aqueous stock solutions were prepared with deionized water, which was further purified by passage through an activated carbon purification cartridge (Barnstead, model D8922, Dubuque, IA).

Synthesis of GUITAR

Synthesis of GUITAR previously was achieved in a flame heated crucible with asphalt.[11] This procedure has been reformed in a tube furnace with a controlled temperature probe. After placing the target substrate in the tube furnace, set the temperature as desired (750 °C – 900 °C). The carbon resource (liquid form) then was introduced by a peristaltic pump into the tube furnace with inert carrier gas (N_2 or Ar) after the furnace has been reached the desired temperature. The duration of the synthetic procedure depends on desired coating thickness and is usually 15 min to 45 min. Then cut off the carbon source and turn off the heating source and allow the tube furnace to be fully cooled down (about 1 hour) with the carrier gas on.

Characterization

SEM All images were produced from a Zeiss Supra 35 scanning electron microscope (SEM) (Carl Zeiss, Germany).

AFM All AFM images were taken on ACS meeting, San Diego by Asylum AFM experts.

XPS The X-ray photoelectron spectroscopy (XPS) apparatus was built in-house at the University of Idaho. The analyses were performed in a vacuum chamber with a base pressure of 1×10^{-10} torr. Measurements were made with the Al Kα emission line (1486.6 eV) and a hemispherical energy analyzer with a resolution of 0.025 eV. The samples were then inserted into the vacuum chamber. During spectral acquisition the samples were grounded and exposed to a 500 eV electron beam to eliminate spurious charging. All spectra were acquired at room temperature. The XPS peaks were fitted to the Gaussian curve, after performing a Shirley background subtraction. For all the fitted peaks, the FWHM were kept to the same value.

XRD X-ray diffraction (XRD) analyses were carried out by employing a Siemens D5000 Diffractometer (Germany) equipped with an FK 60-04 air insulated X-ray diffraction tube with Cu anode, the XRD spectrums were taken with Cu Ka radiation (1.5406 nm) at 40 kV and 30 mA in the range of 2b = 2–60. The graphite powder (300 mesh) samples were obtained from Johnson Matthey Inc. (Seabrook, NewHampshire).

TGA Thermogravimetric analysis (Perkin Elmer, TGA 7 thermogravimetric analyzer, Waltham, MA) was conducted under air atmosphere (at flow rate of 21 sccm) from ambient temperature to 900 °C with a heating rate of 10 °C/min. Samples used in TGA are ground up particles with a size smaller than 1mm * 1mm and flakes with a size of about 0.5 cm^2. 1-2 mg samples were used for each test.

Raman The scanning confocal Raman microscopy on GUITAR was collected with 5 different laser excitation wavelengths. The system used for laser excitation wavelength of 442 nm, 532 nm and 633nm was a Horiba LabRAM HR Evolution Raman microscope (Irvine, California). The optical magnification at the objective was 100X, producing a spot size of roughly 599 nm, 721 nm and 858 nm respectively to the laser wavelength in diameter. Laser Spot Size diameter = 1.22 λ / NA (λ is the wavelength of the laser and NA is the

numerical aperture = 0.90 for 100x objective). Spectral scans were taken at 30 s integration times with 2 averaged accumulations with a spatial resolution of approximately about 300 nm, 361 nm and 430 nm respectively for the wide scans. Spatial Resolution =0.61λ /NA. The spectrum was collected at a laser power of 25% were used with no instability or transient effects observed in the spectra of the sample. Multiple locations across multiple samples were analyzed. The system used for 488 nm, 514 nm was Horiba Jobin Yvon T64000 triple monochromator with a liquid-nitrogen-cooled, multichannel charge-coupled device detector (Irvine, California). The approximate spot diameter on the surface of the sample is about 100um, measured them in macro geometry focusing the laser with a conventional lens. The spectrum was collected at a laser power of 200mW. Spatial resolution is approximately about 330 nm and 348 nm respectively. Multiple locations across multiple samples were analyzed.

1.3 Results and discussion

1.3.1 Morphology-compare to pyrolytic carbon

Pyrolytic carbon is usually observed as a product when heating the hydrocarbon source to a temperature higher than 500 °C in absence of air.[25] According to the recommended terminology by the IUPAC(International Union of Pure and Applied Chemistry) [26] for the description of carbon as a solid, pyrolytic carbon is a carbon material deposited from gaseous hydrocarbon compounds on suitable underlying substrates at temperatures ranging from 700 °C to 2000°C (chemical vapor deposition). Since the synthetic procedure of pyrolytic carbon is very close to that of GUITAR, it is reasonable to compare these two carbon materials.

Multilayered structure can usually be observed in pyrolytic carbon[25], also is seen on GUITAR as in Figure **1**.**1**a. GUITAR grown off a flat surface (e.g. Quartz slides) has a flat basal plane and a layered structure, which appears to be similar to HOPG (highly oriented pyrolytic graphite (Figure **1**.**1**b). The synthetic procedure allowed GUITAR being transformable coating onto desired substrates, such as graphite fiber (Figure **1**.**1**c) and silica nanospring (Figure **1**.**1**d) [27,28]. This confirmed that the GUITAR coating is uniform and layered on substrate with a wide size range from cm to nm. As a carbon based material, the GUITAR coating made nonconductive materials applicable in energy storage devices[29], electrochemical sensors,[30,31,32] and water treatment.

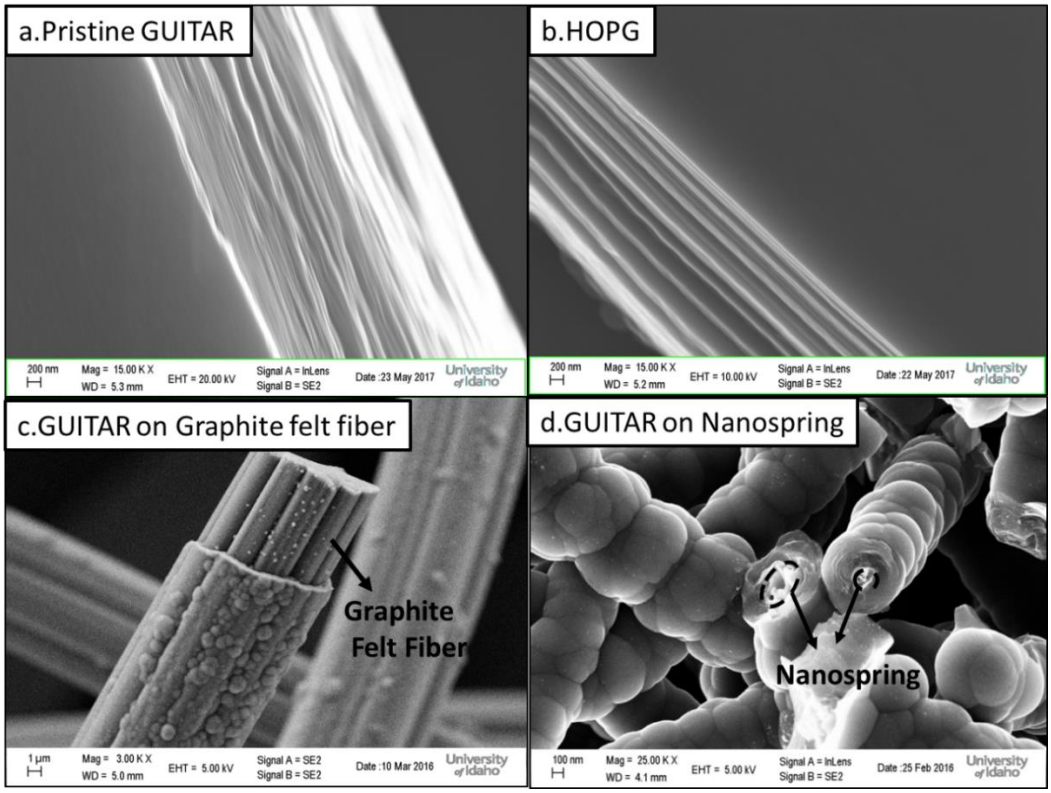

Figure 1.1. Scanning Electron Microscopic figure of a. GUITAR flake (obtained from GUITAR coated quartz), b. Highly Oriented Pyrolytic Graphite (HOPG), c. GUITAR coated graphite felt fiber and d. GUITAR coated silica nanospring.

Though GUITAR basal plane (BP) is microscopically (from SEM) flat, the AFM result indicated it is not atomically flat as in Figure **1**.**2**A. HOPG is a well-known atomically flat carbon material on the basal plane,[33] with occasional step defect across the basal plane with depth of ± 1 nm as in Figure **1**.**2**B. This step defect is missing on BP-GUITAR. Instead, uneven nano-bubble like feature spreads out on the basal plane with waviness amplitude of ± 15 nm.

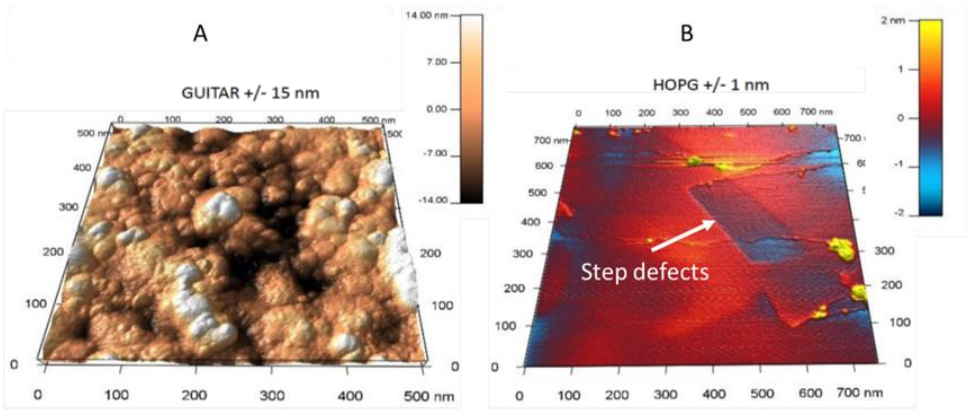

Figure 1.2. AFM of (A) GUITAR and (B) HOPG

On pyrolytic carbon, the graphite crystallites rearrange themselves at a different level of order (Figure **1**.**3**A), depending on the temperature used in the procedure.[25] This diagram indicates the grain boundaries in typical pyrolytic graphite, even in highly ordered examples, such as HOPG. These boundaries or the step defects (as in Figure **1**.**3**A) allowed the electrolyte intercalation when a positive potential is applied on the material.[34, 35, 36, 37] From our previous study on GUITAR, no intercalation can be observed even when scanned to 2.3V vs Ag/AgCl.[13] It is proposed in previous study that on GUITAR basal plane, there is no step defects (Figure **1**.**3**B).

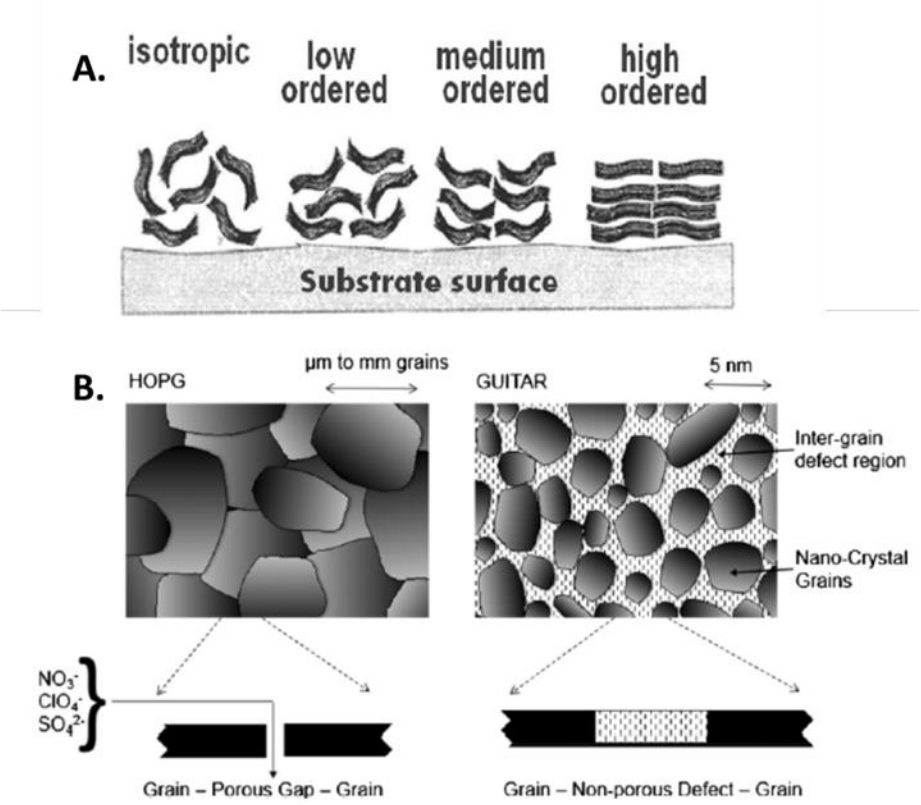

Figure 1.3. A. Scheme of isotropic and anisotropic (low-, medium-, high ordered) texture of pyrolytic carbon (according to Reznik and Huttinger, 2002 Ref 38).Reprint permission obtained from Ref 39. B. Proposed morphological differences between graphite (left) and GUITAR (right). The gaps between graphite grains allow for electrolyte intercalation. GUITAR has smaller grains and more disorder in the inter-grain regions that allow for faster heterogeneous electron transfer in property i and lacks porous defects that allow for electrolyte intercalation. This extends its aqueous anodic limit to 2.1 V. Reprint permission obtained from Ref 13.

1.3.2 XPS and elemental analysis-GUITAR might be a graphite like hydrogenated amorphous carbon

The results of this study yield 98.72% C, 0.20% O and 1.08% H by mass (88.35% C, 0.14% O and 11.51% H by mole) for GUITAR. This matches results obtained with XPS analysis below. It is noteworthy that GUITAR is one of the purest carbon films grown by CVD, and significantly, with no metal contamination and negligible oxygen content. Literature CVD-grown graphene contain metal contamination and 5-30 wt% oxygen. [39,40,41] Elemental

analysis indicates that GUITAR possesses more hydrogen content that would be expected of most graphites but within the range of hydrogenated a-C (a-C:H). [42]

Figure **1**.**4**A shows the full scan XPS spectra of GUITAR where only the C1s peak is observed. In Figure **1**.**4**B the deconvolved C1s peak reveals 3 components, for sp^2-C (85.0%) at 284.2, sp^3-C (15.0%) at 285.4 and a satellite peak typical of sp^2 carbon at 286.9 eV. [43] The sp^2 content of GUITAR is close to literature graphites, which range from 90 to 100%. [44,45] With a-C and DLC electrodes the sp^2 carbon content varies from 10-75%.[46,47,48] Another graphite-like material, turbostratic carbon consists of 70% sp^2 carbon. [49] As discussed in the introduction, increasing the proportion of sp^2 carbon in DSA carbon electrodes decreases resistance to corrosion and increases HET rates for the $Fe(CN)_6^{3-/4-}$ redox probe. [16]

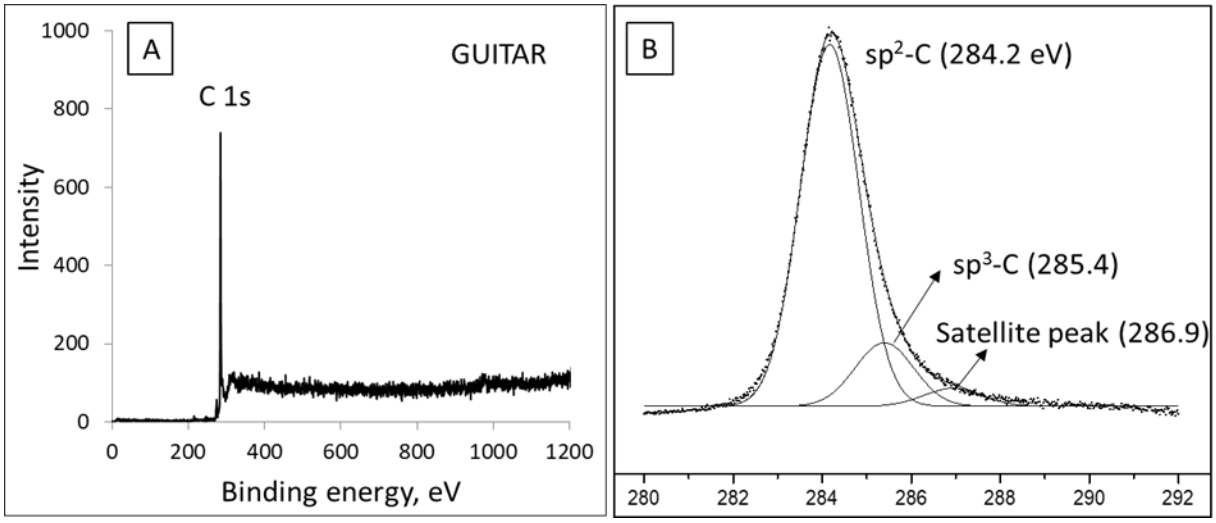

Figure 1.4. (A) Wide scan XPS spectra of GUITAR and (B) deconvolved peaks of the C1s signal.

Depends on the sp^2-sp^3-H% composition, Ferrari and Robertson[50] categorized carbon materials into graphite, diamond, and amorphous carbon. The sp^2-sp^3-H % by atom correlation on different carbon materials is summarized in the ternary phase diagram (Figure **1**.**5**A). [51] [52] Among all the carbon materials, graphite has the highest sp^2 content (90-100% which locates at the sp^2 corner on the diagram. [53,54] In contrast to graphite, the diamond has the highest sp^3 content, which locates at the sp^3 corner. Filling the gap between graphite and diamond, the amorphous carbon which has mixture of sp^2 and sp^3 in the structure locates in

the major part of this diagram. [55,56,57,58] The hydrogenated carbon (a-C:H) was classified into four categories by Casiraghi.[52]

i) Polymer-like a-C:H (PLCH) containing 40–60 atomic% H and up to 60% sp^3-C.

ii) Diamond-like a-C:H (DLCH) with 20–40 atomic% H and lower sp^3-C.

iii) Hydrogenated tetrahedral amorphous carbon (ta-C:H), have 25-30 atomic % H with ~70% sp^3-C.

iv) Graphite-like a-C:H (GLCH) have 20 atomic % H or less with high sp^2-C content. [59, 60]

The GUITAR (85% sp^2 and 15% sp^3 relative to total carbon and 12% H by atom) locates in the lower border of GLCH region. The GLCH was found to also have a layered structure, however with a wavy surface. [60]

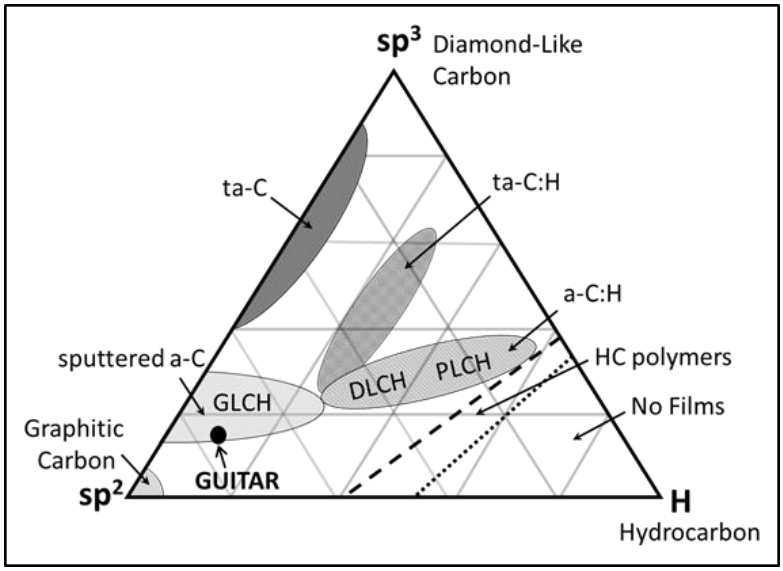

Figure 1.5. Placement of GUITAR (75.1% sp^2-C, 13.2% sp^3-C and 11.5% H by mole) in the sp^2-sp^3-H ternary phase diagram for carbon. Abbreviations: a-C = Amorphous Carbon, a-C:H = Hydrogenated a-C, ta-C = Tetrahedral a-C, ta-C:H = Tetrahedral a-C:H, GLCH = Graphite like a-C:H, DLCH = Diamond like a-C:H and PLCH = Polymer like a-C:H.

1.3.3 Raman Studies of GUITAR Indicate that is has Characteristics of Nano-crystalline Graphite and Graphite-Like Hydrogenated a-C

Figure **1.6**A illustrates the Raman spectrum of GUITAR with different laser excitation wavelengths. In graphitic materials the G-band (1575-1600 cm^{-1}) is associated with the E_{2g} vibrational mode within the graphene lattice. The D-band (1350-1380 cm^{-1}) is associated with a breathing mode that appears with the defects in that lattice.[61,62] With the laser excitation wavelength of 514 nm (2.41 eV), the ratio of the intensities on GUITAR, I(D)/I(G) = 1.16 is with the D and G band position at 1359 and 1591 cm^{-1}. Using that data in the Raman analysis of Figure 5 in reference 42, yields a H atomic % of ~10% which is in good agreement with elemental analysis of this study (11.51% H). In Figure 5 of that reference the G-band position of GUITAR (1591 cm^{-1}) is intermediate to nano-crystalline graphite (nc-G, 1600 cm^{-1}) and graphite-like hydrogenated a-C (GLCH, 1560 cm^{-1} and 16% H). A Raman spectrum of GLCH with 12% atomic H that could not be located in literature. The material with 16% H differs significantly with reported D and G band positions at 1385 and 1569 cm^{-1} respectively, with I(D)/I(G) = 0.60.[63] Another carbon material with exposed nc-graphene edges and a sp^2-C content of 85-87% has similar Raman and electrochemical characteristics (discussed below) with GUITAR.[64] Ferrari's amorphization trajectory offers further insights based on the placement of carbon materials in one of three stages, (1) graphite to nanocrystalline graphite (nc-G, 100% sp^2), (2) nc-G to a-C (up to 20% sp^3) and (3) a-C to tetrahedral a-C (ta-C, up to 85% sp^3). Based on G-positions and I(D)/I(G) ratios, GUITAR is in Ferrari's Stage 2, near the transition with Stage 1. The reported GLCH with 16% H is again in Stage 2 but near the transition to Stage 3.[65,66]

Tuinstra and Koenig noted that the ratio of I(D)/I(G) varied inversely with L_a.[67] However this is not valid for smaller crystal size than 2 nm. $\frac{I(D)}{I(G)} = \frac{C(\lambda)}{L_a}$, C(514nm)=4.4 nm [67 68 69] I(D)/I(G) will increase with increasing disorder, according to TK equation, while decrease with more disorder.[70] For this more disordered or amorphous carbon zone, Ferrari and Robertson proposed a new relationship for carbon with crystal size smaller than 2 nm.[70] $\frac{I(D)}{I(G)} = C'(\lambda){L_a}^2$, C'(514 nm)~0.0055. [7070] Assuming GUITAR might have either grain size, we did calculation with both equations. If GUITAR has a grain size smaller than 2 nm, the $L_{a\ (GUITAR)}$ is 1.5 nm and 3.6 nm if its grain size is lager.[71] (manuscript submitted)

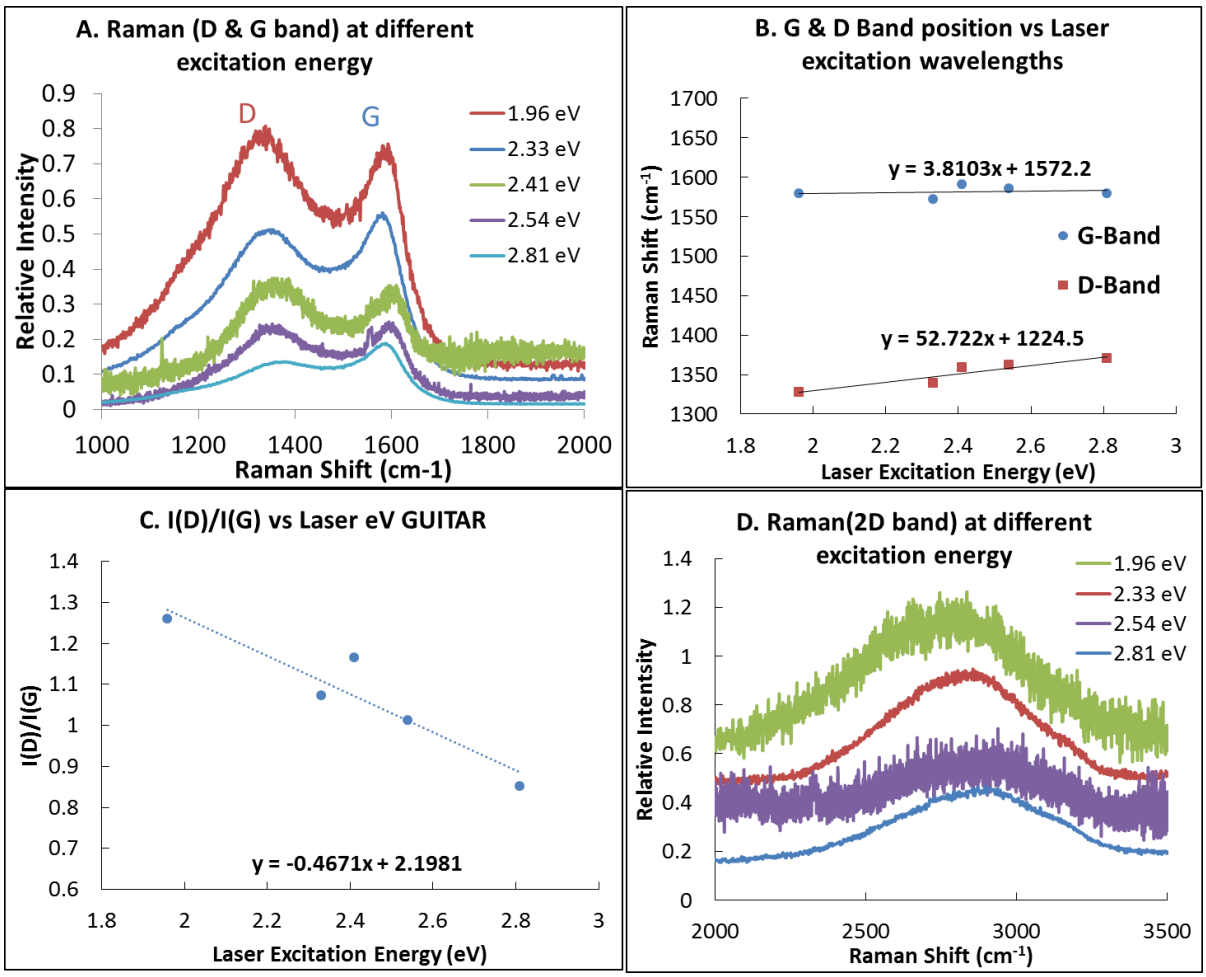

Figure 1.6. A. Raman (D & G band) of GUITAR with laser excitation energy of 2.81 eV (633 nm), 2.54 eV (532 nm), 2.41 eV (514 nm), 2.33 eV (488 nm) and 1.96 eV (442 nm) on GUITAR coating a piece of quartz slide; B. G& D band position dispersion with Laser excitation wavelengths; C. I(D)/I(G) ratio dispersion with laser excitation wavelengths. D. Raman (2D band) of GUITAR with laser excitation energy of 2.81 eV (633 nm), 2.54 eV (532 nm), 2.33 eV (488 nm) and 1.96 eV (442 nm) on GUITAR coating a piece of quartz slide.

Figure **1.6**B and C illustrated the G and D positions and I(D)/I(G) ratio dispersion on the laser excitation wavelengths. The G band on GUITAR is not dispersive with the laser wavelengths. This non-dispersive behavior is commonly seen on graphitic carbons, [50, 72] such as HOPG,[73, 74, 75, 76] nano-crystalline graphite[77, 78] and glassy carbon[79]. The dispersion of G

band can only be observed in more disordered carbon, and is proportional to the degree of disorder.[50] The D band dispersion on GUITAR is 52.7 cm^{-1}/nm, which agrees well with that on other graphitic materials. [72] The D band dispersion is useful for differencing an aromatic-based sample from a diamond-based sample because the 1332 cm^{-1} band in the latter case does not disperse.[72] Moreover, similar to microcrystalline or nanocrystalline graphite, I(D)/I(G) dispersion on GUITAR reached the maximum among all the carbon material as demonstrated by Farrari and Robertson[50] and Merlen et al.[72] As in Figure **1**.**6**D, the 2D bands of GUITAR were collected with different laser activation power. Though the 2D band can be evolved for more information on carbon/hydrogen bonding details, the band is however too broad to extract useful information from. The G and D positions and I(D)/I(G) ratio dispersion study on GUITAR all lead to the same conclusion that GUITAR is like a nano- or micro- crystalline graphite.

1.3.4 XRD-GUITAR has turbostratic structure but not turbostratic carbon

Figure **1**.**7** presented the XRD spectra of GUITAR and HOPG. XRD spectra can be used to calculate the interlayer spacing (d-spacing) distance from Bragg's law ($n\lambda=2d\sin\theta$, n is order of reflection and equals to 1 for all reflections in crystallography, λ = x-ray source wavelength (Å), d = d-spacing or interlayer spacing (Å), and θ= Bragg angle (°)).[80,81,82,83] The (002) line position (25.4°) on GUITAR is close to classical graphite (2θ=26.5-27°)[80 81] and is the characteristic peak for hexagonal graphitic lattice[80], the d-spacing is 0.350 nm. The d-spacing was found 0.335 nm for HOPG, the same as reported d-spacing for crystalline graphite.[84 85] The peak showed around 52-55° can be assigned to (004) plane. For both GUITAR and HOPG, $d_{004} = ½\ d_{002}$, which agrees well with Bragg's law $d_{00nl}=\frac{1}{n}d_{00l.}$ The (002) peak of GUITAR slightly shifted to a smaller angle compared to that of HOPG. This shift of (002) line was due to the insufficient cancellation effect caused by a smaller crystallite size by Fujimoto.[85]

The d-spacing of GUITAR (0.350 nm) is wider than that of HOPG (0.335nm), classical graphites (0.335-0.340 nm)[80, 81], MWCNT (0.340 nm)[9], glassy carbons (0.335-0.342 nm) [86] and onion-like carbon (0.336-0.340 nm) [87, 88]. GUITAR d-spacing (0.350 nm), however, conforms with turbostratic carbons (0.342-0.365 nm) [84,89,90]. It is suggested that carbon with an interlayer spacing more than 0.342 nm is considered to have the turbostratic structure.[89]

Notably, micrographs of turbostratic carbon do not exhibit discernable layer structures [91] as does GUITAR in Figure **1.1**.

Comparing the XRD spectra of GUITAR to that of HOPG as in Figure **1.7**, (002) peak experienced a significant broadening effect. The FWHM increases while the diffraction angle decreases with decreasing crystalline size.[85, 92] The grain size (L_a) can be calculated from Scherrer's law ($L_a=(C\lambda)/(B\cos\theta)$, where, L_a=grain size (Å), C=crystallite shape factor=0.94, B=Full width at half maxima (FWHM) of the peak of interest (Rad) and θ=Bragg angle (°)). The Scherrer's law however will only give a rough estimation on the crystalline size.[88, 90] The shape factor C is a dimensionless constant that varies from 0.89 to 1.39 depending on the geometry of the scattering objects. For a perfect two-dimensional lattice, C is 0.89 [93] and for a cubic three-dimensional crystal, C is 0.94 and for a perfect spherical object, C is 1.39 [94]. Here, the shape factor of GUITAR is selected to be 0.94 as in reference.[95,96] The grain size of GUITAR and HOPG were found to be 1.6 nm (n=3) and 60.9 nm respectively. The 1.6 nm grain size of GUITAR agrees very well with the value derived from the Raman spectrum (1.5nm-3.6 nm) from the previous section. [71]

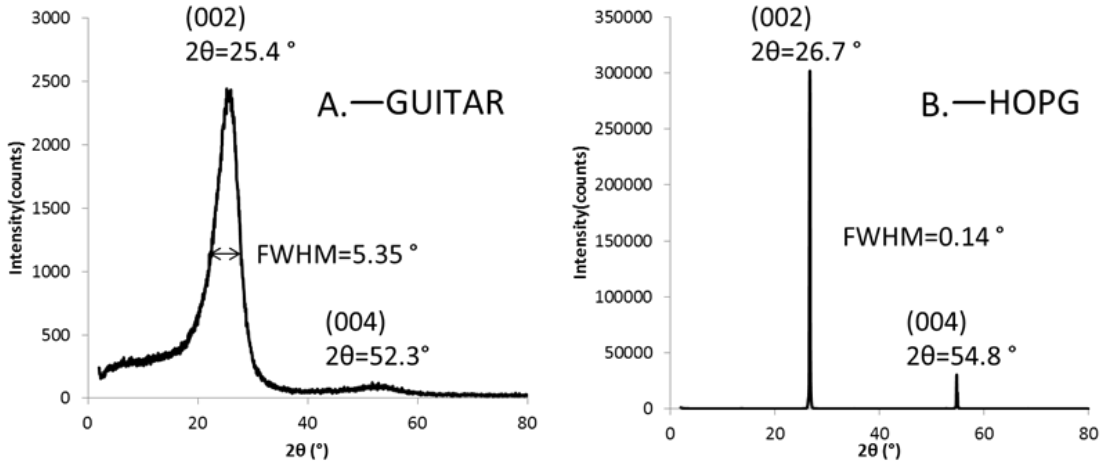

Figure 1.7. XRD of (A) GUITAR and (B) HOPG

1.4 Conclusion

GUITAR was found to have a unique electrochemical behavior. As a DSA with a wide potential window of 3V, GUITAR possesses a fast electron transfer rate (0.012 cm/s) on the

basal plane with high sp^2 content (85%, relative to total carbon). As seen on AFM (Figure **1**.**2**A), it doesn't allow the electrolyte intercalation as there is no step defects or grain boundary on the basal plane as other graphite.[33,34,35,36] The d-spacing of GUITAR (0.350 nm) is wider than that of typical graphite (0.335 nm). [80, 81] This confirmed the turbostratic disorder in GUITAR. The XPS, elemental analysis, Raman and TGA studies on GUITAR lead to a more definitive conclusion that it is nanocrystalline graphite with relatively high sp^3 content (15% relative to total carbon) and a grain size between 1.5 nm to 3.6 nm.

Chapter 2 . Chemically modified GUITAR (pseudo-Graphite from the University of Idaho Thermolyzed Asphalt Reaction) as a voltammetric pH sensor.

Haoyu Zhu, Ricardo Lopez, Hailey Joel Smith, Nolan Nicholas, Prasanna Sankaran, David N. McIlroy, I. Francis Cheng

2.1 Abstract

Voltammetric pH sensing was conducted with an oxidized form of GUITAR (Graphene/Graphite from the University of Idaho Thermolyzed Asphalt Reaction). This modification creates a surface rich of quinoid whose square voltammetric peak potential shifts by -63.3 mV/pH over the range of pH 0 to 11. The response is robust with up to 20 voltammetric runs between pH 0-9 and 2 between pH 10-11. There is no reactivation required between voltammetric scans. Cyclic voltammetric analysis reveals that the surface concentration of quinoid is 2.7×10^{-9} mol/cm^2, which ranks as the highest in literature on a basal plane carbon material. X-ray photoelectron spectroscopy studies confirm this high concentration of oxygen at the basal plane. Further studies indicate that this voltammetric pH sensor is free of interference from Na^+ and K^+ and from the oxygen reduction reaction.

2.2 Introduction

GUITAR (Pseudo-Graphite from the University of Idaho Thermalized Asphalt Reaction) is hypothesized to be a new form of carbon synthesized from a relatively low cost and simple method.[97,98,99] Visual characteristics and micrographs indicate basal and edge morphologies shared with other graphitic materials. However GUITAR differs in electrochemical properties in that its basal plane has fast heterogeneous electron transfer kinetics while the aqueous anodic and cathodic limits exceed other graphitic carbons by 1 V, resulting in a 3 V electrochemical window.[100,101] These features indicate many applications in sensors,[102,103] energy storage and conversion, and water purification.[104] In this report, efforts are directed toward the chemical modification of GUITAR for the voltammetric sensing of pH.

The measurement of pH is of fundamental consideration.[105,106,107,108,109] In this pursuit the glass pH electrode is the most utilized sensor. It is well characterized and an economical device in most instances. [110,111] However, it requires frequent re-calibration and is

mechanically fragile which makes it impractical for many applications. [112, 113, 114, 115] Furthermore, it is difficult to miniaturize this electrode especially for *in vivo* analysis. [115, 116] Due to these limitations, there is a search for alternative pH sensors. Carbon materials show promise as voltammetric based sensors from the standpoints of economic feasibility, ability to be miniaturized and mechanical robustness.[117,118,119,120,121] However, carbon requires surface modification with pH sensitive functional groups for this application. The scheme in Figure 2.1 illustrates the possibility of sensing pH through quinoid functionalities. The cyclic voltammetric half-wave potential ($E_{1/2}$) on these functional groups offers a theoretical linear shift of 59.2 mV per pH unit.

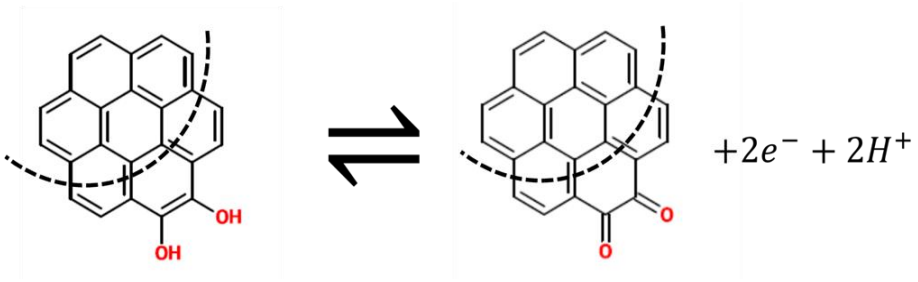

$$E_{1/2} = \text{constant} - 0.0592\, pH$$

Figure 2.1. The mechanism of quinoid/hydroquinoid redox reaction on graphitic electrode and the Nernstian response equation.

This approach has been investigated on carbon electrodes by various preparation methods. In most instances, the modification processes may be time consuming, require re-activation between pH determinations and/or the use of hazardous materials.[113,122,123] In a previous investigation, GUITAR was modified with quinoid functional groups (q-GUITAR) for use in chemical oxygen demand (COD) sensing.[103] The method to form q-GUITAR is rapid, which generally takes less than 20 minutes in 1M sulfuric acid. In this contribution we examined the pH sensing capabilities of this modified material.

2.3 Experimental

Chemicals and Materials. Nitrogen gas (>99.5%) was obtained from Oxarc (Spokane, WA, USA). Sulfuric acid (96.3%), acetic acid (glacial), sodium bicarbonate (powder) and potassium nitrate (crystal) was obtained from the J.T. Baker Chemical Co. (Phillipsburg, NJ, USA). Sodium chloride (crystalline), boric acid, sodium hydroxide and sodium carbonate were obtained from Fisher Chemical (Fair Lawn, NJ, USA). Phosphoric acid was from Macron Fine Chemicals (Center Valley, PA, USA). 1M standardized nitric acid was purchased from Alfa Aesar (Tewksbury, MA, USA). TRIS (base) (tris(hydroxymethyl)aminomethane) and TRIS hydrochloride were obtained from VWR (Radnor, PA, USA). Copper alligator clips (model: CTM-34C) and paraffin wax were obtained from Cal Test Electronics (Yorba Linda, CA, USA) and Royal Oak Enterprises (Roswell, GA, USA). Glass pH combination electrode (PY-P21) was obtained from Sartorius Stedim Plastics GmbH (Goettingen, Germany). All aqueous solutions were prepared with deionized water passed through an activated carbon purification cartridge (Barnstead model D8922, IA, USA). Solutions used for pH detection were 1M HNO_3 (pH=0) as purchased, 0.1M HNO_3 (pH=1), Britton-Robinson Buffer system[124] (pH=2-9, 0.04M phosphoric acid, 0.04M acetic acid and 0.04 boric acid mixture, pH adjusted with 0.2M NaOH), 0.1M carbonate-bicarbonate buffer (pH=10-11). The supporting electrolyte for pH 1-11 buffers was 0.1M KNO_3. For interference studies, pH of 0.1M TRIS was adjusted by 0.1M TRIS hydrochloride in place of the Britton-Robinson buffer at pH= 5.5, 7 and 9 with no supporting electrolyte.

Electrode Fabrication and Electrochemical Setup. GUITAR samples were synthesized as described in previous studies.[97,98,99] Electrode fabrication and geometric area isolation were performed as described previously.[100] All electrochemical studies were conducted in a three-electrode undivided cell with graphite rod counter electrode and Ag/AgCl/3M NaCl (aq) (0.209 V vs SHE) reference electrode. Cyclic voltammetry (CV) and square wave voltammetry (SWV) were carried out using a Bioanalytical Systems EC Epsilon potentiostat (West Lafayette, IN, USA. All the SWVs in this work were collected with a step potential of 4 mV, a potential amplitude of 20 mV and a frequency of 25 Hz.

Electrode Characterization The X-ray photoelectron spectroscopy (XPS) apparatus was built in-house at the University of Idaho. The analyses were performed in a vacuum chamber with a base pressure of 1×10^{-10} torr. Measurements were made with the Al Kα emission line (1486.6 eV) and a hemispherical energy analyzer with a resolution of 0.025 eV. The samples were then inserted into the vacuum chamber. During spectral acquisition the samples were grounded and exposed to a 500 eV electron beam to eliminate spurious charging. All spectra were acquired at room temperature. The XPS peaks were fitted to the Gaussian curve, after performing a Shirley background subtraction. For all the fitted peaks, the FWHM were kept to the same value.

2.4 Results and Discussion

2.4.1 Formation of pH Sensitive Quinoid Groups on GUITAR.

A previous study investigated the formation of quinone-like functional groups on GUITAR. That system was optimized for chemical oxygen demand (COD) sensing.[103] In this contribution, the treatment again forms a quinoid-modified GUITAR (q-GUITAR). However, it was done under slightly different conditions that maximize pH sensing ability. Modification was conducted by applying 2.0 V vs. Ag/AgCl for 150 seconds followed by 15 cyclic voltammetric scans from -0.7 V to 1.0 V to -0.7V with scan rate of 50 mV/s in 1M sulfuric acid. This changed the metallic sheen of GUITAR to a yellowish brown (Figure 2.2). On anodized glassy carbon and related materials, this feature is attributed to a thin oxide layer causing an optical interference.[125,126,127] It is important to note that glassy carbon is an edge plane type electrode.

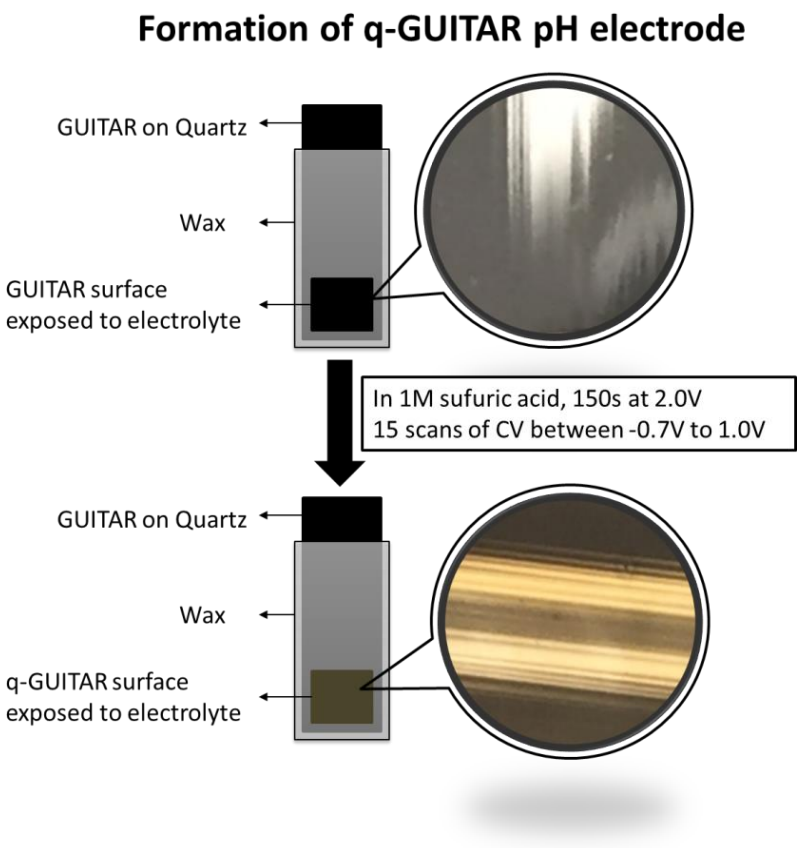

Figure 2.2. Diagram of electrode preparation and formation of the q-GUITAR pH sensor.

Post-modification cyclic voltammetric (CV) studies in 1 M H_2SO_4 are shown in Figure 2.3. The steady–state CV of q-GUITAR in Figure 2.3(a) shows the reduction and oxidation of quinonoid/hydroquinonoid surface functional groups. The broadness of reduction and oxidation peaks indicates pH sensitive quinoid groups in a variety of chemical environments.[117] The peak potentials (Ep) of this CV wave are 322 mV and 426 mV, respectively for the cathodic and anodic branches. Both the reduction and oxidation peak currents (i_p) were found to be linearly dependent on the scan rate, as seen in Figure 2.3(b). This is expected for surface bound redox-active functional groups. **Equation 1** allows for the calculation of surface concentration from the CV wave.

$$\boldsymbol{Q = nFA\Gamma_0^*} \qquad (1)$$

The variables n, F, A and Γ_0^* represent the number of electron transferred, Faraday's constant, electrode area and quinoid surface concentration (mol/cm^2), respectively. The charge, Q is integrated from the shaded area in Figure 2.3(a). On the basal plane (BP) of q-GUITAR, the concentration of quinoid species was found to be 2.7x10^{-9} mol/cm^2, equivalent to 40 % coverage relative to carbon on that surface, if we assume that the GUITAR basal plane has perfect hexagonal crystallinity. Electrochemical formation of quinoid groups on GUITAR compare favorably with other attachment methods on graphite. In general, q-GUITAR has relatively higher concentrations of quinoid when compared to graphitic materials (7.8×10^{-12} mol/cm^2 to 1.1×10^{-9} mol/cm^2).[113,116,122,130] Other examples possess such high surface concentrations (3.6×10^{-9} mol/cm^2 to 2×10^{-8} mol/cm^2) of quinoid are edge-plane rich materials.[128,129] Significantly to our knowledge, there appears to be no other examples of quinoid modification on basal plane (BP) graphite in the literature. This indicates a unique chemical environment in BP-GUITAR relative to BP-graphite. With such high quinoid coverage, the q-GUITAR electrode produces a high square-wave voltammetric pH sensing signal (Figure 5) relative to literature.[113,122,130]

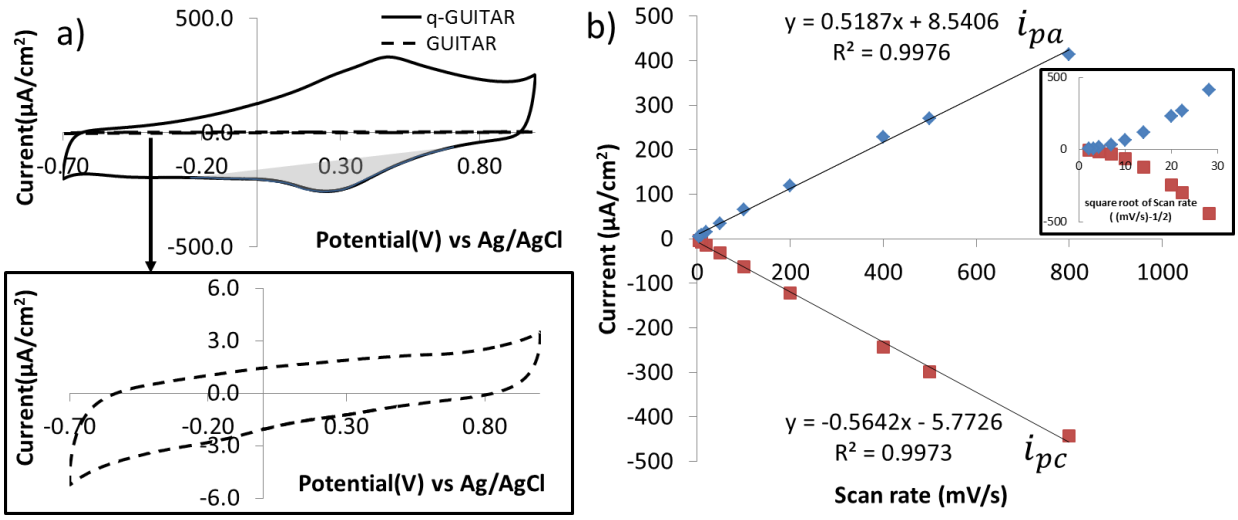

Figure 2.3. a) Steady state Cyclic Voltammetry of q-GUITAR (solid line) and GUITAR (dashed line) in de-aerated 1M sulfuric acid at 50 mV/s. The shaded area indicated the charge integration used to calculate the quinoid surface coverage. b) Quinoid reduction and oxidation peak current collected from steady state CV linearly dependence on the scan rate (average of n=3). The inserted figure shows the non-linear relationship between peak current and square root of the scan rate.

2.4.2 Characterization by X-ray Photoelectron Spectroscopy (XPS).

The wide scan XPS of q-GUITAR in Figure 2.4 reveals C 1s and O 1s peaks. The deconvolved C 1s peaks with their chemical assignments and relative abundances on pristine and q-GUITAR of this study are summarized in Table 2.1 and compared with a previous work. [103]

Table 2.1. Results of the deconvolution of the XPS C 1s peak of pristine GUITAR and q-GUITAR from this and previous work.

	Pristine GUITAR	q-GUITAR	q-GUITAR previous work[103]
C=C/C-C	284.2 eV (C=C, 85 %) 285.4 eV (C-C, 15 %)	284.5 eV (66.4%)	284.5 eV (59.0%)
C-O-C/C-OH	XPS wide scan indicates not oxygen content	285.9 eV (17.5%)	286.1 eV (19%)
C=O		287.4 eV (9.1%)	287.4 eV (11.8%)
COOH		288.8 eV (7.0%)	288.8 eV (10.2%)

The electro-active surface oxygen content of q-GUITAR of this study (sum of the 285.9 eV and 287.4eV peaks) is 26.6% are in relatively good agreement with the electrochemical measurements with **Equation 1** of 40%. The q-GUITAR of that previous study had higher total oxygen content (sum of all oxygen involved peak component) of 41% as measured by XPS.[103] The deconvolved O 1s peak of q-GUITAR indicated two components: C=O at 532.1eV (46.2%) and C-O at 533.2eV (53.8%) (Figure 2.4). It is notable that there was no peak that can be attributed to intercalated water (534.7 eV).[129]

In contrast, after being anodized, other graphitic electrodes undergo electrolyte intercalation at the edge plane, step defects and grain boundaries.[104,131,132,133] The lack of intercalation in GUITAR is unique and has been discussed in previous publications [100,101] and is the hypothesized basis for the GUITAR's resistance to corrosion relative to other graphitic

materials.

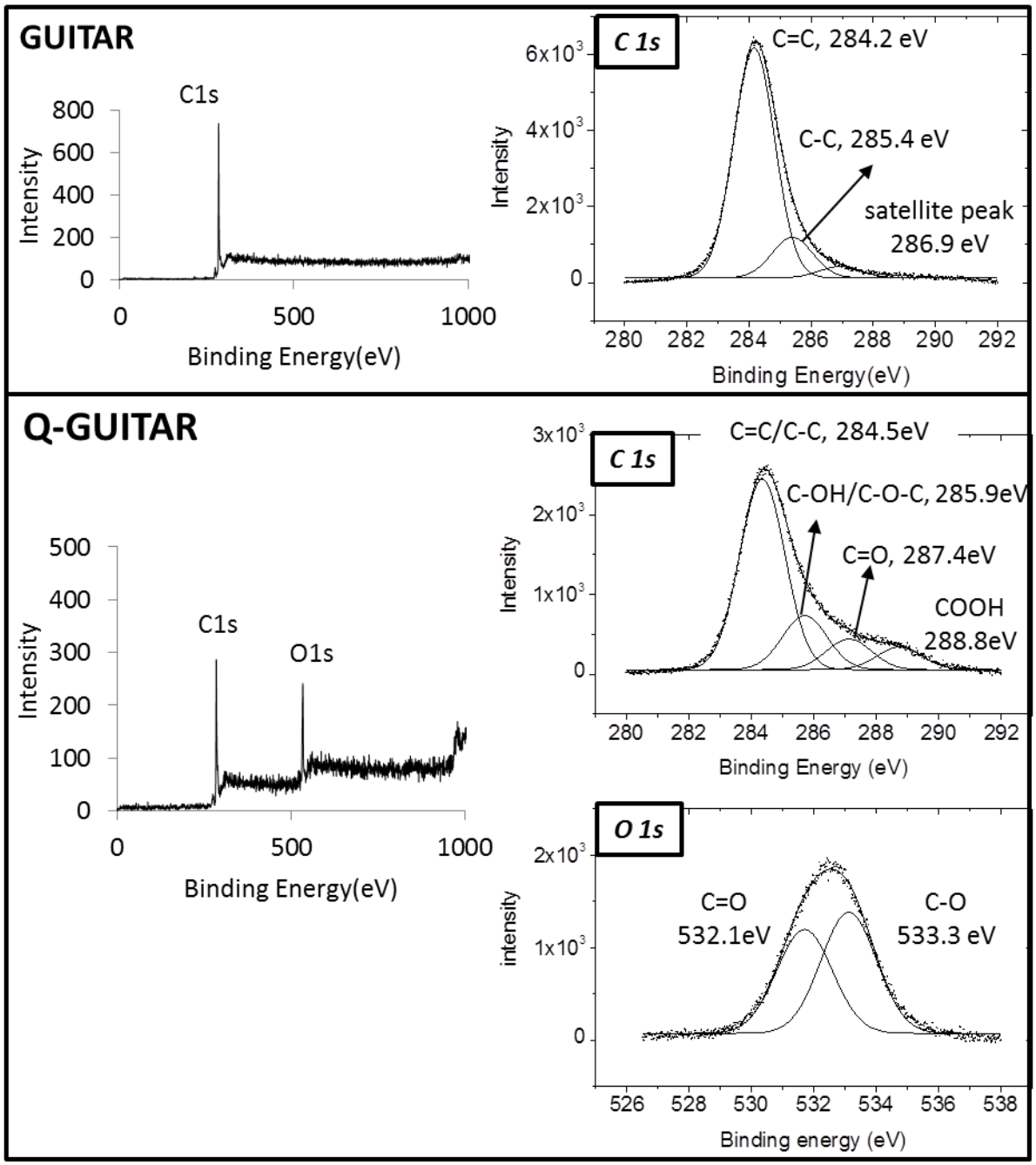

Figure 2.4. X-ray photoelectron spectra and deconvolution of C1s and O1s peak of pristine GUITAR and q-GUITAR of this study.

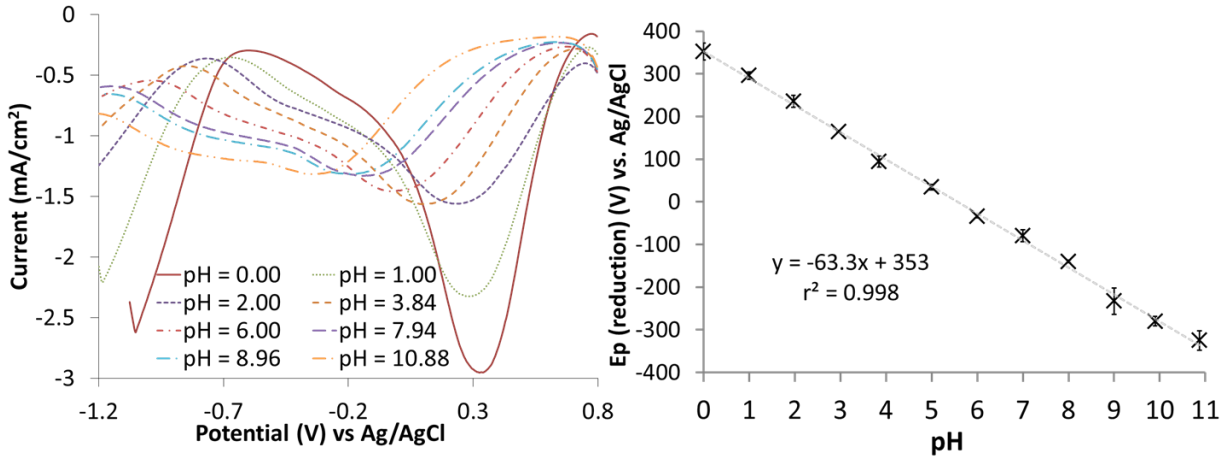

Figure 2.5. (A) left Representative square wave voltammograms of q-GUITAR as a function of pH. All the SWVs were collected on the same electrode without re-activation, under aerobic conditions with 0.1 M KNO_3 supporting electrolyte. (B) right The SWV reduction peak position (Ep) vs. pH, the error bars indicate standard deviation for 5 samples. The slope is -63.3 mV/pH.

2.4.3 Voltammetric pH sensing with q-GUITAR.

The pH response of q-GUITAR was measured by square wave voltammetry (SWV). This is due to its sensitivity relative to other voltammetric techniques.[134] Quinoid reduction peaks from pH 0 to 11 are shown in Figure 2.5(A). The buffers for this study were measured to 0.01 pH units with a calibrated glass pH electrode. It is apparent that the peak current signal decreases with the increasing pH value. This effect has also been observed in the literature with other quinoid modified graphite materials with a variety of hypotheses.[113,122,129,135] The variation in SWV peak potentials with pH is expected through Figure 2.1. That plot is shown in Figure 2.5(B). The average slope of this shift is -63.3 mV/pH with a standard deviation of $\pm$1.1 mV/pH and an intercept of 353 $\pm$ 6 mV for five samples. The slope is near Nernstian in behavior (59.2 mV/pH).

The linear sensing range of q-GUITAR electrodes was established from pH 0 to 11. At pH -1.0 (10 M HNO_3) and below, no current response was observed for the quinoid group reduction. Approximately 50% of the q-GUITAR electrodes (20 samples) are successful at sensing pH - 0.58 (3.8M HNO_3). At pH 0, all 20 sensors were effective. For the upper limit,

pH 12 and above are not possible as the q-GUITAR undergoes oxide layer exfoliation subjected to the voltammetric scan. This has also been observed in anodized glassy carbon electrodes.[136] At pH 11, pH sensing is possible for 2 SWV measurements before an observed shift in that peak potential. At pH 10, 7 measurements are possible without that peak potential shift. At pH 9 the electrode was stable for more than 20 measurements. Overall this pH sensor demonstrates very good stability over the pH range of 0-9. This sensor is very competitive with the literature in terms of need for reactivation between voltammetric runs, overall stability and pH range. [113,116,122,128,129,135]

2.4.4 Possible Interferences.

Two possible interferences were examined. These include the classical interferences with alkali metals on the glass pH membrane and the oxygen reduction reaction (ORR) (**Equation 2**).

$$O_2 + 4H^+ + 4e^- \rightarrow 2H_2O \qquad (2)$$

Na^+ and K^+ Does Not Interfere with pH Sensing.

The classical glass pH electrode suffers from Na^+ and K^+ interferences through competing equilibria with H^+.[137] There is at least one report that indicates this possibility with voltammetry of quinoid derivatives.[138] To examine the possible interference of Na^+ and K^+, TRIS buffer was used in place of the Britton-Robinson buffer, as it is free of alkali metal ions. As evidence in Figure 2.6, the peak position in the absence or the presence of 0.5 M $NaNO_3$ and 0.5 M KNO_3 did not significantly differ from the least squares fit line of Figure 2.5(B). These were not significantly different subjected to the Student's t-test at 99.5% confidence interval. This indicates that Na^+ and K^+ do not interfere with this sensor.

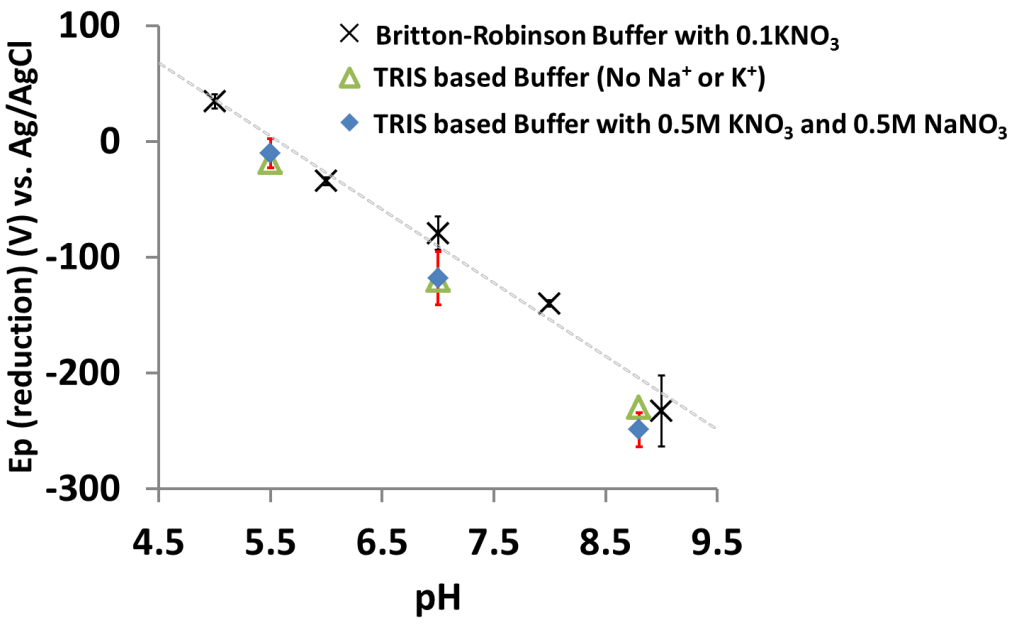

Figure 2.6. The response of the q-GUITAR pH sensor in the presence and absence of K^+ and Na^+. The response in the Britton-Robinson buffer (×) is taken from Figure 2.5(B). The response in the TRIS buffer were collected in the absence (Δ) and in the presence (♦) of 0.5M KNO_3 and 0.5M $NaNO_3$. Black error bars indicate the standard deviation of five electrodes, and red error bars is that of four. The responses in all buffers were not significantly different subjected to 99.5% confidence interval indicating no interferences from K^+ and Na^+.

The Oxygen Reduction Reaction (ORR) Does Not Interfere with pH Sensing.

The ORR was also examined as possible interference. As on many carbon materials, this reaction proceeds in the same potential range for voltammetric pH sensing.[113, 122] Furthermore, the need for O_2 removal would impede its use as a practical sensor. The voltammetric response of q-GUITAR at pH 0 and 9 under air and after deaeration with N_2 purging are shown in Figure 2.7. As evident in the voltammograms, the peak potentials (Ep) are not affected by the presence of dissolved O_2. There is minor contribution to the overall SWV current by the ORR but they occur at potentials more negative to the peak potentials.

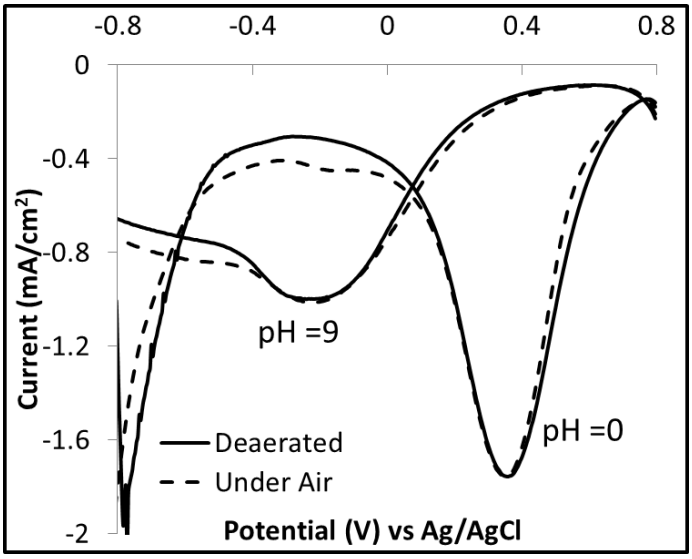

Figure 2.7. Square Wave Voltammetry of q-GUITAR in 1M HNO3 (pH=0) and B-R buffer (pH=9) under air (dashed line) and after deaeration (solid line)

2.5 Conclusion

A significant feature of this sensor is its ease of preparation, good linear range of pH 0-11 and relative durability. Attributes include the ease and speed at which the pH sensitive quinoid groups are formed on the basal plane of GUITAR. It is noteworthy that forming these groups by anodization is difficult or even impossible on basal plane of other sp^2 carbon due to corrosive processes.[104,131,132,133] The GUITAR stands unique in this characteristic. The concentration of the quinoid groups on BP of q-GUITAR is about the same as electrochemically produced moieties of edge plane graphite based sensors. Table 2.2 highlights the sensing performance of the q-GUITAR relative to the literature. In comparison to the glass pH electrode it has a similar linear range with slightly better acidic performance with reliable response down to pH 0. This was only observed with a few other carbon based electrode systems.[139] The overall pH sensing range is very competitive with other sensors and exceeds other anodized carbon electrodes.[129,135,140] The combination of these attributes makes q-GUITAR a competitive pH sensor relative to literature. Furthermore, there is a strong possibility of miniaturization of this sensor[141] along with screen-printed GUITAR particles designs for semi-disposable test strip electrode systems. We will report on these in future contributions.

Table 2.2. Voltammetric pH sensor literature summary.

Quinoid moiety activation or attachment method	Electrode	Slope mV/pH	pH linear range	stability	pH Detection method	ref
N/A	Commercial Glass electrode	53.2 to 63.1	2 to 12		potentiometric	142
Anodization methods	GUITAR	63.3 ± 1.1 (n=5)	0 to 11	20 and more tests for pH 0-9 2 tests for pH 0-11	SWV/reduction	This work
	Carbon fiber	52 ± 2 (n=4)	3 to 9	24 tests in pH 7	SWV/oxidation	129
	Carbon paste	60	3 to 8	N/A	potentiometric	135
	Glassy Carbon	60	2 to 5	4 tests in pH 7	SWV/oxidation	140
Polishing	Edge Plane Pyrolytic Graphite	57 ± 1	1 to 13	Single test Need reactivation	SWV/reduction	113
	Glassy Carbon	59	1 to 13	Single test Need reactivation	SWV/reduction	122
Chemical oxidation	Boron Doped Diamond	59 ± 1	2 to 12	More than 12 tests in	SWV/reduction	123

				pH=2.85		
	Graphite ink	57	1 to 13	Single test	SWV/reduction	130
Covalent bonding	Carbon fiber	38	6.5 to 8.0	45000 tests in pH 7.5	CV/oxidation	128
	Multi wall carbon nanotubes	59.3-60.2	1 to 12	500 tests in pH 6.8	SWV/reduction and oxidation	143
Physical adsorption	Pyrolytic carbon coated quartz nanopipette	54	2 to 12	N/A	CV/mid peak	112
Chemical adsorption	Au coated Carbon fiber	58	5.8 to 8	1000 tests in pH 7.4	CV/mid peak	116
Composite electrode	Carbon paste electrode	60.2	0 to 7	N/A	SWV/oxidation	139
		60	0 to 9	500 tests in pH 4,7,9	SWV/oxidation	
		59.7-62.0	2 to 11	N/A	CV/oxidation	144
		55.8	2 to 10			145

Chapter 3 . Chemically modified GUITAR (pseudo-Graphite carbon from the University of Idaho Thermolyzed Asphalt Reaction) as micro-supercapacitor electrode

Haoyu Zhu, Hailey Joel Smith, Thomas Williams, I. Francis Cheng

3.1 Abstract

A facile anodization treatment was applied on GUITAR and modified GUITAR with an ultrathin oxide film with a thickness of 25 nm. This oxide film presented a high areal capacitance of 890 μF/cm^2 at the current density of 10 μA/cm^2 and 590 μF/cm^2 at 50 μA/cm^2. The stability on q-GUITAR is moderate. But even after 5000 cycles of Galvano charge and discharge tests, the absolute capacitance is still higher than other carbon based micro supercapacitor (MSC) electrodes. With a capacitive potential on the electrode up to 1.7 V, the q-GUITAR oxide film based MSC has an expected energy density of 35.8 mWh/cm^3 at a power density of 1.0 W/ cm^3 and 22.7 mWh/ cm^3 at power density of 8.5 W/cm^3. Such performance is very competitive to the state of the art of other micro energy storage devices. The q-GUITAR based MSC will also be a very cost effect device as the oxide film was formed in-situ, with the GUITAR backbone being used directly as the current collector.

3.2 Introduction

The development and further miniaturization of portable/wearable electronic devices, wireless sensor networks, and micro-electromechanical systems (MEMS) is driving the research towards systems that have smaller dimensions, are maintenance free, and have a higher energy and power density. [146] [147] [148] Micro batteries such as micro lithium ion batteries have a high energy density, but also suffer from a limited lifetime and low power density. [148] [149] As an alternative to the micro batteries, micro supercapacitors (MSCs) provide a new approach for energy storage. Supercapacitors are also known as electrolytic double layer capacitors (EDLC). The supercapacitor stores charge through ions accumulated in the thin double layer formed at the electrode and electrolyte interface. Thus, supercapacitors can be charged and discharged at a much faster rate and have a much longer lifetime.

Though there is no clear definition for MSCs in the literature, this term usually refers to a miniaturized supercapacitor, down to the millimeter or centimeter size. Such a device requires a thin film electrode, which has a thickness less than 10 μm with a high volumetric capacitance. Thus the choice of electrode material is critical for MSCs. Carbonaceous materials have attracted attention due to their good conductivity, cost effectiveness, and in many cases their high specific surface area. The capacitive performance of activated carbon,[150] onion-like carbon,[149] carbon nanotubes,[151 152] graphene or graphene oxide,[147, 148] and their composites,[153, 154] were explored in MSCs. Volumetric capacitance, one of the important performance metrics for carbon based MSCs, is limited up to 35 F/cm^3 for most carbon based MSCs. The carbide-derived carbon exhibited super high capacitance up to 410 F/ cm^3 but suffered from poor electrode integrity.[146, 155, 156] With limited capacitance, the energy density is also limited. The energy stored in a supercapacitor can be calculated from $E = \frac{1}{2}CV^2$, where C is the capacitance of the capacitor; V is the applicable potential window on the capacitor. In aqueous systems, most carbon electrode materials have a capacitive window of 0.8 V to 1 V, as limited by the thermodynamic potential limit of water.[153, 157 158]

GUITAR is hypothesized to be a new carbon allotrope synthesized from a relatively low cost and simple method.[159,160,161] Its electrochemical properties differ from graphite in that its basal plane has fast heterogeneous electron transfer kinetics while the aqueous anodic and cathodic limits exceed other graphitic carbons by 1 V, resulting in a 3 V electrochemical window in aqueous systems.[162, 163] The wide potential window is due to the lack of electrolyte intercalation, as there are no step defects on the basal plane of GUITAR, as discussed in Chapter 1. This unique feature made the anodization of GUITAR possible without causing exfoliation, unlike graphitic electrodes. [164 165] In this study, anodization was applied on GUITAR to form a quinoid rich oxide film in-situ, as described in a previous chapter. The quinoid modified GUITAR (q-GUITAR) is evaluated as an ultracapacitor electrode. The ultrathin oxide film formed in-situ exhibited a high capacitance and a wide potential window, which leads to a high energy density with a moderate power density.

3.3 Experimental

Chemicals. Nitrogen gas (>99.5%) was obtained from Oxarc (Spokane, WA, USA). Sulfuric acid (96.3%) was obtained from the J.T. Baker Chemical Co. (Phillipsburg, NJ, USA). Potassium hydroxide is obtained from the EMD (Darmstadt, Germany). Copper alligator clips (model: CTM-34C) and paraffin wax were obtained from Cal Test Electronics (Yorba Linda, CA, USA) and Royal Oak Enterprises (Roswell, GA, USA). All aqueous solutions were prepared with deionized water passed through an activated carbon purification cartridge (Barnstead model D8922, IA, USA). Quartz was obtained from technical glass products (Painesville Twp., Ohio).

Electrochemcial characterization. GUITAR samples were synthesized as described in previous studies.[159, 160, 161] Electrode fabrication and geometric area isolation were performed as described previously.[166,] All electrochemical studies were conducted in a three-electrode undivided cell with graphite rod counter electrode and Ag/AgCl/3M NaCl (aq) (0.209 V vs SHE) reference electrode. Cyclic voltammetry (CV) and controlled potential electrolysis was carried out using a Bioanalytical Systems EC Epsilon potentiostat (West Lafayette, IN, USA). Cyclic charge and discharge tests were taken on MITs Arbin instrument.

Formation of q-GUITAR and exposure of sub-GUITAR. In a previous chapter, the quinoid modified GUITAR (q-GUITAR) was formed after being held in 1M sulfuric acid at 2.0 V vs Ag/AgCl for 150s, followed by 15 scans of cyclic voltammetry between -0.7V to 1.0V (as in Figure 3.1, from I. GUITAR to II. q-GUITAR). This treatment formed a thin oxide film on the surface of GUITAR. This oxide layer can be destabilized by a cyclic voltammetry scan between 0.8 V to -1.0 V for 5 cycles in 0.1 M potassium hydroxide (basic electrolyte, pH > 12). Following a rinse with DI water, the oxide layer can then be removed as indicated in Figure 3.1, from II. q-GUITAR to III. sub-GUITAR. The sublayer GUITAR (sub-GUITAR) has almost the same metallic sheen as GUITAR.

Physical characterization TEM. Transmission electron microscopy (TEM) observations were conducted with a JEOL 1200 EX II TEM at 120 kV. The freestanding GUITAR flakes adhere well to the copper TEM grids. The exfoliated oxide film was in DI water or in isopropanol and carefully pipetted on to the copper TEM grids and then dried in air. **AFM** The atomic force microscopy image was obtained with NTEGRA AFM from NT-MDT

spectrum Instruments (Moscow, Russia) operating in contacting mode in air at room temperature. The line etched silicon probe was obtained from Bruker Nano Inc. (Tucson, AZ). It was made of Antimony (n) doped Si with a tip height of 10-15 μm and radius of 8 nm, and a cantilever spring constant of 40 N/m, nominally. A scan area of 50 μm × 50 μm was taken on partially exfoliated q-GUITAR sample.

3.4 Result and discussion

3.4.1 Characterization of qGUITAR oxide film.

In a previous chapter, the quinoid modified GUITAR (q-GUITAR) was formed after being electrochemically treated. This treatment created a thin oxide film on GUITAR. The surface discoloration was again observed and can be attributed to this thin oxide layer causing an optical interference. [167,168,169]

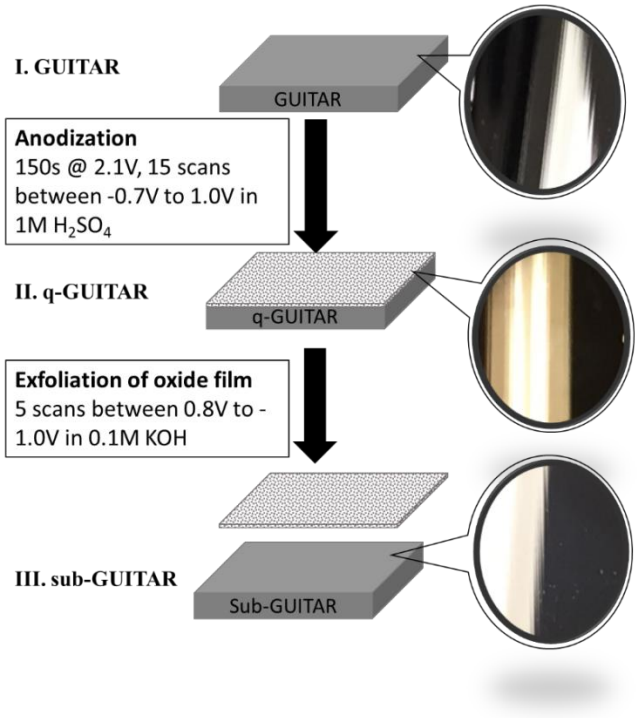

Figure 3.1. Diagram of formation of q-GUITAR and exposure of sub-GUITAR upon removal of oxide film.

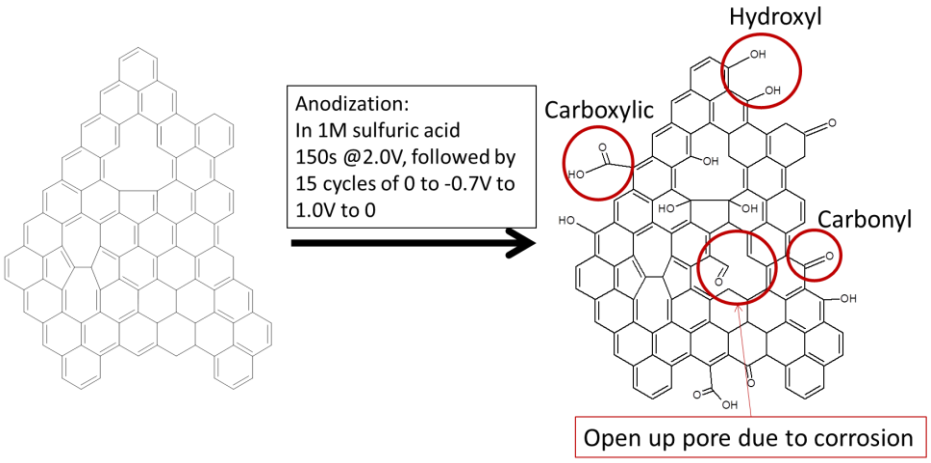

Figure 3.2. Proposed mechanism of anodization treatment on GUITAR.

The mechanism of the anodization treatment is proposed in Figure 3.2. Aside from the formation of hydroxyl, carbonyl, and carboxylic groups on GUITAR, it is also highly possible that the treatment causes pit corrosion on the basal plane of GUITAR. The porous structure of the oxide film is confirmed by the TEM, seen in Figure 3.3. Compared to the intact structure of GUITAR (Figure 3.3A), it is obvious that there are pores with a diameter ranging from 10-30 nm randomly distributed on q-GUITAR oxide film (Figure 3.3B). The anodization treatment penetrates through multiple layers of the GUITAR electrode. The porous structure allows more for the surface area on the oxide film to be accessible to ions, which leads directly to a higher capacitance.

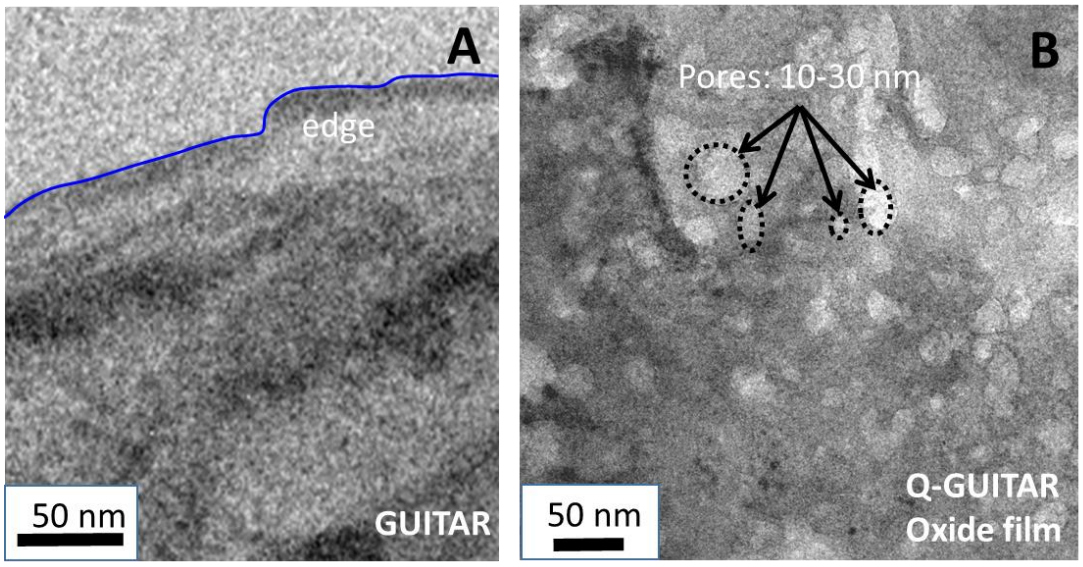

Figure 3.3. TEM of A. GUITAR flake, B. oxide film exfoliated from q-GUITAR. Pores with a diameter range of 10-30 nm presented.

3.4.2 Evaluation of q-GUITAR as MSC electrode- Areal capacitance

Figure 3.4A presents the cyclic voltammetry (CV) of GUITAR, q-GUITAR and sub-GUITAR in deaerated 1M sulfuric acid. The CV of an ideal capacitor is supposed to be rectangular. The current on the flat region of the CV curve can be used to calculate the double layer capacitance on the electrode.

$$C = \frac{i_+ - i_-}{scan\ rate \times electrode\ area},$$

where i_+ and i_- are the current at a potential (0.8V for this study, indicated by two black dots in Figure 3.4A) where it is flat, or no faradaic current exists. The areal double layer capacitance on GUITAR was found to be 15 ± 1 μF/cm^2, 750 ± 100 μF/cm^2 on q-GUITAR and 58 ± 12 μF/cm^2 on sub-GUITAR, where more than three samples were tested for each electrode material. The areal capacitance on q-GUITAR is 50 times higher than that of GUITAR, which is a result of the porous structure of the top oxide film layer as indicated in Figure **3.3**B. The steady–state CV of q-GUITAR in Figure 2A (II. q-GUITAR) presents the redox peaks of quinonoid/hydroquinonoid surface functional groups. These functional groups have been studied previously for pH sensing.[170]

On sub-GUITAR, the areal capacitance is slightly higher than, but at the same magnitude as, that of GUITAR. The capacitance of an electrolytic double layer capacitor (EDLC) can be calculated in the same fashion as conventional capacitors.

$$\boldsymbol{C = \varepsilon \frac{A}{d}},$$

where ε represents the permeativity of the electrolyte, A is the accessible area of the electrode to electrolyte, and d is the distance between the electrolyte to the electrode. The residual oxides make sub-GUITARs surface more hydrophilic than pristine GUITAR, which results in a smaller distance (d) between the aqueous electrolyte and the electrode surface. Thus, the capacitance on sub-GUITAR (58 ± 12 μF/cm^2) is slightly higher than that on GUITAR (15 ± 1 μF/cm^2).

The capacitance loss from q-GUITAR to sub-GUITAR electrode, after removal of the oxide film, implies that the high capacitance on q-GUITAR can largely be attributed to the oxide film. Also, The similar capacitance values of sub-GUITAR and pristine GUITAR indicated both electrodes have similar surface structure. To further confirm this, the $Fe(CN)_6^{3-/4-}$ redox probe was used to diagnose the surface change on GUITAR.[171, 172] As in Figure 3.4B, the cyclic voltammetry of I. GUITAR and III. sub-GUITAR in 1mM $K_3Fe(CN)_6$, 1M KCl almost overlapped each other. On q-GUITAR, the cyclic voltammetry distorted with no obvious peak in the same potential range. Such behavior indicates a much slower heterogeneous electron transfer (HET) rate on the q-GUITAR electrode, which can be attributed to the oxygenation on the electrode surface.[173] The peak separation on sub-GUITAR (93 mV) is slightly higher than that of GUITAR (88 mV). The slightly wider peak separation (or slightly slower HET rate) again confirms the existence of surface oxide residue on sub-GUITAR.

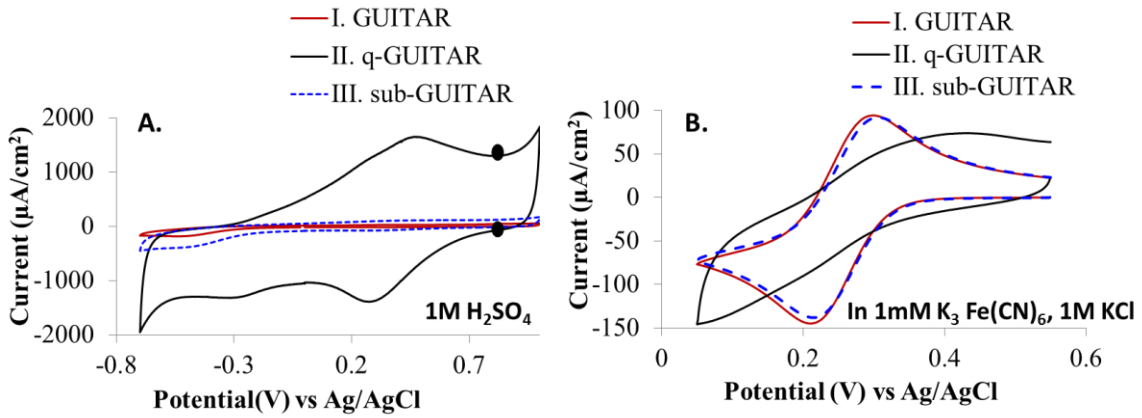

Figure 3.4. Steady state CV of GUITAR (Red solid line), q-GUITAR (black solid line), and sub-GUITAR (blue dashed line) in A. deaerated 1M sulfuric acid and B. 1mM Potassium Ferricyanide, 1M KCl, with a scan rate of 50 mV/s.

3.4.3 Evaluation of q-GUITAR as MSC electrode -Volumetric Capacitance

The gravimetric capacitance is usually used to evaluate the conventional supercapacitor, but is meaningless on a microscale device or a thin film device, as the weight of a microscale device is almost negligible.[174] Instead, volumetric capacitance becomes much more important. It can be obtained by dividing the areal capacitance by the thickness of the active material on the electrode. Atomic force microscopy (AFM) was used to find the thickness of the oxide film on q-GUITAR, seen in Figure 3.5A. The sample was obtained by partially submerging the q-GUITAR electrode in 0.1M KOH solution. Five cycles of cyclic voltammetry between 0.8V to -1.0V were taken on the electrode. After being rinsed by DI water, the oxide film exfoliated from the portion of the electrode that was submerged and electrochemically treated in KOH. The partially exfoliated q-GUITAR electrode is displayed in Figure 3.5B. The AFM probe was then focused on the artificial step defect created by the partial removal of the oxide film. The height distribution profile (Figure 3.5C) was taken across the step, as the shaded area in Figure 3.5A. The height difference between sub-GUITAR and q-GUITAR is equivalent to the thickness of the oxide film, which was found to be 25 nm.

Thus, the areal capacitance is 750 ± 100 μF/cm^2 on q-GUITAR, which is primarily from the 25 nm thick oxide film. This leads to a volumetric capacitance of 300 F/cm^3. Most reported

carbon thin film or micro electrodes have an effective electrode thickness of 1-10 µm. [147, 149] The oxidized q-GUITAR film has a thickness that is almost one magnitude thinner when compare to other carbon electrodes. This is an important milestone in the development of micro-electronic devices with ultra-small and thin dimensions. The thin oxide film exhibits a much higher volumetric capacitance than that of most carbon based micro electrodes, whose capacitance can range from 1F/cm^3 to 35 F/cm^3. [147, 149, 175 176] The carbide-derived carbon was reported with super high capacitance up to 410 F/ cm^3 in aqueous systems.[146, 155, 156] However, the carbide derived carbon usually required TiC as a starting material. The removal of Ti will cause electrode cracking, thus a poor electrode integrity.[155] The q-GUITAR electrode does not have the electrode integrity issue as the oxide film was formed in situ.

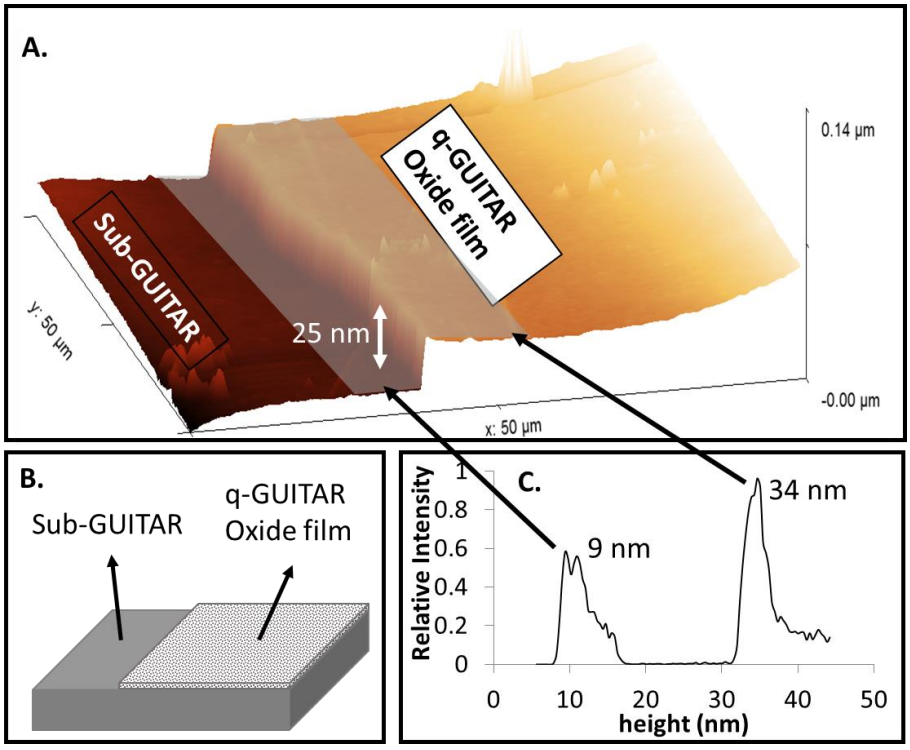

Figure 3.5. A. AFM of partially exfoliated q-GUITAR. The step indicates where the q-GUITAR film has been removed. B. Diagram of partially exfoliated q-GUITAR. C. Height distribution in the shaded step area. The height difference is the thickness of the q-GUITAR film: 25 nm.

3.4.4 Galvano charge and discharge and stability

The Galvano charge and discharge (GCD) was also investigated on q-GUITAR electrode at different current densities. As suggested by Ruoff et al,[177] the 10th cycle of the GCD tests at each current density are shown in Figure 5A. For an ideal capacitor, the GCD curve is expected to be triangular. The slightly distorted GCD curve on q-GUITAR was due to the pseudo-capacitance, of which the charge was from faradaic electron transfer, from the oxide groups. This behavior is also seen on other supercapacitors with appreciable amounts of pseudo-capacitance.[178 179 180] From the GCD tests, the capacitance can be calculated from $C = \frac{i}{\Delta V/\Delta t}$, where i is the current density applied to the electrode and $\Delta V/\Delta t$ is the slope for the discharge curve. The GCD curves as in Figure 3.6A were collected at current density from 10 to 100 μA/cm^2. The capacitance retention at different current density is as in the inserted figure in Figure 3.6A. Areal capacitance is 0.89 mF/cm^2 at 10 μA/cm^2; dropped to 0.59 mF/cm^2 at 50 μA/cm^2, maintained 0.57 mF/cm^2 at 100 μA/cm^2.

As seen in Figure 3.6C, the stability of the capacitance and charge efficiency on the q-GUITAR electrode has also been tested over 5000 cycles of GCD test at current density of 50 μA/cm^2. The capacitance retention (%) was obtained by comparing the capacitance after each cycling batch against the initial capacitance. Through 5000 cycles, the q-GUITAR electrode didn't lose any charge efficiency, which maintained about 99%. The initial drop of capacitance might be due to the loss of less stable oxide groups. After the initial loss of 20 % following the first 1000 cycles, the capacitance was more stable, and only dropped 10 % over the following 4000 cycles. While this loss of capacitance is not negligible, the absolute capacitance on q-GUITAR is still very competitive when compared to other carbon based MSC electrodes, as in Figure 3.6D. The initial capacitance of q-GUITAR is 233 F/cm^3 which dropped to 194 F/cm^3 at 1000th cycle, and 163 F/cm^3 at 5000th cycle. The capacitance at 5000th cycle is still much higher than that of carbon nanotube (CNT),[181] onion like carbon (OLC),[149] activated carbon (AC),[149, 150]and graphene [149, 153, 157, 182] based MSC electrodes, and comparable to that of carbide derived carbon (CDC).[155, 156]

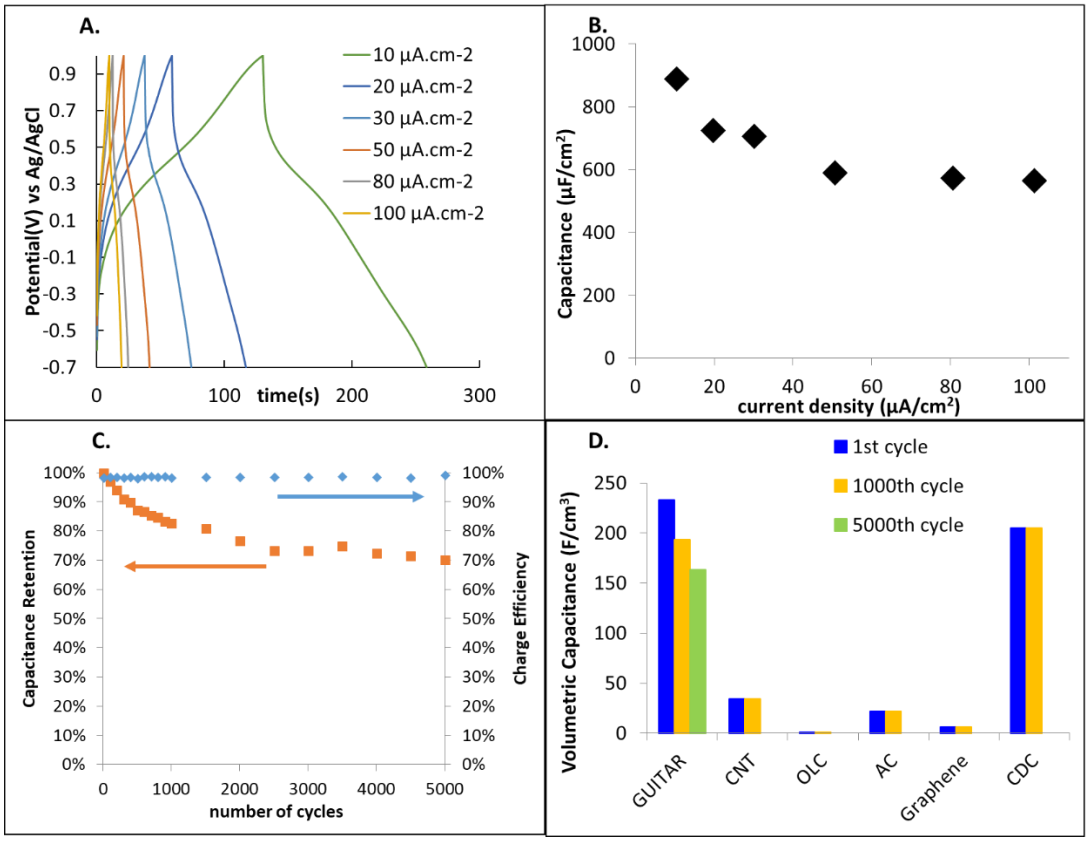

Figure 3.6. A. Cyclic charge and discharge curves tested at various current density in deaerated 1M H2SO4; B. Capacitance retention at different current density; C. Capacitance retention over 5000 cycles (Orange dot to the left vertical axis and charge efficiency stability over 5000 cycles (blue dot to the right vertical axis). D Capacitance stability comparison to state of the art for first and 1000th and 5000th cycle. CNT-Carbon nanotubes; OLC-Onion Like Carbon; AC-Activated Carbon; CDC-Carbide derived carbon. [147] [149] [150] [153] [155] [156] [157] [181] [182]

3.4.5 Ragone plot expectation-Energy density vs power density

From the single electrode performance on q-GUITAR, energy and power density can be estimated for a q-GUITAR based MSC device. The energy (E) that can be stored in a capacitor is calculated based on the capacitance: $E = \frac{1}{2}CV^2$, where C is the capacitance on the capacitor, and V is the applicable potential on the capacitor, which is 1.7V for q-GUITAR. The term C is equal to a quarter of the electrode capacitance, which was obtained from GCD curve at a certain current density. To test the electrode performance at different

current density (power density), the GCD curves were collected at current densities from 10 to 100 μA/ cm^2. The power (P) can be calculated from $P = \frac{E}{t_{dsicharge}}$, where E is the energy; $t_{discharge}$ is the time for the discharge.

As seen in Figure 3.7, the volumetric energy and volumetric power of a q-GUITAR capacitor estimated from a single electrode performance is compared to the state of the art in the literature. The expectation of volumetric energy on q-GUITAR is 21 - 33 mWh/cm^3 at the power density range of 7.8 - 0.9 W/cm^3. The volumetric energy on q-GUITAR is at the high end among the observed literature, even better than the commercial thin film lithium ion batteries.[148 149 183] However, the power density is moderate compare to the carbon based MSCs.[147, 148, 149, 150, 153, 155, 157, 184, 185, 186] The q-GUITAR oxide film electrode has appreciable amount of pseudo-capacitance. Thus, its power density is in a comparable range to other pseudo-capacitors, such as the metal oxides [175, 186, 187 188] and the conducting polymers based MSCs. [189 190] The MSC with the highest energy density and power density to date is an asymmetric MSC, which used MnO_2 and polypyrrole for each side, with nanoporous gold serving as the current collector. [191] The cost of a q-GUITAR based MSC will be much lower.

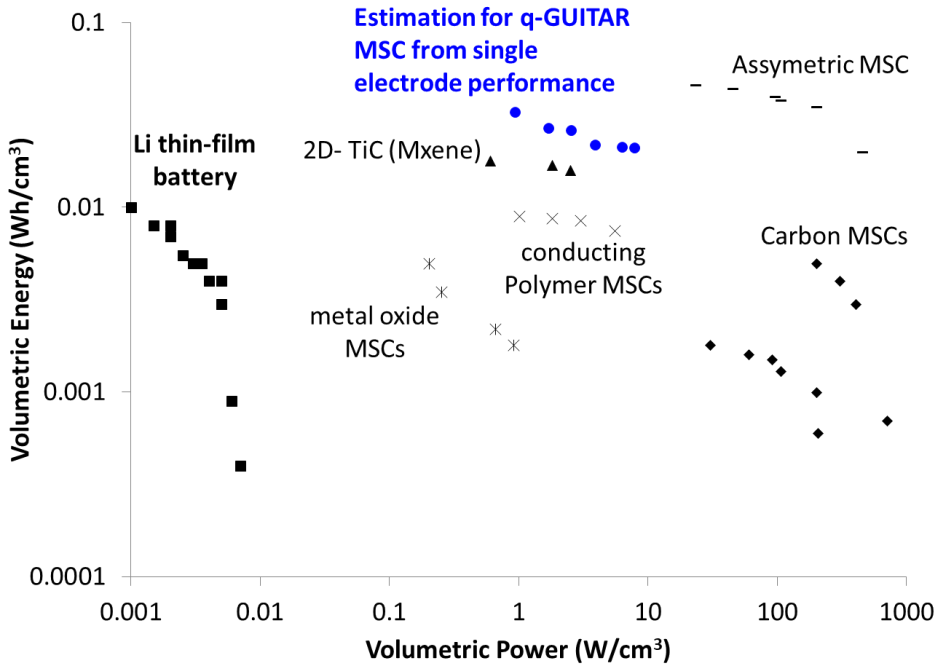

Figure 3.7. Comparison of volumetric energy and volumetric power expected for q-GUITAR based device to the state of the art in the literature. Li Thin film battery,[148, 149, 183] metal oxide

MSCs,[175 , 186, 187 ,188] conducting polymer MSCs, [189][189], [190]Carbon MSCs, [147, 148, 149 , 150, 153, 155, 157, 184, 185, 186] asymmetric MSCs (MnO2 on gold/polypyrrole on gold),[191] and 2D TiC MSCs.[183]

3.5 Conclusion

A modified GUITAR electrode was introduced as a micro supercapacitor electrode, which presented a high volumetric capacitance. The high capacitance was attributed to the nanopores in the thin oxide film formed in situ on the GUITAR electrode, without losing conductivity in the GUITAR backbone. The backbone GUITAR can be directly used as the current collector, which made it even more cost effective. The estimated energy and power density on a q-GUITAR based device was also very competitive with the state of the art of other micro energy storage devices. This was due to a much wider capacitive potential window (1.7V) as the energy density is proportional to the square of the potential window. This unique modified GUITAR provided a new and promising alternative for future micro supercapacitor electrode material selection.

Chapter 4 . Amine functionalized GUITAR and its potential applications

Haoyu Zhu, Kabir Humanyun, Ronald Wright, Nolan W. Nicholas, Elena Echeverria, Dave McIlroy, I. Francis Cheng

4.1 Abstract

Amine groups were introduced to the surface of GUITAR via the electrochemical oxidation of carbamate ions in situ. This is the first time a N content as high as 8% was reported on the basal plane of a flat carbon electrode. Confirmed by XPS N 1s peak, all the N content can be attributed to amine groups. Such high amine content on the GUITAR basal plane is surprisingly comparable to that on edge plane rich carbon materials. The successfully aminated GUITAR (am-GUITAR) electrode demonstrated a superior resistance to both air and solution aging effects over other graphite electrodes. The separation of $Fe(CN)_6^{3-/4-}$ redox peaks, which directly examines the heterogeneous electron transfer(HET) rate, on am-GUITAR was barely impacted by any aging effects over 4 days of exposure to both air and solution. The am-GUITAR also presented a competitive performance in sensing hypochlorite ions (free chlorine) with both chronoamperometric(CA) detection and cyclic voltammetric(CV) detection. The limits of detection (LOD) are 4.4 μM and 6.2 μM and the sensitivities are 73 μA/mM-cm^2 and 297 μA/mM-cm^2 with CA and CV respectively. The linear ranges are 0- 2000 μM for both CA and CV detection method. The am-GUITAR was also explored for its potential use in further functional group attachments. The di-hydroquinone group has been successfully attached to am-GUITAR. The stability of this attachment was demonstrated over five tests, with 10 minutes a soaking in phosphate buffer solution in between each test.

4.2 Introduction

GUITAR (Graphenic carbon from the University of Idaho Thermalized Asphalt Reaction) is hypothesized to be a new carbon allotrope synthesized from a relatively low cost and simple method.[192,193,194] Visual characteristics and micrographs indicate basal and edge morphologies shared with other graphitic materials. However GUITAR differs in

electrochemical properties in that its basal plane has fast heterogeneous electron transfer kinetics while the aqueous anodic and cathodic limits exceed other graphitic carbons by 1 V, resulting in a 3 V electrochemical window.[195,196] The fast heterogeneous electron transfer on GUITAR was reasoned to a finite density of state at the fermi level which might be due to the high density of defects on GUITAR basal plane.[197] These defects might provide sites that can be easily activated and functionalized. In a previous study, the oxidation treatment introduced the quinoid group on GUITAR with a surface concentration of 2.7E-9 mol/cm^2, equivalent to 40 % coverage relative to carbon on that surface. This compares favorably with other attachment methods on graphite.[198]

To activate the carbon surface for different applications, functionalizations other than oxidation have also been widely explored.[199] One of the extensively studied functional groups is the amino group, which enhances the surface hydrophilicity, provides strong interactions to target molecules, and provides a pathway for further functionalization. Amine functionalized carbon has been reported as sensors with a higher sensitivity toward NO_2^-,[200] Pb^{2+},[201] and free chlorine[202], and as supercapacitor electrode materials with higher capacitance and better capacitive desalination performance.[203 204] It was also reported as a good cross linker, readily bonding to other functional groups such as catechol,[205] carboxylated ferrocene,[206] and polymers.[207 208]

Amine groups have also been introduced on other carbon materials successfully. The N content on amianted graphene was reported to be 3.2% - 8.8%, [201, 206, 209, ,210] 10-15% on aminated Glassy Carbon, [200, 205, 211, 212,] and up to 20.6% on aminated CNT.[207] It is noteworthy that these examples are all edge rich materials. To our knowledge, there have been no successful amine attachments reported on a basal plane rich carbon material observed in the literature. In this study, an electrochemical amination method is applied to the GUITAR basal Plane. Verified by X-ray Photo Spectroscopy (XPS) and scanning electron microscopy/ energy dispersive x-ray spectroscopy (SEM/EDX), aminated GUITAR has a N content of 8% (by XPS), which is comparable to that on aminated edge plane carbon materials. All the amine groups were confirmed to be primary amines. The am-GUITAR will be evaluated with $Fe(CN)_6^{3-/4-}$ redox couple for heterogeneous electron transfer (HET) rate when fresh and after being aged. The sensing ability toward free chlorine and further functional group attachment will also be discussed on am-GUITAR.

4.3 Experimental

Materials and Chemicals. Sodium hypochlorite (5% m/m) were obtained from Acros Organics (NJ, USA). Potassium iodide (101.1%), potassium iodate (99.6%), sodium thiosulfate (99.5-101.0%) and starch (1% w/v) were obtained from J. T. Baker (PA, USA) for standardization of sodium hypochlorite. Potassium monophosphate (99.6%), potassium diphosphate (99.8%) and potassium chloride (99.7%) were obtained from Fisher Scientific (Waltham, NJ, USA). Ammonium Carbamate (99%) was obtained from Sigma Aldrich (St. Louis, MO, USA). Paraffin wax was obtained from Royal Oak Enterprises (GA, USA). All aqueous solutions were prepared with deionized water purified by passage through an activated carbon purification cartridge obtained from Barnstead - model D8922 (IA, USA). The sodium hypochlorite solutions were standardized by iodometric titration and used within three days.[213] 1M PBS solution was prepared by mixing.

Characterizations. XPS The X-ray photoelectron spectroscopy (XPS) apparatus was built in-house at the University of Idaho. The analyses were performed in a vacuum chamber with a base pressure of 1×10^{-10} torr. Measurements were made with the Al Kα emission line (1486.6 eV) and a hemispherical energy analyzer with a resolution of 0.025 eV. The samples were then inserted into the vacuum chamber. During spectral acquisition the samples were grounded and exposed to a 500 eV electron beam to eliminate spurious charging. All spectra were acquired at room temperature. The XPS peaks were fitted to the Gaussian curve, after performing a Shirley background subtraction. For all the fitted peaks, the FWHM were kept to the same value. The Scanning Electron Microscope (SEM) images were produced from a Zeiss Supra 35 scanning electron microscope (SEM) (Carl Zeiss, Germany).

Electrode Fabrication and Electrochemical Setup. GUITAR samples were synthesized as described in previous studies. [192] [193] [194] Electrode fabrication and geometric area isolation were performed as described previously.[195] Amination on GUITAR was achieved by applying 1.1V vs Ag/AgCl on GUITAR in 0.1M ammonium carbamate solution buffered by 0.1M PBS (pH=8.9). The 2,5-dihydroquinone amide GUITAR (DHQ-am-GUITAR) was obtained by pipetting 30 μL 10 mM 2,5 dihydroxyl benzoic acid (2,5-DHBA) buffered by 0.1M 2-(N-morpholino)ethanesulfonic acid (MES) (pH=4) onto am-GUITAR electrode. After one hour, rinse off the residue solution with DI water. All electrochemical studies were

conducted in a three-electrode undivided cell with graphite rod counter electrode and Ag/AgCl/3M NaCl (aq) (0.209 V vs SHE) reference electrode. Cyclic voltammetry (CV) and chronoamperometric (CA) studies were carried out using a Bioanalytical Systems (BASi) EC Epsilon potentiostat (West Lafayette, IN, USA).

4.4 Result and Discussion

4.4.1 Characterization of am-GUITAR and GUITAR

The GUITAR electrode was held at 1.1V for 16 hours in 0.1M Ammonium Carbamate with 0.1M PBS (pH=8.9).[202 214 215] The possible mechanism of formation of am-GUITAR is shown in Figure 4.1. The C-N bond in the carbamate ion will break down to generate CO_2 and an amino radical. The amino radical formed at the electrode and electrolyte interface will attack the electrode surface to form a bond in situ. Thus the resulted functionalities are expected to be primary amine groups.

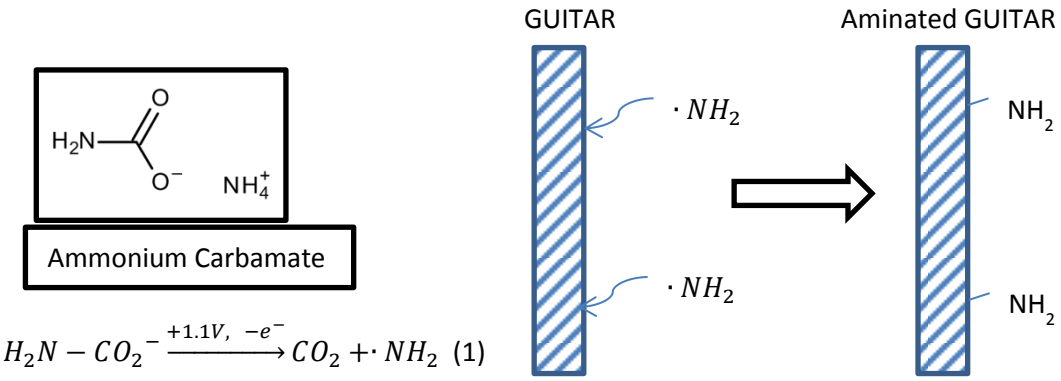

Figure 4.1 Amination of carbon and GUITAR electrodes by the electrochemical oxidation of ammonium carbamate.

The SEM of am-GUITAR shares the same microscopic appearance as that of GUITAR (Figure 4.2A & B). After a 16 hour electrochemical amination at 1.1V, the GUITAR electrode is still intact. The energy dispersive x-ray spectroscopy (EDX) associated with SEM indicated a high percentage of nitrogen and oxygen content on am-GUITAR, as seen in Figure 4.2C and D. The X-ray Photoelectron Spectroscopy (XPS) of GUITAR and am-

GUITAR is shown in Figure 4.3. On am-GUITAR, N 1s (around 400 eV) and O 1s (around 532 eV) appeared on the XPS wide scan, while GUITAR only has one C 1s peak. Using CasaXPS quantification to analyze the wide scan on am-GUITAR surface, the elemental composition is 82.2% carbon, 9.8% oxygen, and 8.0% nitrogen. As suggested by UKSAF[216] and NIST database[217], the N 1s peak around 398- 400 eV is from aromatic or alphatic amino signal, while the peaks around 400-402 eV is from amido signal. In deconvoluted N 1s peak, the single component at 399.8 eV can be assigned to the amine group.

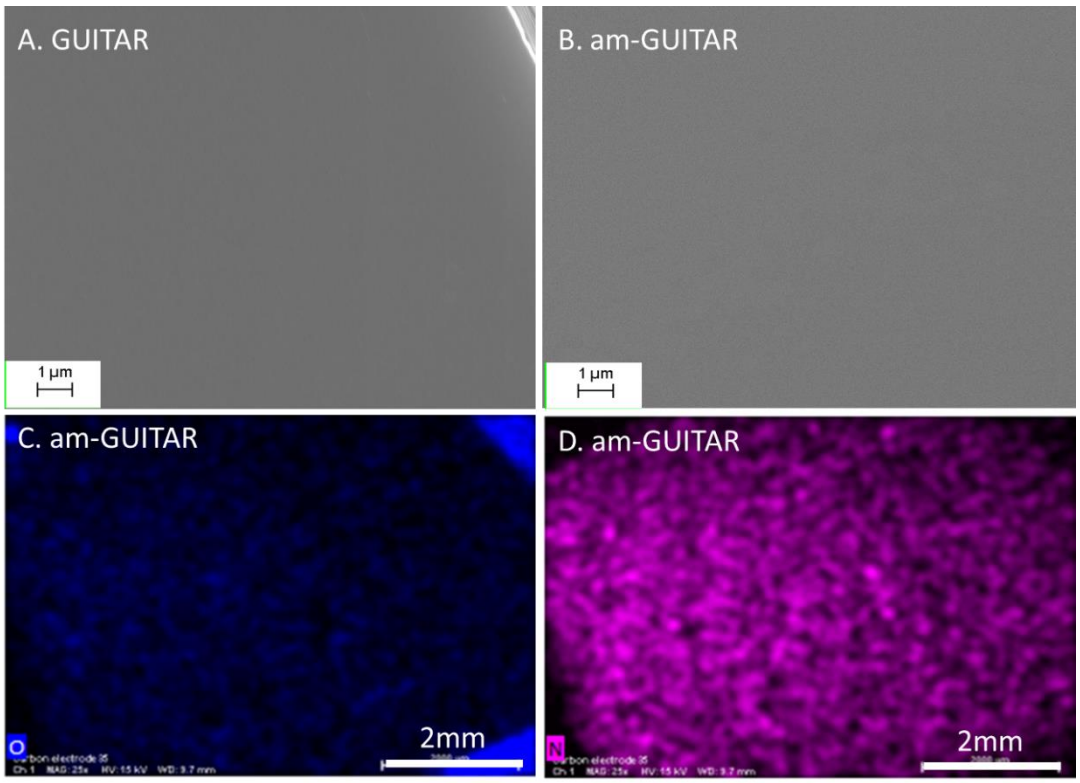

Figure 4.2: SEM of A.GUITAR and B. aminated GUITAR. The energy dispersive x-ray spectroscopy (EDX) on am-GUITAR of C. oxygen and D. nitrogen distribution on a piece of aminated GUITAR electrode.

Amine groups can directly or indirectly attached to other carbon electrodes. Successful direct amination on glassy carbon was reported through electro-oxidation of carbamate or carbamic acid, which resulted in a N content of 10 to 15 at. %.[200, 205, 211, 212] The direct amination can also be achieved by replacing the oxygen in a carbonyl group with an amine through a

reductive Leuckart Reaction, which yielded 3.2 at. % of nitrogen on graphene oxide.[209] Indirect attachment of amine usually requires a carboxylated carbon surface. Using crosslinkers, the -NH_2 will replace the -OH and be linked to the carbonyl carbon. Such reactions planted 4.4 to 8.8 at. % N content in aminated graphene oxide.[201, 206, 210] and 13.4 at.% to 20.6 at.% N content in aminated CNT. [207] It is noteworthy that these carbon materials are all rich in edge plane exposure. Wildgoose et al[212] has reported the electrochemical amination on basal plane pyrolytic graphite (BPPG) failed as the XPS N 1s were observed at 402.1 eV, which was assigned to ammonium ions. There is no successful direct amination being reported on the basal plane rich carbon materials. Thus, the amination on GUITAR is remarkable as it is the only reported basal plane amination, with a N content comparable to that of edge plane carbon materials.

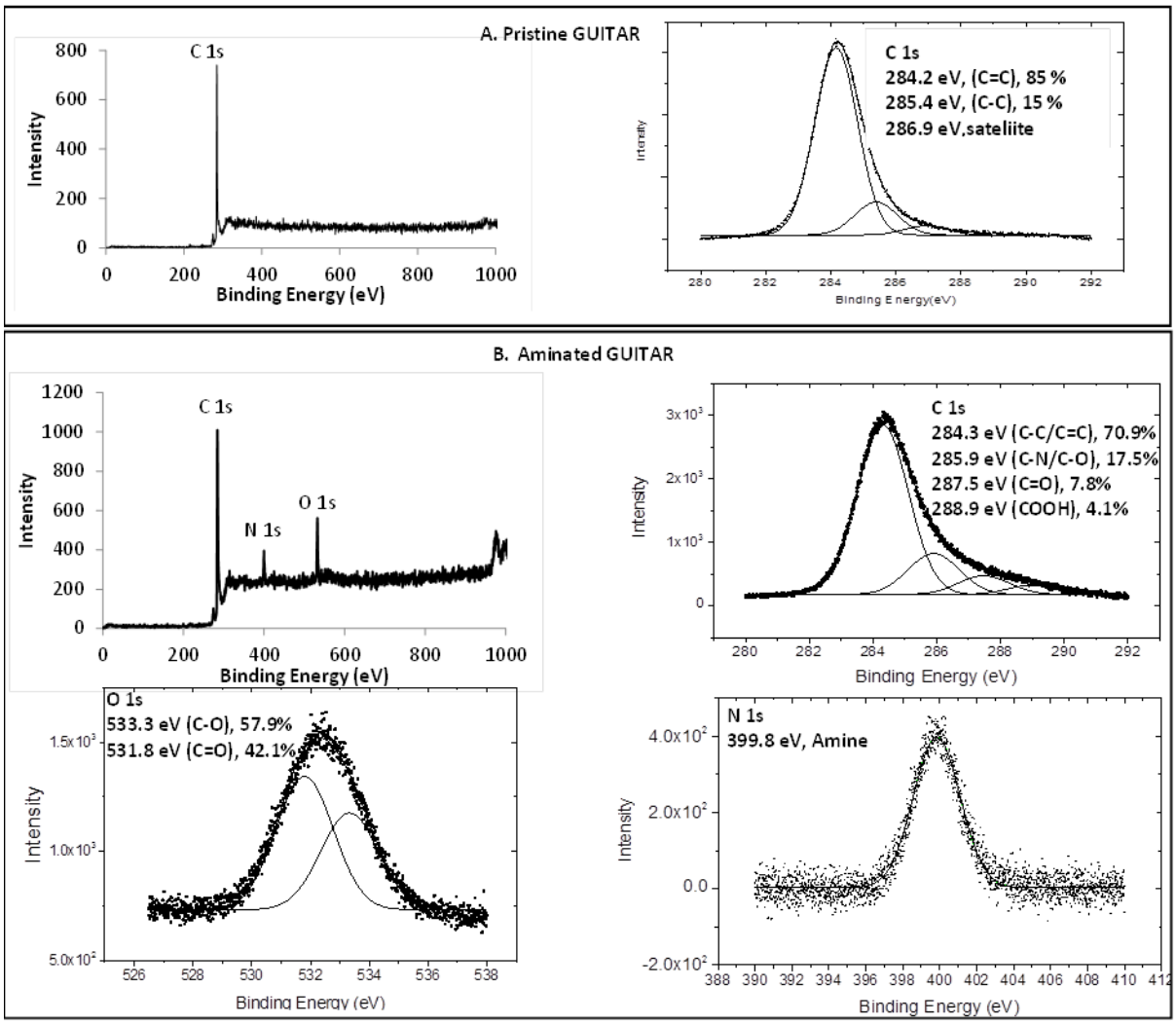

Figure 4.3 (a) Wide scan XPS spectra of pristine GUITAR and deconvoluted C1s peak by Origin; (b) Wide scan XPS spectra Aminated GUITAR and deconvoluted C1s, O1s and N1s peak by Origin. The deconvolution was obtained through fitting with Gaussian curve with Origin. For each deconvoluted peak, the component peaks had the same FWHM.

4.4.2 Resistance to aging effect.

The $Fe(CN)_6^{3-/4-}$ redox couple is a very simple quasi-reversible system often used to characterize new electrode systems [218] and very sensitive to surface structure.[219] Peak to peak separation (ΔEp) of this redox couple effectively represents the heterogeneous electron transfer rate (HET). [220] Thus, they are employed in this study as probe to monitor the change

of HET on GUITAR and am-GUITAR electrodes. On the am-GUITAR basal plane (BP), the peak separation was 66 mV ±3 mV, which is slightly smaller than that on GUITAR BP (73 mV ±3 mV) indicating a very fast HET rate.[195] A control experiment was also done on GUITAR by holding the electrode at 1.1V for 16 hours in 0.1M PBS. The peak separation on the control GUITAR electrode went up to 118 mV right after the treatment. This demonstrates that the fast HET can be partially attributed to the amine groups.

In previous work, the GUITAR BP electrode was found to experience a decrease in HET (increase in ΔEp) subject to exposure from air or ferricyanide solution (1mM $K_3Fe(CN)_6$, 1M KCl).[195] In that study, ΔEp on GUITAR was increased from 73 mV to 125 mV after 24 hours exposure to air. In this work, the exposure length is extended to 96 hours. The CVs on GUITAR and am-GUITAR after different exposure time to air is shown in Figure 4.4 A1-2. The exposure to air for 96 hours had a much smaller impact on the peak separation of am-GUITAR (from 66 mV to 102mV) than that on GUITAR (from 73 mV to 247 mV). The peak separation is also plotted in Figure 4.4 A3. It is obvious that on am-GUITAR, the peak separation is much more stable than that of GUITAR under exposure to air. The air aging effect was also significant on HOPG basal plane. The peak separation on HOPG was increased from 60 mV to 590 mV after being exposed for 3 hours to dry air.[220] On basal plane pyrolytic graphite (BPPG), ΔEp went from 227 mV to 596 mV and this value went from 89 mV to 137 mV on edge plane pyrolytic graphite (EPPG) after 24 hours of exposure to air.[195] Generally on graphite electrodes, a drastic increase of peak separation (or decreased HET rate) was observed. The decreased HET rate was possibly due to oxygenation on step edge or defects. [195 220]

A similar aging effect was also observed when the electrodes were exposed to the ferricyanide solution (1mM $K_3Fe(CN)_6$, 1M KCl). As seen in Figure 4.4 B1, the peak separation was not affected at all on am-GUITAR after 96 hours of exposure. On GUITAR, the peak separation was increased from 73 mV to 110 mV after 36 hours exposure and a pair of adsorption peaks appeared between 0.20V to 0.25V vs Ag/AgCl as in Figure 4.4 B2. This adsorption peak current kept increasing with longer exposure time to the solution. Unwin et al reported the same solution aging effect on HOPG, where the peak separation increased from 60 mV to over 590 mV after 3 hours of exposure to the solution(1mM $K_3Fe(CN)_6$, 1M KCl). [220] They claimed it might be due to possible Prussian blue deposition, but didn't

observe the adsorption peak.[220] Such aging effects have also been reported on Pt, the reason for which was assigned to either the formation of polymeric hexacyanoferrate[218 221 222] or the absorbed Ferri/Ferrocyanide on the electrode surface.[223]

The am-GUITAR presents a unique resistance to both air and ferricyanide solution aging effects. As seen in the proposed mechanism in **Figure 4.5**, there are two possible reasons for the superior resistance to aging effects. The first possibility is the amine layer acting as a protective layer to the polymerization of the electrolyte and to the oxygenation from air oxidation. The GUITAR surface under the amine blanket remains electrochemically active to electron transfer. Thus, even after aging, the HET rate is still fast. The other hypothesis is the passivation from solution and air still occurred on GUITAR surface, while the amino groups perform as the electron transfer pathway between the redox species in the solution to the electrode surface. The amine in the aqueous solution might be easily protonated and will have better interaction with negatively charge ferricyanide ions. Thus a fast HET rate was maintained on am-GUITAR.

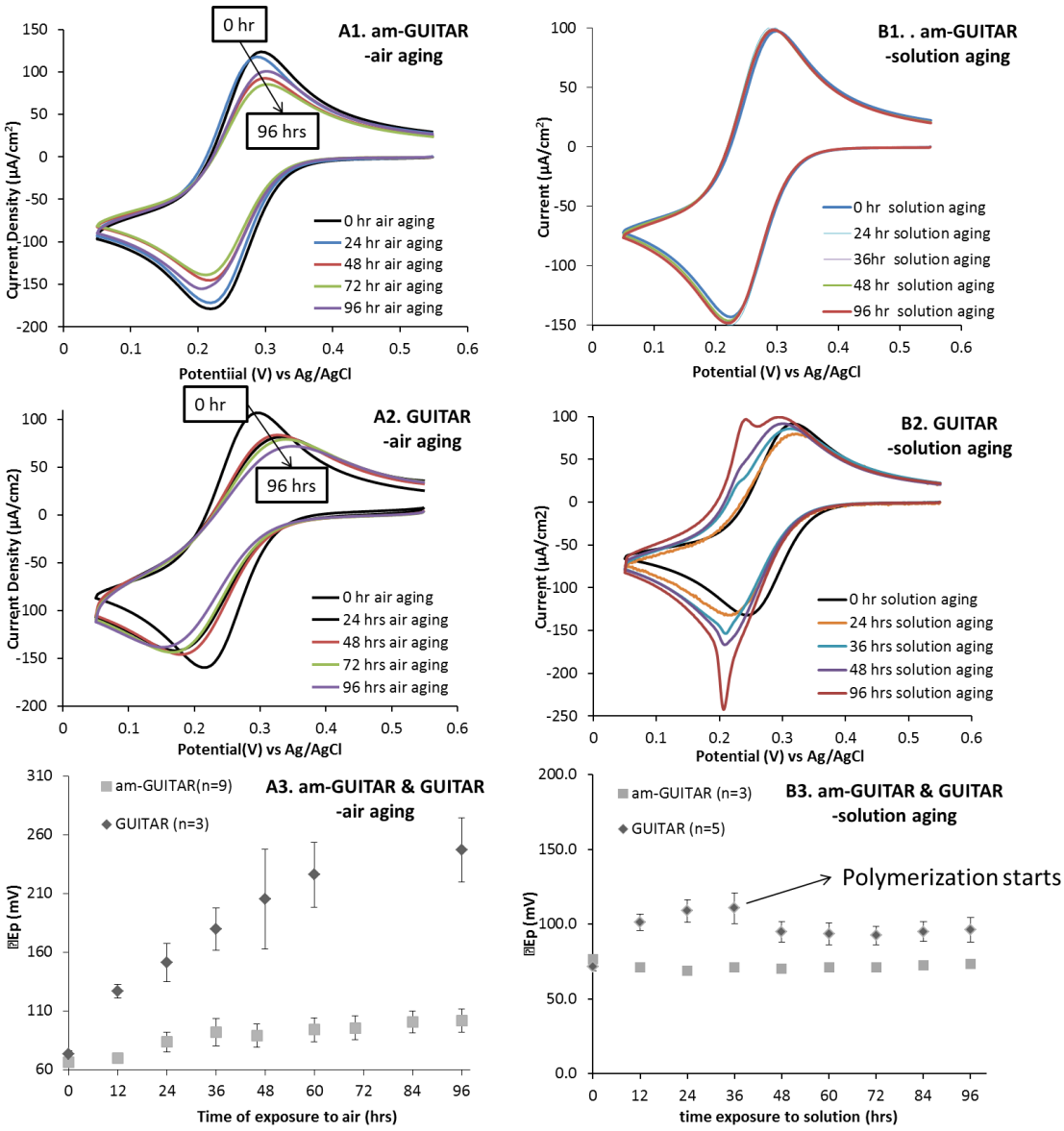

Figure 4.4: Cyclic voltammetries of 1mM ferricyanide, 1M KCl on (A) am-GUITAR and (B) GUITAR being exposed to (1) air and (2) ferricyanide solution for 0 to 96 hrs with time increment of 12 hrs. (C) the redox peak separation vs the time of exposure to (1) air and (2) ferricyanide solution.

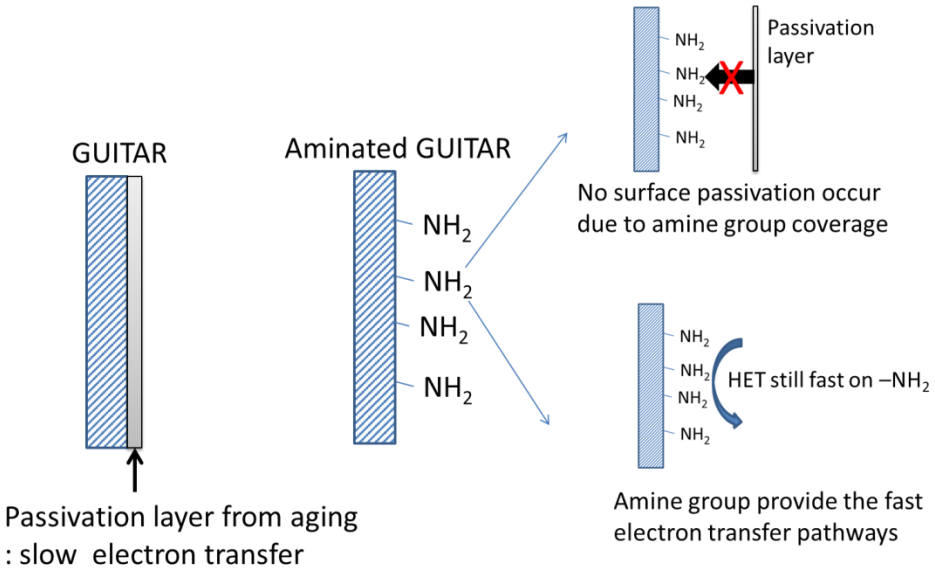

Figure 4.5: Scheme of the Passivation on GUITAR from aging and resistance to aging effect on aminated GUITAR.

4.4.3 Improvement of electrode sensitivity and HET to ClO- reduction

The amino functionalized carbon electrode has been explored as a chemical sensor to a great extent. The amine group provides a stronger interaction between the electrode and the target molecules. [200 201 203 204] The am-GUITAR was found to have a faster electron transfer rate for ClO^- reduction reaction. As in Figure 4.6 curve i and ii, GUITAR and am-GUITAR were both tested with cyclic voltammetry at 50 mV/s with a scanning window of 0.6 V to -1.0 V in deaerated 1 mM NaClO, 0.1 M PBS solution. The peak (around -50 mV to -200 mV) is assigned to the reduction reaction of ClO^-.

$$ClO^- + 2e^- + 2H^+ = Cl^- + H_2O \qquad E^{0'} = 1.49V \text{ (vs SHE) at pH 7} \qquad (1)$$

The peak position of hypochlorite reduction on am-GUITAR was shifted positively by 150 mV compare to that on GUITAR (from -0.2 V to -0.05 V vs Ag/AgCl). Such peak position shift demonstrates a marked improvement in HET by the amine group on the electrode surface. The faster kinetics might be due to the strong ionic interaction between protonated amine to the hychlorite ion. [200 201 203 204]

The oxygen reduction reaction (ORR) interference was also examined with cyclic voltammetry (CV). The CVs were conducted on am-GUITAR in 1 mM NaClO, 0.1 M PBS in air (Figure 6 iii) and after deaeration (Figure 6 ii). The peak around -0.5 V vs Ag/AgCl (ORR peak) disappeared after deaeration. The ClO^- reduction peak (-0.05 V vs Ag/AgCl) position and amplitude were not affected at all with absence or presence of the ORR peak. This clearly indicated the ORR does not interference with ClO^- reduction. This made ClO^- detection practical in air.

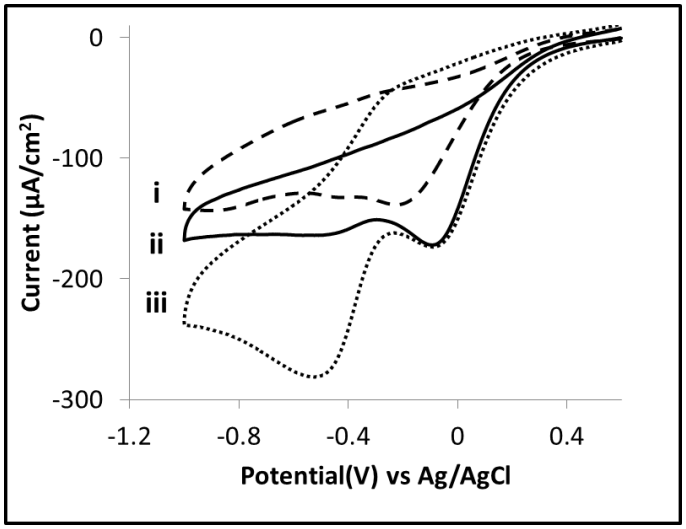

Figure 4.6: Cyclic voltammetry of (i) GUITAR in N_2 deaerated; (ii) am-GUITAR in N_2 deaerated and (iii) am-GUITAR under air in 1mM free chlorine with 0.1M PBS (pH=7.5)

4.4.4 Detetction of ClO^- (free chlorine)

The detection of ClO^- (free chlorine) on am-GUITAR was examined with both chronoamperometry (CA) and cyclic voltammetry (CV) (Figure 4.7). The CAs shown in Figure 4.7a were collected at -0.05 V vs Ag/AgCl in 0.1 M PBS with NaClO concentration of 0 to 2000 µM with 500 µM as the concentration increment. The current was then collected at 120s for the calibration curve in Figure 4.7b. The CV shown in Figure 4.7c was collected in the 0.1 M PBS with NaClO concentration ranging from 0 to 2000 µM, with 500 µM as increments. Only the peak current was collected for the calibration curve in Figure 7d. On CA and CV, limits of detection (LOD) are 4.4 µM and 6.2 µM respectively, with sensitivities of 73 µA/mM-cm^2 and 297 µA/mM-cm^2. The linear ranges are 0- 2000 µM for both CA and CV. The detection of free chlorine on other electrodes from literature is listed in **Table 4-1**.

The amino group improved the sensitivity by 32% for CA and 37% with CV when compared to pristine GUITAR. Especially with CV detection, the am-GUITAR sensor almost presents the best sensitivity compare to the literature. The Au and Pt based sensors have the highest sensitivity among the literature reported values.[224 225 226] However, it is noteworthy that GUITAR is much more cost effective compared to the noble metals. The detection concentration range is much wider on am-GUITAR than that on Au and Pt electrodes. Thus, am-GUITAR is a competitive hypochlorite detector with a high sensitivity in a wide detection range, at a much lower cost.

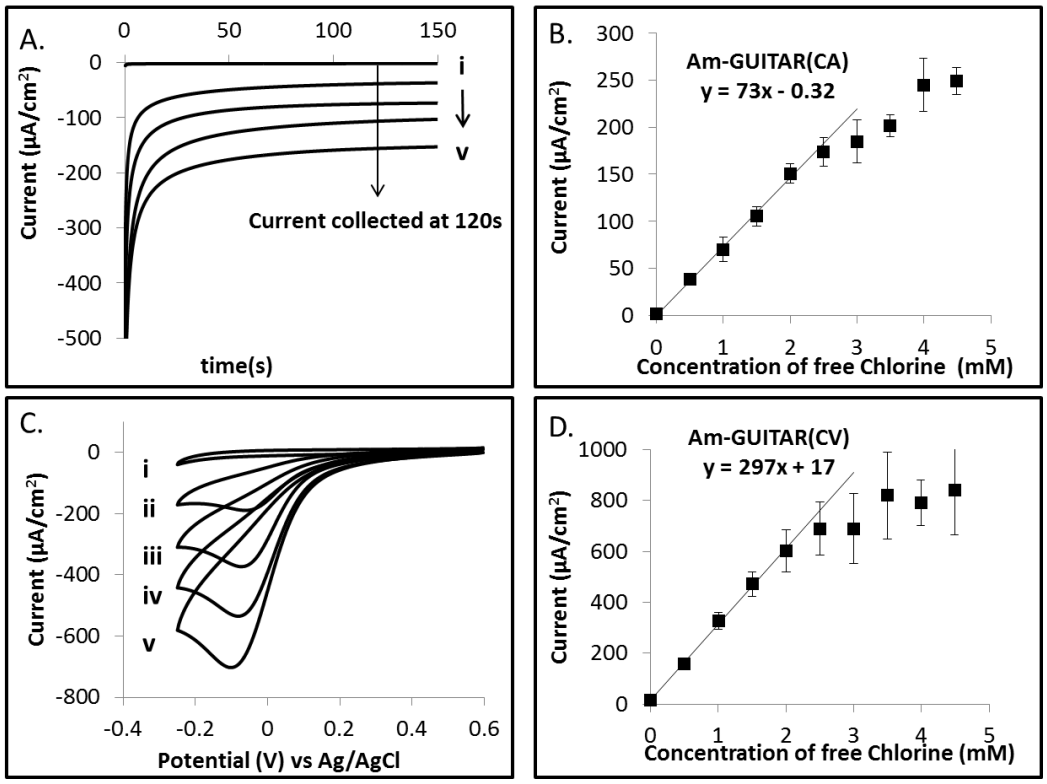

Figure 4.7: (a) chronoamperometry of am-GUITAR in (i-v) 0-2000 µM NaClO in 0.1M PBS(pH=7.5) at -0.05V vs Ag/AgCl; (b) calibration curve of ClO^- detection on am-GUITAR based on the chronoamperometric current collected at 120s; (c) cyclic voltammetry of am-GUITAR in (i-v) 0-2000 µM NaClO in 0.1M PBS(pH=7.5) at scan rate of 50mV/s; (d) calibration curve of ClO^- detection on am-GUITAR based on the cyclic voltammetry ClO^- reduction current collected at -0.05V vs Ag/AgCl.

Table 4-1. Comparison of free chlorine detection on GUITAR and am-GUITAR electrode to the literature.

Material	Sensitivity ($\mu A/mM\text{-}cm^2$)	LOD (μM)	Linear range (μM)
Au[224 225 226]	720	0.2 - 0.4	0.2 - 300
Pt[224 227 228]	670	0.2 - 1.4	2.8 - 60
Am-GUITAR(CV) **This work**	**297**	**6.2**	**0-2000**
Aminated glassy carbon[229]	283	1.55	200-2000
Au micro electrode[230]	278	1.5	0 - 80
Glassy carbon[229]	230		0-2000
GUITAR (CV)[231]	**215.8**	**1**	**0 - 5000**
Polymelamine modified screen printed carbon electrode[232]	210	5.5	10-7000
Au-NPs-PEDOT/GC[233]	209	1	1-932
Am-GUITAR(CA) **This work**	**73**	**4.4**	**0-2000**
Carbon nanotube/epoxy resin[225]	75	0.4	0.4 - 80
GUITAR (CA) [231]	**55.2**	**0.5**	**200 - 2200**
Boron doped diamond[234]	38	0.16	400 - 2000
CuO-NPs/MWCNT/epoxy resin[235]	17	0.085	
Aminated-pencil graphite[202]	15		0.8-116
AuNPs/poly-MnTAPP/GC[236]	5	24.7	

4.4.5 Further surface modification

Surface bonded amino groups provide a pathway for further functional group attachment. Carboxylated ferrocene was reported to attach to an aminated surface for a higher sensitivity to H_2O_2.[206] Different polymers have also been attached to aminated carbon nanotubes to create more material systems.[207 208] As discussed in a previous chapter, the quinoid modified

GUITAR electrode can be developed into a pH sensor. As an expansion on that study, an effort was made toward further attachment of hydroquinone groups. The mechanism for this attachment is shown in Figure 4.8A. The primary amine group was bonded to the carboxylic carbon in the 2,5-Dihydroxybenzoic acid (DHBA) through the cross linker ethyl-3-[3-dimethylaminopropyl]carbodiimide (EDC). As in Figure 4.8B, steady state CV on am-GUITAR and dihyroquinone attached am-GUITAR (DHQ-am-GUITAR) was obtained in 0.1M PBS. The rectangular CV on am-GUITAR indicated pure capacitive behavior with no faradaic electron transfer process. The appearance of a pair of peaks on DHQ-am-GUITAR indicated the successful attachment of the dihydroquinone group. These peaks can be assigned to the redox reaction of surface bonded dihydroquinone as indicated in the below equation.

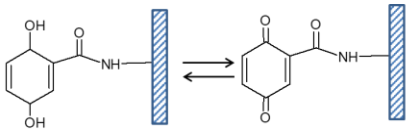

$$+2H^+ + 2e^-$$

The coverage of dihydroquinone can be calculated from $\boldsymbol{Q = nFA\Gamma_0^*}$. The variables n, F, A and Γ_0^* represent the number of electron transferred, Faraday's constant, electrode area, and quinoid surface concentration (mol/cm^2), respectively. The charge, Q is integrated from the shaded area in **Figure 4.8**B**.** On the basal plane (BP) of DHQ-am-GUITAR, the surface concentration of dihydroquinone was found to be 3.3×10^{-11} mol/cm^2, equivalent to 0.5 % coverage relative to carbon on that surface. This assums that the GUITAR basal plane has a perfect hexagonal crystallinity. The utilization of amine groups is only 5%. The yield of the reaction is yet to be improved.

The stability of the surface attached DHQ has also been evaluated. The electrode was left in 0.1 M PBS solution for 10 minutes between tests. As in **Figure 4.8**B, the first CV (fresh) on the electrode is overlaid with the fifth CV (after 50 minutes soaking). There is no difference between two CV scans, which indicated a good stability of the surface attached dihydroquinone.

Future work involves the optimization of reaction conditions to obtain a higher yield and utilization of amine groups. The pH sensing ability of this DHQ-am-GUITAR is also to be evaluated in the future.

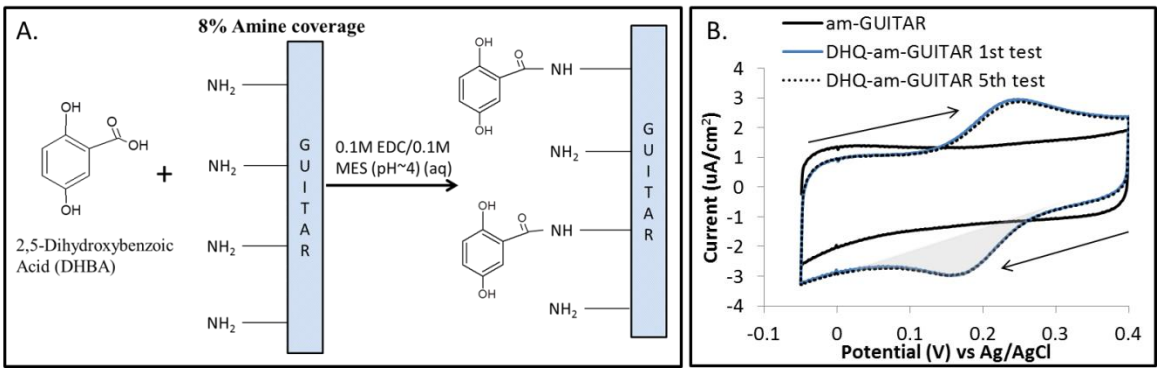

Figure 4.8 A. Diagram of Attachment of 2,5-Dihydroxybenzoic acid (DHBA) onto am-GUITAR surface, which catalyzed by the cross linker ethyl-3-[3-dimethylaminopropyl]carbodiimide (EDC) buffered by 0.1 M 2-(N-morpholino)ethanesulfonic acid (MES) (pH=4). B. Steady state cyclic voltammetry on am-GUITAR and dihyroquinone attached am-GUITAR (DHQ-am-GUITAR) in 0.1M PBS (pH=7.5). The DHQ-am-GUITAR electrode was tested after being soaked in 0.1 M PBS solution for every 10 minutes. The 1st test (fresh) and 5th test (after 50 minutes soaking) were shown and overlapped each other.

4.5 Conclusion

Amination of GUITAR was introduced as a new approach to functionalize the GUITAR surface for sensors and further modification purposes. Aminated GUITAR has been evaluated in sensing free chlorine and for further quinone attachment. On am-GUITAR, the chlorite reduction peak position has been shifted positively by 150 mV and the sensitivity toward free chlorine was improved by about 30% compared to that on GUITAR. With a wide detection range (0-2000 uM) and high sensitivity at a low cost, am-GUITAR is a competitive detector for free chlorine. Evaluation on further surface attachment of hydroquinone was successful, but the coverage of hydroquinone is yet to be optimized. It is noteworthy and unique that amine coverage on the basal plane GUITAR is high, and in the range of other edge rich aminated materials. There is no other basal plane carbon that has been successfully aminated. Aminated GUITAR has demonstrated its superior resistance to air and solution aging effects over other graphite electrodes. The heterogeneous electron transfer rate on am-

GUITAR is not impacted at all after being aged in air or being soaked in ferricyanide solution.

Chapter 5 . Conclusion-GUITAR, a material ready to be functionalized

5.1 Conclusion

Physical characterizations and various applications on GUITAR have been discussed in this dissertation. The characterization results indicated GUITAR (pseudo-**G**raphite from **U**nviersity of **I**daho **T**hermalyzed **A**sphalt **R**eaction) a unique hydrocarbon material. The electrochemical behavior of GUITAR was also found very outstanding, which made it possible to be functionalized in many different approaches. Below is a summary of the important findings of this dissertation:

1. GUITAR is new hydrocarbon material, whose sp^2, sp^3 and hydrogen composition has not been reported previously. Visual characteristics and micrographs indicated basal and edge morphologies shared with other graphitic materials. However, GUITAR has very different electrochemical properties in that its basal plane has fast heterogeneous electron transfer kinetics while the aqueous anodic and cathodic limits exceed other graphitic carbons by 1 V, resulting in a 3 V electrochemical window. [237,238] These features indicate a unique defective structure and many applications in sensors,[239,240] energy storage and conversion, and water purification.[241] To sum up, GUITAR is a pseudo-graphite with high sp^3 content (15% relative to total carbon) and a nano grain size between 1.5 nm to 3.6 nm.
2. The high anodic limit on basal plane of GUITAR (BP-GUITAR) allowed the quick electrochemical modifying approach. The anodization in sulfuric acid introduced the quinoid groups onto GUITAR. The quinoid group modified GUITAR is noted as q-GUITAR. The quinoid coverage on q-GUITAR basal plane was found to be the highest among the literature reported carbon-based pH electrode. This q-GUITAR electrode has multiple applications.
    - It has been utilized as a pH sensor. The square voltammetric peak potential shifts by -63.3 mV/pH over the range of pH 0 to 11. The response is robust with up to 20 voltammetric runs between pH 0-9 and 2 between pH 10-11. There is no reactivation required between voltammetric scans. Further studies

indicate that this voltammetric pH sensor is free of interference from Na^+ and K^+ and from the oxygen reduction reaction.

- It has also been utilized as a micro super capacitor electrode, which presented a high volumetric capacitance. The estimated energy and power density on a q-GUITAR based device was very competitive with the state of the art of other micro energy storage devices. This was benefitted from a much wider capacitive potential window (1.7V) as the energy density is proportional to the square of the potential window and the high volumetric capacitacne.

3. The amino radical was formed at GUITAR electrode and then attached on the electrode surface in-situ. The amine content was found to be 8% on the basal plane of GUITAR (BP-GUITAR). A similar amination approach has been reported on basal plane graphite, the N 1s XPS of which, however, only indicated ammonium ion. [242] The amine content on BP-GUITAR is surprisingly comparable to that on edge plane rich carbon materials. The amino group functionalized GUITAR (am-GUITAR) was found very resistant to the aging effect both in air and in ferricyanide solution. The aging effect slows down the heterogeneous electron transfer rate which can be determined by the peak separation of ferri/ferrocynide redox couple. GUITAR (BP-GUITAR and EP-GUITAR), glassy carbon, graphite (BPPG, EPPG) were all subject to such aging effect. Such aging has also been reported pronounced on HOPG electrode. [243]

    - The am-GUITAR can be used as a chemical sensor. The am-GUITAR was found to have a very good sensitivity to reduction of hypochlorite ion. The limits of detection (LOD) are 4.4 μM and 6.2 μM and the sensitivities are 73 μA/mM-cm^2 and 297 μA/mM-cm^2 with CA and CV respectively. The linear ranges are 0- 2000 μM for both CA and CV detection method.

4. The oxide (carbonyl, hydroxyl, and carboxyl groups) and amino groups (primary amine) introduced onto GUITAR basal plane allowed lot applications. More importantly, the carboxyl group and primary amine made possible further functionalization. The two most used reactions for this purpose are esterification and amide bond formation.[244]

- The dihydroquinone (DHQ) has been successfully attached on the am-GUITAR basal plane. This DHQ attached am-GUITAR demonstrated stable redox peaks on cyclic voltammetric curves over 5 tests (10 minutes soaking in 0.1M phosphate buffer soluition between each test)

The pursuit of materials, which can be readily modified with different functional groups, has been the focus of many researches. In search of such materials, carbon materials showed promise from the standpoints of economic feasibility, ability to be miniaturized and mechanical robustness. [245, 246, 247] Functionalization on carbon takes place at either basal sp^2 carbon or edges and defect sites. [244] On basal plane, sp^2 carbon can be functionalized from addition reactions onto the unsaturated C=C bond. [244, 245] Radical addition reaction has been successfully reported on Carbon nanotubes (CNTs), [248 249 250 251] Onion like carbon (OLC), [252] and Graphene. [253 254 255] The cycloaddition has also been reported on graphene, [244, 256] CNT,[244] and OLC. [244 257] However, due to the low chemical reactivity of the sp^2 carbon on basal plane (C_{60} however is an exception[258]), the coverage of the functionalities is usually low (below or around 1%). [244] The edge plane and defect sites are more reactive for modification and are usually rimmed with oxygen-containing functional groups.[244] Carbon nanotubes (CNTs), [245] graphene, [244, 259] and doped diamond [247] have been extensively studied to explore the possible functionalization approaches. One drawback, which is shared by the CNTs, Graphene and doped diamond, is the cost and scalability. GUITAR was synthesized from a quick and low cost method and a low cost initiator. The defective basal plane made it unique and ready to be modified with a high coverage of functional groups, which made it very competitive to other carbon materials.

5.2 Other ongoing applications of functionalized GUITAR

The possibility to be functionalized by different methods made GUITAR a very promising candidate for a lot other applications as well. Some of the other ongoing studies are listed below.

5.2.1 The q-GUITAR electrode as Chemical Oxygen Detector (COD)

The q-GUITAR has also been exploited as a COD sensor. The COD sensing performance of q-GUITAR was quantified with glucose, potassium hydrogen phthalate (KHP), lactic acid, and sodium dodecyl benzenesulfonate (SDBS). At a constant potential of 1.6 V vs. Ag/AgCl

q-GUITAR anodes have the largest linear range of 0 to 10000 ppm (as glucose) reported in literature. The limit of detection (40 ppm) and sensitivity are competitive with other electrode systems. The q-GUITAR electrode system is stable over 10 tests and can be re-treated to gain the sensitivity back.

5.2.2 Nitrogen doped chemically treated GUITAR as fuel cell electrode

Chemically modified GUITAR electrode that surpasses the performance of other graphite, carbon, and graphene electrodes in the application of the oxygen reduction reaction (ORR) electrode in fuel cells and metal/air batteries.

In fuel cells the anode consumes fuel e.g. H_2 in the following:

$$2H_2 \rightarrow 4H^+ + 4e^- \qquad E^0 = 0.0\ V$$

Other fuels are also possible including e.g. methanol and ethanol. The cathode consumes oxygen as:

$$O_2 + 4H^+ + 4e^- \rightarrow 2H_2O \qquad E^0 = 1.23\ V$$

The combination of reactions above give a theoretical 1.23 V, however fuels cells generate less than this given losses due to resistance and slow electrode kinetics. The ORR cathode requires catalysts that increase the rate of this reaction for improvement of overall fuel performance. Present designs require platinum catalysts dispersed on a high surface area carbon substrate (PtC) for this application.[260] The nitrogen doping on GUITAR demonstrated the improvement in ORR catalytic performance. The nitrogen doping shifts the ORR onset potential by +125 mV and increases the current density by greater than 35%. This is one of the highest current densities reported in literature. [261,262,263,264] The durability of the nitrogen doped GUITAR carbon black composite electrode is demonstrated in the following figure and exceeds the durability of other literature N-doped carbons. When held at -450 mV vs. Ag/AgCl an NGC composite electrode in 0.1 M KOH retains 96% of its initial performance after 92 hours of continuous used as a rotated disk electrode at 800 rpm. The commercial PtC catalyst system experienced a 22% loss under the same conditions as the NGC electrodes. Other literature reported N-doped carbon materials which experience losses of 5-20% after 1 to 50 hours.[263, 265,266]

5.3 Future works

5.3.1 Dihydroquinone attached am-GUITAR as a pH sensor

The dihydroquinone (DHQ) bonded am-GUITAR electrode demonstrated stable cyclic voltammetric (CV) curves over 5 tests (10 minutes soaking in 0.1M phosphate buffer soluition between each test). Compared to q-GUITAR electrode, the chemical environment of quinone on DHQ-am-GUITAR was expected to be less complicated. The redox peaks on CV curve is expected to be sharper, thus which leads to a better signal to background response.

5.3.2 Heavy metal detection

The q-GUITAR and am-GUITAR were expected to provide chelating sites for the heavy metal ions, such as Cd, Pb, Hg and As. Thus, a better sensitivity and selectivity toward different heavy metal ion can be expected.

5.3.3 Lithium ion Intercalation Battery (LIB) electrode

It is expected that the fast HET rate and good resistance to corrosion will aid in GUITAR's performance as an anode in the Li-ion battery (LIB). In terms of charge-discharge cycling the defect-rich BP will allow for more efficient intercalation/penetration into the bulk. Other graphitic systems are limited to intercalation through the edge planes.

5.3.4 Other attachment on q-GUITAR and am-GUITAR

The two most used reactions to extend the functionality on oxidized carbon and aminated carbon are esterification and amide bond formation. The unique defective structure on BP-GUITAR made such extention possible on both q-GUITAR and am-GUITAR. For example, the attachment of polymer and DNA onto am-GUITAR or q-GUITAR through amide bonds will allow more bio sensing applications. The attachment of porphyrins will allow the photoluminescence on GUITAR.

Reference

1 P. R. Wallace, The Band Theory of Graphite. Physical Review. 1947, 71, 622.

2 A. K. Geim; K. S. Novoselov. The rise of graphene. Nature Materials, 2007, 6, 183–191.

3 Eswaraiah, V., S. S. J. Aravind, and S. Ramaprabhu. Top down method for synthesis of highly conducting graphene by exfoliation of graphite oxide using focused solar radiation. J. Mater. Chem. 21, 2011: 6800–6803.

4 Zhi, L. and K. Mullen. A bottom-up approach from molecular nanographenes to unconventional carbon materials. J. Mater. Chem. 18, 2008: 1472–1484.

5 I. O. Gyan, H. Zhu, I. F. Cheng. Ch.18 Low-Cost and Simple Method for Graphene Synthesis. CRC Graphene Science Handbook. Chapter 18, Volume 4

6 T. E. Benavidez, R. Martinez-Duarteb and C. D. Garcia. Analytical methodologies using carbon substrates developed by pyrolysis. Analytical Methods 2016, 8, 4163–4176.

7 S. Guoab and S. Dong. Graphene nanosheet: synthesis, molecular engineering, thin film, hybrids, and energy and analytical applications. Chemical Society Review 2011, 40, 2644-2672.

8 M. Mojica, J. A. Alonso and F. Méndez, Synthesis of fullerenes. J. Phys. Org. Chem., 2013, 26, 526-539.

9 K. B. Teo, C. Singh, M. Chhowalla and W. I. Milne, Catalytic Synthesis of Carbon Nanotubes and Nanofibers, Encyclopedia of Nanoscience and Nanotechnology, 2003, vol. X, American Scientific Publisher, Stevenson, CA 91381, USA, pp. 1–22.

10 G. M. Jenkins and K. Kawamura, Structure of Glassy Carbon. Nature, 1971, 231, 175-176.

11 I. F. Cheng, Y. Xie, R. A. Gonzales, P. R. Brejna, J. P. Sundararajan, B. A. F. Kengne, D. E. Aston, D. N. McIlroy, J. D. Foutch, P. R. Griffiths. Synthesis of graphene paper from pyrolyzed asphalt. Carbon 2011, 49, 2852-2861.

12 Y. Xie, S. D. McAllister, S. A. Hyde, J. P. Sundararajan, B. A. F. Kengne, D. N. McIlroy, I. F. Cheng. Sulfur as an important co-factor in the formation of multilayer graphene in the thermolyzed asphalt reaction. Journal of Material Chemistry 2012, 22, 5723-5729.

13 I.O. Gyan, P.M. Wojcik, D.E. Aston, D.N. McIlroy, I.F. Cheng. A Study of the Electrochemical Properties of a New Graphitic Material: GUITAR, ChemElectroChem 2015, 2(5), 700-706.

14 I.O. Gyan, I.F. Cheng. Electrochemical study of biologically relevant molecules at electrodes constructed from GUITAR, a new carbon allotrope. Microchemical Journal 2015, 122, 39-44.

15 H. Kabir, I.O. Gyan, J.D. Foutch, H. Zhu, I.F. Cheng. Application of GUITAR on the negative electrode of the Vanadium redox flow battery: improved V3+/2+ heterogeneous electron transfer with reduced hydrogen gassing. Journal of Carbon Research C 2016, 2(2), 13.

16 Y. Tanaka, M. Furuta, K. Kuriyama, R. Kuwabara, Y. Katsuki, T. Kondo, A. Fujishima, K. Honda. Electrochemical properties of N-doped hydrogenated amorphous carbon films fabricated by plasma-enhanced chemical vapor deposition methods. Electrochimica Acta 2011, 56(3), 1172-1181.

17 H.B. Martin, A. Argoitia, U. Landau, A.B. Anderson, J.C. Angus. Hydrogen and oxygen evolution on Boron-Doped Diamond electrodes. Journal of the Electrochemical Society 1996, 143(6), L133-L136.

18 K.W. Hathcock, J.C. Brumfield, C.A. Goss, E.A. Irene, R.W. Murray. Incipient Electrochemical Oxidation of Highly Oriented Pyrolytic Graphite: Correlation between Surface Blistering and Electrolyte Anion Intercalation. Analytical Chemistry 1995, 67(13), 2201-2206.

19 P.E. Sharel, Y.R. Kim, D. Perry, C.L. Bentley, P.R. Unwin, Nanoscale Electrocatalysis of Hydrazine Electro-Oxidation at Blistered Graphite Electrodes. ACS Applied Materials & Interfaces 2016, 8(44), 30458-30466.

20 S. Maass, F. Finsterwalder, G. Frank, R. Hartmann, C. Merten. Carbon support oxidation in PEM fuel cell cathodes. Journal of Power Sources 2008, 176(2), 444-451.

21 C.C.Villarreal, T. Pham, P. Ramnani, A. Mulchandani. Carbon allotropes as sensors for environmental monitoring. Current Opinion in Electrochemistry 2017, 3(1), 106-113.

22 Kristin K. Cline, Mark T. McDermott, Richard L. McCreery. Anomalously Slow Electron Transfer at Ordered Graphite Electrodes: Influence of Electronic Factors and Reactive Sites. Journal of Physical Chemistry, 1994, 98, 5314-5319.

23 Richard L. McCreery, Mark T. McDermott. Comment on Electrochemical Kinetics at Ordered Graphite Electrodes. Analytical Chemistry 2012, 84, 2602-2605.

24 Xiaobo Ji, Craig E. Banks, Alison Crossley, Richard G. Compton. Oxygenated Edge Plane Sites Slow the Electron Transfer of the Ferro-/Ferricyanide Redox Couple at Graphite Electrodes. ChemPhysChem 2006, 7, 1337-1344.

25 B. K. Kwiecińska, S. Pusz. Pyrolytic carbon — Definition, classification and occurrence. International Journal of Coal Geology 2016, 163, 1–7.

26 E. Fitzer, K. H. Kochling, H. P. Boehm, H. Marsh. Recommended terminology for the description of carbon as a solid. IUPAC recommendations. Pure Appl. Chem. 1995. 67, 473–506.

27 D. N. McIlroy, D. Zhang, and Y. Kranov, M. Grant Norton. Nanosprings. Appllied Physical Letter 2001, 79, 1540-1542.

28 Daqing Zhang*, Abdullah Alkhateeb, Hongmei Han, Hasan Mahmood, and David N. McIlroy, M. Grant Norton. Silicon Carbide Nanosprings. Nano Letters, 2003, 3, 983–987

29 Kabir, H.; Gyan, I. O.; Foutch, J. D.; Zhu, H.; Cheng, I. F. Application of GUITAR on the Negative Electrode of the Vanadium Redox Flow Battery: Improved V3+/2+ Heterogeneous Electron Transfer with Reduced Hydrogen Gassing. C--Open Access Carbon Res. J. 2016, 2, 13.

30 Gyan, I. O.; Cheng, I. F. Electrochemical study of biologically relevant molecules at electrodes constructed from GUITAR, a new carbon allotrope. Microchem. J. 2015, 122, 39-44.

31 Kabir, H.; Zhu, H.; Lopez, R.; Nicholas, N. W. and Cheng, I. F. Electrochemical Determination of Chemical Oxygen Demand (COD) on Functionalized GUITAR Electrodes. Unpublished work.

32 H. Zhu, R. Lopez, H. J. Smith, N. Nicholas, P. Sankaran, D. N. McIlroy, I. F. Cheng. Chemically modified GUITAR (Graphene from the University of Idaho Thermolyzed Asphalt Reaction) as a voltammetric pH sensor. Unpublished work.

33 R. Kostić, M. Mirić∗ , T. Radić, M. Radović, R. Gajić and Z.V. Popović. Optical Characterization of Graphene and Highly Oriented Pyrolytic Graphite. Acta Physica Polonica A 2009. 116, 718-821.

34 C. A. Goss, J. C. Brumfield, E. A. Irene, R. W. Murray. Imaging the incipient electrochemical oxidation of highly oriented pyrolytic graphite. Anal. Chem. 1993, 65, 1378–1389.

35 D. C. Alsmeyer, R. L. McCreery. In situ Raman monitoring of electrochemical graphite intercalation and lattice damage in mild aqueous acids. Anal. Chem. 1992, 64, 1528–1533.

36 Alliata, R. Kçtz, O. Hass, H. Siegenthaler, In Situ AFM Study of Interlayer Spacing during Anion Intercalation into HOPG in Aqueous Electrolyte. Langmuir 1999, 15, 8483 – 8489.

37 D. Alliata, P. H•ring, O. Haas, R. Kçtz, H. Siegenthaler. Anion intercalation into highly oriented pyrolytic graphite studied by electrochemical atomic force microscopy. Electrochemical Communication 1999, 1, 5–9.

38 B. Reznik, D. Gerthsen, K. J. Huttinger. Micro- and nanostructure of the carbonmatrix of infiltrated carbon fiber felts. Carbon 2001, 39, 215–229.

39 D.A.C. Brownson, M.G. Mingot, C.E. Banks. CVD graphene electrochemistry: biologically relevant molecules. Physical Chemistry Chemical Physics 2011, 13, 20284–20288.

40 R. Hawaldar, P. Merino, M.R. Correia, I. Bdikin, J. Gracio, J. Mendez, J.A. M. Gago, M.K. Singh. Large-area high-throughput synthesis of monolayer graphene sheet by Hot Filament Thermal Chemical Vapor Deposition. Scientific Reports 2012, 2, 682.

41 R. John, A. Ashokreddy, C. Vijayan, T. Pradeep. Single- and few-layer graphene growth on stainless steel substrates by direct thermal chemical vapor deposition. Nanotechnology 2011, 22, 165701.

42 C. Casiraghi, A.C. Ferrari, J. Robertson. Raman spectroscopy of hydrogenated amorphous carbons. Physical Review B 2005, 72, 085401.

43 R. Blume, D. Rosenthal, J.P. Tessonnier, H. Li, A.K. Gericke, R. Schlogl. Characterizing Graphitic Carbon with X-ray Photoelectron Spectroscopy: A Step-by-Step Approach. ChemCatChem 2015, 7, 2871-2881.

44 W. Xie, K.M. Ng, L.T. Weng, C.M. Chan. Characterization of hydrogenated graphite powder by X-ray photoelectron spectroscopy and time-of-flight secondary ion mass spectrometry. RSC Advances 2016, 6, 80649–80654.

45 S.K. Jerng, D.S. Yu, J.H. Lee, C. Kim, S. Yoon, S.H. Chun. Graphitic carbon growth on crystalline and amorphous oxide substrates using molecular beam epitaxy. Nanoscale Research Letters 2011, 6(1), 565.

46 F. Atchison, T. Bryś, M. Daum, P. Fierlinger, A. Foelske, M. Gupta, R. Henneck, S. Heule, M. Kasprzak, K. Kirch, R. Kötz, M. Kuźniak, T. Lippert, C.F. Meyer, F. Nolting, A. Pichlmaier, D. Schneider, B. Schultrich, P. Siemroth, U. Straumann. Structural characterization of diamond-like carbon films for ultracold neutron applications. Diamond & Related Materials 2007, 16, 334–341.

47 J.C. Lascovich, R. Giorgi, S. Scaglione. Evaluation of the sp2/sp3 ratio in amorphous carbon structure by XPS and XAES. Applied Surface Science 1991, 47, 17-21.

48 R.J. Yeo. Ultrathin carbon-based overcoats for extremely high density magnetic recording. 2017, ISBN 978-981-10-4881-4.

49 A. Wollbrink, K. Volgmann, J. Koch, K. Kanthasamy, C. Tegenkamp, Y. Li, H. Richter, S. Kamnitz, F. Steinbach, A. Feldhoff, J. Caro. Amorphous, turbostratic and crystalline carbon membranes with hydrogen selectivity. Carbon 2016, 106, 93-105.

50 A. C. Ferrari and J. Robertson. Resonant Raman spectroscopy of disordered, amorphous, and diamondlike carbon. Physical Review B, 2001, 64, 075414

51 W. Jacob, and W. Möller. On the structure of thin hydrocarbon films. Appl. Phys. Lett. 1993, 63, 1771-1773.

52 C. Casiraghi, A. C. Ferrari, and J. Robertson. Raman spectroscopy of hydrogenated amorphous carbons. Physical Review B, 2005, 72, 08540

53 W. Xie, Kai Mo Ng, Lu-Tao Weng, Chi-Ming Chan. Characterization of hydrogenated graphite powder by X-ray photoelectron spectroscopy and time-of-flight secondary ion mass spectrometry. RSC Adv., 2016, 6, 80649–80654

54 S.-K. Jerng, D. S.Yu, J. H. Lee, C. Kim, S. Yoon, S.-H.Chun. Graphitic carbon growth on crystalline and amorphous oxide substrates using molecular beam epitaxy. Nanoscale Res Lett. 2011, 6, 565.

55 K. Honda, H. Naragino, Y. Shimai. Control of Electric Conductivity and Electrochemical Activity of Hydrogenated Amorphous Carbon by Incorporating Boron Atoms. Journal of The Electrochemical Society, 2014, 161, B207-B215.

56 F. Atchison, T. Bryś, M. Daum, P. Fierlinger, A. Foelske, M. Gupta, R. Henneck, S. Heule, M. Kasprzak, K. Kirch, R. Kötz, M. Kuźniak, T. Lippert, C.-F. Meyer, F. Nolting, A. Pichlmaier, D. Schneider, B. Schultrich, P. Siemroth, U. Straumann. Structural characterization of diamond-like carbon films for ultracold neutron applications. Diamond & Related Materials 2007, 16, 334–341.

57 J. C. Lascovich, R. Giorgi, S. Scaglione. Evaluation of the sp2/sp3 ratio in amorphous carbon structure by XPS and XAES. Applied Surface Science 1991, 47, 17-21.

58 R.J. Yeo. Ultrathin carbon-based overcoats for extremely high density magnetic recording. 2017, ISBN 978-981-10-4881-4

59 T.M. Manhabosco, A.P.M. Barboza, R.J.C. Batista, B.R.A. Neves, I.L. Müller. Corrosion, wear and wear–corrosion behavior of graphite-like a-C:H films deposited on bare and nitrided titanium alloy. Diamond & Related Materials 2013, 31, 58–64.

60 A.M.M. Santos, R.J.C. Batista, L.A.M. Martins, M. Ilha, M.Q. Vieira, D.R. Miquita, F.C.R. Guma, I.L. Müller, T.M. Manhabosco. Corrosion and cell viability studies of

graphite-like hydrogenated amorphous carbon films deposited on bare and nitrided titanium alloy. Corrosion Science 2014, 82, 297-303.

61 A.M. Dimiev, S. Eigler. Graphene Oxide: Fundamentals and Applications. 2016, ISBN: 978-1-119-06940-9. DOI:10.1002/9781119069447.

62 A. Ochoa, B. Valle, D.E. Resasco, J. Bilbao, A.G. Gayubo, P. Castano. Temperature Programmed Oxidation Coupled with In Situ Techniques Reveal the Nature and Location of Coke Deposited on a Ni/La2O3-αAl2O3 Catalyst in the Steam Reforming of Bio-oil. ChemCatChem 2018, 10, 2311-2321.

63 T.M. Manhabosco, A.P.M. Barboza, R.J.C. Batista, B.R.A. Neves, I.L. Müller. Corrosion, wear and wear–corrosion behavior of graphite-like a-C:H films deposited on bare and nitrided titanium alloy. Diamond & Related Materials 2013, 31, 58–64.

64 Liangliang Huang, Yuanyuan Cao, Dongfeng Diao. Nanosized graphene sheets induced high electrochemical activity in pure carbon film. Electrochimica Acta 262 (2018) 173-181.

65 A.C. Ferrari. Determination of bonding in diamond-like carbon by Raman spectroscopy. Diamond and Related Materials 2002, 11, 1053-1061.

66 Andrea Carlo Ferrari and John Robertson. Raman spectroscopy of amorphous, nanostructured, diamond-like carbon, and nanodiamond. Philosophical Transactions of the Royal Society London A 2004, 362, 2477-2512.

67 F. Tuinstra and J. L. Koening, Raman Spectrum of Graphite. J. Chem. Phys. 1970, 53, 1126-1130.

68 D. S. Knight and W. B. White. Characterization of diamond films by Raman spectroscopy. Journal of Material Research 1989, 4, 385–393.

69 M. J. Matthews, M. A. Pimenta, G. Dresselhaus, M. S. Dresselhaus and M. Endo. Origin of dispersive effects of the Raman D band in carbon materials Phys. Rev. B 1999, 59, R6585.

70 A. C. Ferrari and J. Robertson. Interpretation of Raman spectra of disordered and amorphous carbon. Physical Review B 2000, 61, 14095-14107.

71 P.M. Wojcik, N. Rajabi, H. Zhu, D. Estrada, P. Davis, K. Livingston, K.M. Yocham, T. Pandhi, I.F. Cheng, D.N. McIlroy. The negative temperature coefficient, electrical resistivity, and surface morphology of single carbon coated silica nanospring. Journal of Applied Physics 2018 (Manuscript Submitted).

72 A. Merlen, J. Buijnsters, C. Pardanaud. A Guide to and Review of the Use of Multiwavelength Raman Spectroscopy for Characterizing Defective Aromatic Carbon Solids:

from Graphene to Amorphous Carbons. Coatings, MDPI AG Multidisciplinary Digital Publishing Institute, 2017, 7 (10), 153.

73 S. Prawer, R.J. Nemanich. Raman spectroscopy of diamond and doped diamond. Philos. Trans. R. Soc. 2004, 362, 2537–2565.

74 P. H. Tan, Y.M. Deng, and Q. Zhao. Temperature-dependent Raman spectra and anomalous Raman phenomenon of highly oriented pyrolytic graphite. Phys. Rev. B 1998, 58, 5435-5439.

75 Z. Wang, X. Huang, R. Xue, and L. Chen. Dispersion effects of Raman lines in carbons. Journal of Applied Physics 1998, 84, 227-231.

76 Y. Kawashima and G. Katagiri. Fundamentals, overtones, and combinations in the Raman spectrum of graphite. Physical Review B 1995, 52, 10053.

77 L. G. Cançado, A. Jorio, M. A. Pimenta. Measuring the absolute Raman cross section of nanographites as a function of laser energy and crystallite size. Phys. Rev. B 2007, 76, 064304.

78 L. G. Cançado, K. Takai, T. Enoki, M. Endo, Y. A. Kim, H. Mizusaki, A. Jorio, L. N. Coelho, R. Magalhaes-Paniago, M. A. Pimenta. General equation for the determination of the crystallite size La of nanographite by Raman spectroscopy. Applied Physical Letter 2006, 88, 163106.

79 V. Wang, D. C. Alsmeyer, and R.L. McCreery. Raman Spectroscopy of Carbon Materials: Structural Basis of Observed Spectra. Chemistry of Material 1990, 2, 557-563.

80 M. Fang, K. Wang, H. Lu, Y. Yang and S. Nutt. Covalent polymer functionalization of graphene nanosheets and mechanical properties of composites. Journal of Material Chemistry, 2009, 19, 7098–7105

81 K. Zhang, Y.Zhang and S. Wang. Enhancing thermoelectric properties of organic composites through hierarchical nanostructures. Scientific Reports. 2013, 3, 3448.

82 Adam H. R. Palser. Interlayer interactions in graphite and carbon nanotubes. Physical Chemistry Chemical Physics, 1999, 1, 4459-4464.

83 K. Spyrou, P. Rudolf. An Introduction to Graphene: Functionalization of Graphene, 1, 2014 Wiley- VCH Verlag GmbH & Co. KGaA. ISBN: 9783527672790.

84 Y. Hishiyama and M. Nakamura. X-ray diffraction in oriented carbon films with turbostratic structure. Carbon, 1995, 33, 1399-1403.

85 H. Fujimoto. Theoretical X-ray scattering intensity of carbons with turbostratic stacking and AB staking structures. Carbon 2003, 41, 1585–1592.

86 S. S. Bukalov, Ya. V. Zubavichus, L.A. Leites, A. I. Sorokin, A. S. Kotosonov. Structural changes in industrial glassy carbon as a function of heat treatment temperature according to raman spectroscopy and x-ray diffraction data. Nanosystems: physics, chemistry, mathematics, 2014, 5, 186–191.

87 R. Bajpai, L. Rapoport, K. Amsalem, H. D. Wagner. Rapid growth of onion-like carbon nanospheres in a microwave oven. CrystEngComm, 2016, 18, 230–239

88 R. Borgohain, J. Yang, J. P. Selegue, D. Y. Kim. Controlled synthesis, efficient purification, and electrochemical characterization of arc-discharge carbon nano-onions. Carbon 2014, 66, 272-284.

89 L. M. Malard, M.A. Pimenta, G. Dresselhaus, M.S. Dresselhaus. Raman spectroscopy in graphene. Physics Reports 2009, 473, 51-87.

90 C. J. Thambiliyagodage, S. Ulrich, P.T. Araujo, M. G. Bakker. Catalytic graphitization in nanocast carbon monoliths by iron, cobalt and nickel nanoparticles. Carbon 2018, 134, 452-463.

91 A. Wollbrink, K. Volgmann, J. Koch, K. Kanthasamy, C. Tegenkamp, Y. Li, H. Richter, S. Kamnitz, F. Steinbach, A. Feldhoff, J. Caro. Amorphous, turbostratic and crystalline carbon membranes with hydrogen selectivity. Carbon 2016, 106, 93-105.

92 Z. Q. Li, C. J. Lu, Z. P. Xia, Y. Zhou, Z. Luo. X-ray diffraction patterns of graphite and turbostratic carbon. Carbon 2007, 45, 1686–1695.

93 R. Kainhofer, One way to get the Scherrer formula for size broadening, TU Vienna, http://reinhold.kainhofer.com/Physics/Scherrer/

94 A. L. Patterson. The Scherrer Formula for X-Ray Particle Size Determination, Physical Review, 1939, 56, 978-982.

95 B. Andonovic, M. Temkov, A. Ademi, A. Petrovski, A. Grozdanov, P. Paunović, A. Dimitrov. Laue functions model vs scherrer equation in determination of graphene layers number on the ground of xrd data. Journal of Chemical Technology and Metallurgy 2014, 49, 545-550.

96 T. Ida. Chapter 6. Diffraction from small crystallites. Crystal Structure Analysis. 2015. http://www.crl.nitech.ac.jp/~ida/education/CrystalStructureAnalysis/6/6e.pdf

97 Cheng, I. F.; Xie, Y.; Gonzales, R. A.; Brejna, P. R.; Sundararajan, J. P.; Kengne, B. A. F.; Aston, D. E.; McIlroy, D. N.; Foutch, J. D.; Griffiths, P. R. Synthesis of graphene paper from pyrolyzed asphalt. Carbon 2011, 49, 2852-2861.

98 Xie, Y.; McAllister, S. D.; Hyde, S. A.; Sundararajan, J. P.; Kengne, B. A. F.; McIlroy, D. N.; Chen, I. F. Sulfur as an important co-factor in the formation of multilayer graphene in the thermolyzed asphalt reaction. J. Mater. Chem. 2012, 22, 5723-5729.

99 Gyan, I. O.; Zhu, H.; Cheng, I. F. Ch.18 Low-Cost and Simple Method for Graphene Synthesis. CRC Graphene Science Handbook. Chapter 18, Volume 4

100 Gyan, I. O.; Wojcik P. M.; Aston D. E.; McIlroy D. N.; Cheng I. F. A Study of the Electrochemical Properties of a New Graphitic Material: GUITAR . ChemElectroChem 2015; 2; 700-706.

101 Cheng, I. F.; Xie, Y.; Gyan, I. O.; Nicholas, N. R. Highest Measured Anodic Stability in Aqueous Solutions: Graphenic Electrodes from the Thermolyzed Asphalt Reaction. RSC Adv. 2013, 3, 2379-2384.

102 Gyan, I. O.; Cheng, I. F. Electrochemical study of biologically relevant molecules at electrodes constructed from GUITAR, a new carbon allotrope. Microchem. J. 2015, 122, 39-44.

103 Kabir, H.; Zhu, H.; Lopez, R.; Nicholas, N. W. and Cheng, I. F. Electrochemical Determination of Chemical Oxygen Demand (COD) on Functionalized GUITAR Electrodes. Unpublished work.

104 Kabir, H.; Gyan, I. O.; Foutch, J. D.; Zhu, H.; Cheng, I. F. Application of GUITAR on the Negative Electrode of the Vanadium Redox Flow Battery: Improved V3+/2+ Heterogeneous Electron Transfer with Reduced Hydrogen Gassing. C--Open Access Carbon Res. J. 2016, 2, 13.

105 Bian, S. W.; Mudunkotuwa, I. A.; Rupasinghe, T.; Grassian, V. H. Aggregation and Dissolution of 4 nm ZnO Nanoparticles in Aqueous Environments: Influence of pH, Ionic Strength, Size, and Adsorption of Humic Acid. Langmuir 2011, 27, 6059–6068.

106 Gillies R. J.; Raghunand, N.; Garcia-Martin M. L.; Gatenby, R. A. pH imaging. A review of pH measurement methods and applications in cancers . IEEE Eng. Med. Biol. Mag. 2004, 23, 57–64.

107 Kurkdjian, A.; Guern, Intracellular pH: measurement and importance in cell activity. J. Annu. Rev. Plant Biol. 1989, 40, 271–303.

108 Slonczewski, J. L.; Fujisawa, M.; Dopson, M.; Krulwich, T. A. Cytoplasmic pH measurement and homeostasis in bacteria and archaea. Adv. Microb. Physiol. 2009, 55, 1–79.

109 Harter, R.D. Effect of soil pH on adsorption of lead, copper zinc, and nickel. Soil Sci. Soc. Am. J. 1982, 47, 47–51.

110 Boyes, W.; Instrumentation Reference Book; Butterworth-Heinemann: Boston, 2010, 374−395.

111 Pungor, E.; Toth, K. Ion-selective membrane electrodes. A review. Analyst 1970, 95, 625−648.

112 Michalak, M.; Kurel, M.; Jedraszko, J.; Toczydlowska, D.; Wittstock, G.; Opallo, M.; Nogala, W. Voltammetric pH Nanosensor. Anal. Chem. 2015, 87, 11641−11645.

113 Lu, M.; Compton, R. G. Voltammetric pH sensor based on an edge plane pyrolytic graphite electrode. Analyst 2014, 139, 2397-2403.

114 Salvo, P.; Melai, B.; Calisi, N.; Paoletti, C.; Bellagambi, F.; Kirchhain, A.; Trivella, M. G.; Fuoco, R.; Francesco, F. D. Review: Graphene-based devices for measuring pH. Sens. Actuators, B 2017, 256, 976-991

115 Korostynska, O.; Arshak, K.; Gill, E.; Arshak, A. Review Paper: Materials and Techniques for In Vivo pH Monitoring. IEEE Sens. J. 2008, 8, 20-28.

116 Zhou, J.; Zhang, L.; Tian, Y. Micro Electrochemical pH Sensor Applicable for Real-Time Ratiometric Monitoring of pH Values in Rat Brains. Anal. Chem. 2016, 88, 2113−2118.

117 Kahlert, H. Functionalized carbon electrodes for pH determination. J. Solid State Electrochem. 2008, 12, 1255-1266.

118 Ang, P. K.; Chen, W.; Wee, A.T.; Loh, K.P. Solution-gated epitaxial graphene as pH sensor. J. Am. Chem. Soc. 2008, 130, 14392–14393.

119 Paek, K.; Yang, H.; Lee, J.; Park, J.; Kim, B. J. Efficient colorimetric pH sensor based on responsive polymer—quantum dot integrated graphene oxide. ACS Nano 2014, 8, 2848–2856.

120 Kimmel, D. W.; LeBalnc, G.; Meschievitz, M. E.; Cliffel, D. E. Electrochemical Sensors and Biosensors. Anal. Chem. 2012, 84, 685-707.

121 Leventis, H. C.; Streeter, I.; Wildgoose, G. G.; Lawrence, N. S.; Jiang, L.; Jones, T. G. J.; Compton, R. G. Derivatised carbon powder electrodes: reagentless pH sensors. Talanta 2004, 63, 1039−1051.

122 Lu, M.; Compton, R. G. Voltammetric pH sensing using carbon electrodes: glassy carbon behaves similarly to EPPG. Analyst 2014, 139, 4599-4605.

123 Ayres, Z. J.; Borrill, A. J.; Newland, J. C.; Newton, M. E.; Macpherson, J. V. Controlled sp2 Functionalization of Boron Doped Diamond as a Route for the Fabrication of Robust and Nernstian pH Electrodes. Anal. Chem. 2016, 88, 974−980.

124 Britton, H. T. S.; Robinson, R. A. Universal buffer solutions and the dissociation constant of veronal. J. Chem. Soc. 1931, 0, 1456-1462.

125 Rojo, A.; Rosenstratten, A.; Anjo, D. Characterization of a Conductive Carbon Film Electrode for Voltammetry. Anal. Chem. 1986, 58, 2988-2991.

126 Kepley, L. J.; Bard, A. J. Ellipsometric, Electrochemical, and Elemental Characterization of the Surface Phase Produced on Glassy Carbon Electrodes by Electrochemical Activation. Anal. Chem. 1988, 60, 1459-1467.

127 Cabanis, G. E.; Diamantis, A. A.; Murphy Jr., W. R.; Linton, R. W.; Meyer, T. J. Electrocatalysis of Proton-Coupled Electron-Transfer Reactions at Glassy Carbon Electrodes. J. Am. Chem. Soc. 1985, 107, 1845-1853.

128 Makos, M. A.; Omiatek, D. M.; Ewing, A. G.; Heien, M. L. Development and Characterization of a Voltammetric Carbon-Fiber Microelectrode pH Sensor. Langmuir 2010, 26, 10386–10391

129 Anderson, A.; Phair, J.; Benson, J.; Meenan, B.; Davis, J. Investigating the use of endogenous quinoid moieties on carbon fibre as means of developing micro pH sensors. Mater. Sci. Eng. C. 2014, 43, 533-537.

130 Galdino, F. E.; Smith, J. P.; Kwamou, S. I.; Kampouris, D. K.; Iniesta, J.; Smith, G. C.; Bonacin, J. A.; Banks, C. E. Graphite Screen-Printed Electrodes Applied for the Accurate and Reagentless Sensing of pH. Anal. Chem. 2015, 87, 11666−11672.

131 Parvez,; Li, K. R.; Puniredd, S. R.; Hernandez, Y.; Hinkel, F.; Wang, S.; Feng, X.; Müllen, K. Electrochemically Exfoliated Graphene as Solution-Processable, Highly Conductive Electrodes for Organic Electronics. ACS Nano 2013, 7, 3598–3606.

132 Parvez, K.; Wu, Z. S.; Li, R.; Liu, X.; Graf, R.; Feng, X.; Müllen, K. Exfoliation of Graphite into Graphene in Aqueous Solutions of Inorganic Salts. J. Am. Chem. Soc. 2014, 136, 6083−6091.

133 Cao, J.; He, P.; Mohammed, M. A.; Zhao, X.; Young, R. J.; Derby, B.; Kinloch, I. A.; Dryfe, R. A. W. Two-Step Electrochemical Intercalation and Oxidation of Graphite for the Mass Production of Graphene Oxide. J. Am. Chem. Soc. 2017, 139, 17446−17456.

134 Osteryoung, J. G.; Osteryoung, R. A. Square wave voltammetry. Anal. Chem. 1985, 57, 101A-110A.

135 Phair, J.; Newton, L.; McCormac, C.; Cardosi, M. F.; Leslie, R.; Davis, A disposable sensor for point of care wound pH monitoring. J. Analyst 2011, 136, 4692-4695.

136 Beilby, A. L.; Sasaki,T. A.; Stem, H. M. Electrochemical Pretreatment of Carbon Electrodes as a Function of Potential, pH, and Time. Anal. Chem. 1995, 67, 976-980.

137 Dole, M. The Theory of the Glass Electrode. J. Am. Chem. Soc. 1931, 53, 4260–4280.

138 Batchelor-McAuley, C.; Li, Q.; Dapin, S. M.; Compton, R. G. Voltammetric Characterization of DNA Intercalators across the Full pH Range: Anthraquinone-2,6-disulfonate and Anthraquinone-2-sulfonate. J. Phys. Chem. B 2010, 114, 4094-4100.

139 Tsionsky, M.; Gun, G.; Glezer, V.; Lev, O. Sol-Gel-Derived Ceramic-Carbon Composite Electrodes: Introduction and Scope of Applications . Anal. Chem. 1994, 66, 1747-1753.

140 Paixão, T. R.L.C.; Kosminsky, L.; Bertotti, M. Use of electrochemically pretreated glassy carbon electrodes as pH sensors in potentiometric titrations. Sens. Actuators B 2002, 87, 41–46.

141 https://davemcilroy.wordpress.com/guitar-nanosprings/

142 Sigma-Aldrich Labware notes: Checking pH Electrode Functionality.

143 Wildgoose, G. G.; Leventis, H. C.; Streeter, I.; Lawrence, N. S.; Wilkins, S. J.; Jiang, L.; Jones, T. G. J.; Compton, R. G. Abrasively Immobilised Multiwalled Carbon Nanotube Agglomerates: A Novel Electrode Material Approach for the Analytical Sensing of pH. ChemPhysChem 2004, 5, 669- 677.

144 Dai, C.; Chan, C. W. I.; Barrow, W.; Smith, A.; Song, P.; Potier, F.; Wadhawan, J. D.; Fisher, A. C.; Lawrence, N. S. A Route to Unbuffered pH Monitoring: A Novel Electrochemical Approach. Electrochim. Acta 2016, 190, 879–886.

145 Dai, C.; P. Song; Wadhawan, J. D.; Fisher, A. C.; Lawrence, N. S. Screen Printed Alizarin-Based Carbon Electrodes: Monitoring pH in Unbuffered Media. Electroanalysis 2015, 27, 917– 923.

146 P. Huang, C. Lethien, S. Pinaud, K. Brousse, R. Laloo, V. Turq, M. Respaud, A. Demortiere, B. Daffos, P. L. Taberna, B. Chaudret, Y. Gogotsi and P. Simon, On-chip and freestanding elastic carbon films for micro-supercapacitors. Science, 2016, 351, 691–695.

147 W. Gao, N. Singh, L. Song, Z. Liu, A. L. Reddy, L. Ci, R. Vajtai, Q. Zhang, B. Wei and P. M. Ajayan, Direct laser writing of micro-supercapacitors on hydrated graphite oxide films. Nat. Nanotechnol., 2011, 6, 496–500.

148 M. F. El-Kady and R. B. Kaner, Scalable fabrication of high-power graphene micro-supercapacitors for flexible and on-chip energy storage. Nat. Commun., 2013, 4, 1475.

149 D. Pech, M. Brunet, H. Durou, P. Huang, V. Mochalin, Y. Gogotsi, P.-L. Taberna and P. Simon. Ultrahigh-power micrometre-sized supercapacitors based on onion-like carbon. Nat. Nanotechnol., 2010, 5, 651–654.

150 D. Pech, M. Brunet, P.-L. Taberna, P. Simon, N. Fabre, F. Mesnilgrente, V. Cone´de´ra and H. Durou, Elaboration of a microstructured inkjet-printed carbon electrochemical capacitor. J. Power Sources, 2010, 195, 1266–1269.

151 H. Ben, M. Julian, W. Shuang, I. Jung Bin, C. Carlo, P. Dimos, P. G. Costas and M. Roya, Highly flexible, all solid-state micro-supercapacitors from vertically aligned carbon nanotubes. Nanotechnology, 2014, 25, 055401.

152 S.-K. Kim, H.-J. Koo, A. Lee and P. V. Braun, Selective wetting-induced micro-electrode patterning for flexible micro-supercapacitors. Adv. Mater., 2014, 26, 5108–5112.

153 M. Beidaghi and C. Wang, Micro- Supercapacitors Based on Interdigital Electrodes of Reduced Graphene Oxide and Carbon Nanotube Composites with Ultrahigh Power Handling Performance. Adv. Funct. Mater., 2012, 22, 4501–4510.

154 B. Song, L. Li, Z. Lin, Z.-K. Wu, K.-S. Moon and C.-P. Wong, Water-dispersible graphene/polyaniline composites for flexible micro-supercapacitors with high energy densities. Nano Energy, 2015, 16, 470–478.

155 J. Chmiola, C. Largeot, P.-L. Taberna, P. Simon and Y. Gogotsi, Monolithic carbide-derived carbon films for micro-supercapacitors. Science, 2010, 328, 480–483.

156 P. Huang, M. Heon, D. Pech, M.Brunet, P.-L. Taberna, Y. Gogotsi, S. Lofland, J. D. Hettinger, P. Simon. Micro-supercapacitors from carbide derived carbon (CDC) films on silicon chips. Journal of Power Sources, 2013, 225, 240-244.

157 J. Lin, C. Zhang, Z. Yan, Y. Zhu, Z. Peng, R. H. Hauge,D. Natelson and J. M. Tour, 3-Dimensional graphene carbon nanotube carpet-based microsupercapacitors with high electrochemical performance. Nano Lett., 2013, 13, 72–78.

158 M. El-Kady, V. Strong, S. Dubin and R. Kaner. Laser scribing of high-performance and flexible graphene-based electrochemical capacitors. Science, 2012, 1326, 1326–1330.

159 I. F. Cheng, Y. Xie, R. A. Gonzales, P. R. Brejna, J. P. Sundararajan, B. A. F. Kengne, A. E., Aston, D. N., McIlroy, J. D., Foutch, P. R., Griffiths. Synthesis of graphene paper from pyrolyzed asphalt. Carbon 2011, 49, 2852-2861.

160 Y. Xie, S. D. McAllister, S. A. Hyde, J. P. Sundararajan, B. A. F. Kengne, D. N. McIlroy, I. F. Cheng. Sulfur as an important co-factor in the formation of multilayer graphene in the thermolyzed asphalt reaction. J. Mater. Chem. 2012, 22, 5723-5729.

161 I. O. Gyan, H. Zhu, I. F. Cheng. Ch.18 Low-Cost and Simple Method for Graphene Synthesis. CRC Graphene Science Handbook. Chapter 18, Volume 4

162 I. O. Gyan, P. M. Wojcik, D. E. Aston, D. N. McIlroy, I. F. Cheng. A Study of the Electrochemical Properties of a New Graphitic Material: GUITAR . ChemElectroChem 2015; 2; 700-706.

163 I. F. Cheng, Y. Xie, I. O. Gyan, N. R. Nicholas. Highest Measured Anodic Stability in Aqueous Solutions: Graphenic Electrodes from the Thermolyzed Asphalt Reaction. RSC Adv. 2013, 3, 2379-2384.

164 P. Khanra, T. Kuila, S. H. Bae, N. H.Kimb and J. H. Lee. Electrochemically exfoliated graphene using 9-anthracene carboxylic acid for supercapacitor application. J. Mater. Chem., 2012, 22, 24403-24410.

165 A. Ambrosi and M. Pumera. Electrochemically Exfoliated Graphene and Graphene Oxide for Energy Storage and Electrochemistry Applications. Chem. Eur. J. 2016, 22, 153 – 159.

166 I. O. Gyan, P. M. Wojcik, D. E. Aston, D. N. McIlroy, I. F. Cheng. A Study of the Electrochemical Properties of a New Graphitic Material: GUITAR . ChemElectroChem 2015, 2, 700-706.

167 A. Rojo, A. Rosenstratten, and D. Anjo. Characterization of a Conductive Carbon Film Electrode for Voltammetry. Anal. Chem. 1986, 58, 2988-2991.

168 L. J. Kepley, and A. J. Bard. Ellipsometric, Electrochemical, and Elemental Characterization of the Surface Phase Produced on Glassy Carbon Electrodes by Electrochemical Activation. Anal. Chem. 1988, 60, 1459-1467.

169 C. E. Cabanis, A. A. Diamantis, W. R. Murphy Jr., R. W. Linton, and T. J. Meyer. Electrocatalysis of Proton-Coupled Electron-Transfer Reactions at Glassy Carbon Electrodes. J. Am. Chem. Soc. 1985, 107, 1845-1853.

170 H. Zhu, R. Lopez, H. Joel Smith, N. Nicholas, P. Sankaran, D. N. McIlroy, and I. F. Cheng. Chemically modified GUITAR (Graphenic carbon from the University of Idaho Thermolyzed Asphalt Reaction) as a voltammetric pH sensor. Manuscript to be submitted.

171 G.W. Bishop, B.K. Ahiadu, J. L. Smith, J.D. Patterson. Use of Redox Probes for Characterization of Layer-by-Layer Gold Nanoparticle-Modified Screen-Printed Carbon Electrodes. J. of The Electrochemical Society 2017, 164 (2), B23-B28.

172 A. N. Patel, M. G. Collignon, M. A. O'Connell, W. O. Y. Hung, K. McKelvey, J. V. Macpherson, and P. R. Unwin. A New View of Electrochemistry at Highly Oriented Pyrolytic Graphite. J Am. Chem. Soc. 2012, 134, 20117−20130

173 X. Ji, C. E. Banks, A. Crossley, and R. G.Compton. Oxygenated edge plane sites slow the electron transfer of the ferro-/ferricyanide redox couple at graphite electrodes. ChemPhysChem 2006, 7, 1337−1344.

174 Y. Gogotsi, P. Simon, True Performance Metrics in Electrochemical Energy Storage. Science, 2011, 334, 917–918.

175 T. M. Dinh, K. Armstrong, D. Guay, and D. Pech. High-resolution on-chip supercapacitors with ultra-high scan rate ability. J. Mater. Chem. A 2014, 2, 7170–7174.

176 J. Lin, Z. Peng, Y. Liu, F. Ruiz-Zepeda, R. Ye, E. L. G. Samuel, M. Jose Yacaman, B. I. Yakobson and J. M. Tour. Laser-induced porous graphene films from commercial polymers. Nat. Commun. 2014, 5, 5714.

177 M.D. Stoller and R.S. Ruoff. Best practice methods for determining an electrode material's performance for ultracapacitors. Energy Environ. Sci., 2010, 3, 1294–1301.

178 W. Chen, C. Xia, R.B. Rakhi, H.N. Alshareef. A general approach toward enhancement of pseudocapacitive performance of conducting polymers by redox-active electrolytes. Journal of Power Sources 2014, 267, 521-526.

179 P. Yuan, N. Zhang, D. Zhang, T. Liu, L. Chen, R. Ma, G. Qiu, X. Liu. Controllable synthesis of layered Co–Ni hydroxide hierarchical structures for high-performance hybrid supercapacitors. Journal of Physics and Chemistry of Solids 2016, 88, 8–13.

180 Y. Zou, I.A. Kinloch and R. A. W. Dryfe. Nitrogen-doped and crumpled graphene sheets with improved supercapacitance. J. Mater. Chem. A, 2014, 2, 19495–19499

181 Y. Q. Jiang, Q. Zhou and L. Lin, Planar MEMS supercapacitor using carbon nanotube forests. IEEE 22nd Int. Conf. Micro Electro Mech. Syst., 2009, 587–590.

182 J. J. Yoo, K. Balakrishnan, J. Huang, V. Meunier, B. G. Sumpter, A. Srivastava, M. Conway, A. L. M. Reddy, J. Yu, R. Vajtai and P. M. Ajayan, Ultrathin Planar Graphene Supercapacitors. Nano Lett., 2011, 11, 1423–1427.

183 Y.-Y.Peng, B.Akuzum, N. Kurra, M.-Q. Zhao, M. Alhabeb, B. Anasori, E. Caglan Kumbur, H.N. Alshareef, M.-D.Ger and Y. Gogotsi. All-MXene (2D titanium carbide) solid-state microsupercapacitors for on-chip energy storage. Energy Environ. Sci., 2016, 9, 2847-2854.

184 Z. S. Wu, K. Parvez, X. Feng and K. Müllen, Graphene-based in-plane micro-supercapacitors with high power and energy densities. Nat. Commun., 2013, 4, 2487.

185 Z. S. Wu, K. Parvez, X. Feng and K. Müllen, Photolithographic fabrication of high-performance all-solid-state graphene-based planar micro-supercapacitors with different interdigital fingers. J. Mater. Chem. A, 2014, 2, 8288–8293.

186 N. Kurra, Q. Jiang and H. N. Alshareef, A general strategy for the fabrication of high performance microsupercapacitors. Nano Energy, 2015, 16, 1–9.

187 N. Kurra, N. A. Alhebshi and H. N. Alshareef, Microfabricated Pseudocapacitors Using Ni(OH)2 Electrodes Exhibit Remarkable Volumetric Capacitance and Energy Density. Adv. Energy Mater., 2015, 5, 1401303.

188 W. Si, C. Yan, Y. Chen, S. Oswald, L. Han and O. G. Schmidt. On chip, all solid-state and flexible micro-supercapacitors with high performance based on MnOx/Au multilayers. Energy Environ. Sci., 2013, 6, 3218–3223.

189 Q. Jiang, N. Kurra and H. N. Alshareef, Marker Pen Lithography for Flexible and Curvilinear On-Chip Energy Storage. Adv. Funct. Mater.,2015, 25, 4976–4984.

190 K. Wang, H. Wu, Y. Meng and Z. Wei, Conducting polymer nanowire arrays for high performance supercapacitors. Small, 2014, 10, 14–31.

191 C. Zhang, J. Xiao, L. Qian, S. Yuan, S. Wang, and P. Lei. Planar integration of flexible microsupercapacitors with ultrafast charge and discharge based on interdigital nanoporous gold electrodes on a chip. J. Mater. Chem. A, 2016, 4, 9502-9510.

192 I. F. Cheng, Y. Xie, R. A. Gonzales, P. R. Brejna, J. Pricilla Sundararajan, B. A. Fouetio Kengne, D. E. Aston, D.N. McIlroy, J. D. Foutch, P. R. Griffiths. Synthesis of graphene paper from pyrolyzed asphalt. Carbon 2011, 49, 2852-2861.

193 Y.Xie,; McAllister, S. D.; Hyde, S. A.; Sundararajan, J. P.; Kengne, B. A. F.; McIlroy, D. N.; Chen, I. F. Sulfur as an important co-factor in the formation of multilayer graphene in the thermolyzed asphalt reaction. J. Mater. Chem. 2012, 22, 5723-5729.

194 Gyan, I. O.; Zhu, H.; Cheng, I. F. Ch.18 Low-Cost and Simple Method for Graphene Synthesis. CRC Graphene Science Handbook. Chapter 18, Volume 4

195 Gyan, I. O.; Wojcik P. M.; Aston D. E.; McIlroy D. N.; Cheng I. F. A Study of the Electrochemical Properties of a New Graphitic Material: GUITAR . ChemElectroChem 2015; 2; 700-706.

196 Cheng, I. F.; Xie, Y.; Gyan, I. O.; Nicholas, N. R. Highest Measured Anodic Stability in Aqueous Solutions: Graphenic Electrodes from the Thermolyzed Asphalt Reaction. RSC Adv. 2013, 3, 2379-2384.

197 Humayun Kabir, Haoyu Zhu, O. Charles Nwamba, Jeremy May, Elena Echeverria, Thomas Williams, Yuwei Kan, Abraham Clearfield, David N. McIlroy, I. Francis Cheng. An sp2-Carbon Corrosion Resistance Electrode: Graphite from the University of Idaho Thermolyzed Asphalt Reaction (GUITAR). Manuscript in preparation.

198 Haoyu Zhu, Ricardo Lopez, Hailey Joel Smith, Nolan Nicholas, Prasanna Sankaran, David N. McIlroy, I. Francis Cheng. Chemically modified GUITAR (Graphenic carbon from the University of Idaho Thermolyzed Asphalt Reaction) as a voltammetric pH sensor. Manuscript to be submitted.

199 Ashraful Alam, Chaoying Wan, Tony McNally. Surface amination of carbon nanoparticles for modification of epoxy resins: plasma-treatment vs. wet-chemistry approach. European Polymer Journal 2017, 87, 422–448

200 Xiuyun Wang, Tingting Cao, Qinglu Zuo, Shuo Wu, Shunichi Uchiyama and Hiroaki Matsuura. Sensitive nitrite detection using a simple electrochemically aminated glassy carbon electrode. Anal. Methods, 2016, 8, 3445–3449

201 Bin Wang, Bin Luo, Minghui Liang, Ali Wang, Jie Wang, Yan Fang, Yanhong Chang and Linjie Zhi. Chemical amination of graphene oxides and their extraordinary properties in the detection of lead ions. Nanoscale, 2011, 3, 5059-5066

202 Si Pan, M. Jamal Deen, and Raja Ghosh. Low-Cost Graphite-Based Free Chlorine Sensor. Anal. Chem. 2015, 87, 10734−10737.

203 Cheng-Meng Chen,abf Qiang Zhang,bc Xiao-Chen Zhao,bef Bingsen Zhang,bd Qing-Qiang Kong,a Mang-Guo Yang,a Quan-Hong Yang,a Mao-Zhang Wang,a Yong-Gang Yang,a Robert Schl€oglb and Dang Sheng Su. Hierarchically aminated graphene honeycombs for electrochemical capacitive energy storage. J. Mater. Chem., 2012, 22, 14076–14084

204 Ahmed G. El-Deen, Remko M. Boom, Hak Yong Kim, Hongwei Duan, Mary B. Chan-Park, and Jae-Hwan Choi. Flexible 3d nanoporous graphene for desalination and biodecontamination of brackish water via asymmetric capacitive deionization. ACS Appl. Mater. Interfaces 2016, 8, 25313−25325

205 Aiko Kanazawa, Takuro Daisaku, Takeyoshi Okajima, Shunichi Uchiyama, Susumu Kawauchi, and Takeo Ohsaka. Characterization by Electrochemical and X‑ray Photoelectron Spectroscopic Measurements and Quantum Chemical Calculations of N‑Containing Functional Groups Introduced onto Glassy Carbon Electrode Surfaces by Electrooxidation of a Carbamate Salt in Aqueous Solutions. Langmuir 2014, 30, 5297−5305

206 Fan L., Zhang Q., Wang K., Li F. and Niu L. Ferrocene functionalized graphene: preparation, characterization and efficient electron transfer toward sensors of H2O2. J Mater. Chem., 2012, 22, 6165-6170.

207 T. Ramanathan, F. T. Fisher, R. S. Ruoff, and L. C. Brinson. Amino-Functionalized Carbon Nanotubes for Binding to Polymers and Biological Systems. Chem. Mater. 2005, 17, 1290-1295

208 T. Ramanathan, H. Liu, L. C. Brinson. Functionalized SWNT/Polymer Nanocomposites for Dramatic Property Improvement. Journal of Polymer Science: Part B: Polymer Physics, 2005, 43, 2269–2279.

209 Héctor Aguilar-Bolados , Daniela Vargas-Astudillo, Mehrdad Yazdani-Pedram, Gabriela Acosta-Villavicencio, Pablo Fuentealba, Ahirton Contreras-Cid, Raquel Verdejo, and Miguel A. López-Manchado. Facile and Scalable One-Step Method for Amination of Graphene Using Leuckart Reaction. Chem. Mater. 2017, 29, 6698−6705.

210 Yizhe Hu, Jianfeng Shen, Na Li, Min Shi, Hongwei Ma, Bo Yan, Wenbin Wang, Weishi Huang, Mingxin Ye. Amino-Functionalization of Graphene Sheets and the Fabrication of Their Nanocomposites. Polymer Composites—-2010

211 Shunichi Uchiyama, Hiroaki Watanabe, Haruhito Yamazaki, Aiko Kanazawa, Hiroshi Hamana and Yoshio Okabe. Journal of the Electrochemical Society 2007, 154, F31-F35.

212 Gregory G. Wildgoose, Adam T. Masheter, Alison Crossley, John H. Jones, Richard G. Compton. Electrolysis of Ammonium Carbamate: A Voltammetric and Xray Photoelectron Spectroscopic Investigation into the Modification of Carbon Electrodes. Int. J. Electrochem. Sci., 2007, 2, 809 – 819.

213 B. Wang, J. Anzai. A Facile Electrochemical Detection of Hypochlorite Ion based on Ferrocene Compounds. Int. J. Electrochem. Sci. 2015, 10, 3260-3268.

214 Randall S. Deinhammer, Mankit Ho, James W. Anderegg, and Marc D. Porter. Electrochemical Oxidation of Amine-Containing Compounds: A Route to the Surface Modification of Glassy Carbon Electrodes. Langmuir 1994,10, 1306-1313

215 Allison J. Downard. Electrochemically assisted covalent modification of carbon electrodes. Elecroanalysis 2000, 12, 1085-1095

216 http://www.uksaf.org/

217 http://srdata.nist.gov/xps/

218 C. M. Pharr and P. R. Griffiths. Step-Scan FT-IR Spectroelectrochemical Analysis of Surface and Solution Species in the Ferricyanide/Ferrocya2nide Redox Couple. Anal. Chem. 1997, 69, 4665-4672

219 K. K. Cline, M. T. McDermott, R. L. McCreery, Anomalously Slow Electron Transfer at Ordered Graphite Electrodes: Influence of Electronic Factors and Reactive Sites. J. Phys. Chem. 1994, 98, 5314.

220 Anisha N. Patel, Manon Guille Collignon, Michael A. O'Connell, Wendy O. Y. Hung, Kim McKelvey, Julie V. Macpherson, and Patrick R. Unwin. A New View of Electrochemistry at Highly Oriented Pyrolytic Graphite. J. Am. Chem. Soc. 2012, 134, 20117−20130.

221 Huang, W.; McCreery R. Electron transfer kinetics of Fe(CN)63-/4- on laser-activated and CN−-modified Pt electrodes. J. Electroanal. Chem. 1992, 326, 1.

222 Kunimatsu, K.; Shigematsu, Y.; Uosaki, K.; Kitz, H. Study of the Fe(CN)3−6/Fe(CN)4−6 redox system on Pt by EMIRS: Part I. Infrared spectra of the intermediates in the charge transfer. J. Electroanal. Chem. 1989, 262, 195

223 Wieckowski, A.; Szklarczyk M. The state of the polycrystalline platinum electrode during the heterogeneous electron-transfer reaction: Fe(CN)63−+eFe(CN)64− . J. Electroanal. Chem. 1982, 142, 157

224 Campo, F. F. D.; Ordeig, O.; Muñoz, F. J. Improved free chlorine amperometric sensor chip for drinking water applications. Analytica Chimica Acta 2005, 554, 98–104.

225 Monllau, R. O.; Orozco, J.; Sánchez, C. F.; Baeza, M.; Bartrolí, J.; Jorquera, C. J.; Céspedes, F. Flow injection analysis system based on amperometric thin-film transducers for free chlorine detection in swimming pool waters. Talanta 2009, 77(5), 1739−1744.

226 Tsaousis, A. N.; Huber, C. O. Flow-injection amperometric determination of chlorine at a gold electrode. Analytica Chimica Acta 1985, 178, 319-323.

227 Awad, M. I.; Sata, S.; Ohsaka, T. Simultaneous Electroanalysis of Hypochlorite and H2O2: Use of I−/I2 as a Probing Potential Buffer. Electroanalysis 2005, 17(9), 769–775.

228 Ordeig, O.; Mas, R.; Gonzalo, J.; Campo, F.J.D.; Muñoz, F. J. ontinuous Detection of Hypochlorous Acid/Hypochlorite for Water Quality Monitoring and Control. Electroanalysis 2005, 17(18), 1641-1648.

229 Watanabe, Hiroaki; Uchiyama, Shunichi. Hypochlorite Sensor Using Amino-Group-Modified Carbon Electrode. Bunseki Kagaku 2007, 56(6), 433-437.

230 Lee, W. H.; Ma, X. M. Austin. Development of a Gold Microelectrode and its Application for Evaluating Free Chlorine Consumption by Metal Surfaces. J. Biosens & Bioelectron. 2015, 1(2), 1006.

231 Humayun Kabir, Peng Yi Ma, Nicholas Renn and I. Francis Cheng. Amperometric Determination of Free Chlorine on GUITAR Electrodes. Manuscript to be submitted.

232 Senthilkumar, Krishnan; Zen, Jyh-Myng. Free chlorine detection based on EC' mechanism at an electroactive polymelamine-modified electrode. Electrochemistry Communications 2014, 46, 87–90.

233 Tsai, Tsung-Hsuan; Lin, T. Kuo-Chiang; Chen, Shen-Ming. Electrochemical Synthesis of Poly(3,4-ethylenedioxythiophene) and Gold Nanocomposite and Its Application for Hypochlorite Sensor. Int. J. Electrochem. Sci. 2011, 6, 2672-2687.

234 Murata, M.; Ivandini, T. A.; Shibata, M.; Nomura, S.; Fujishima, A.; Einaga, Y. Electrochemical detection of free chlorine at highly boron-doped diamond electrodes. J. of Electroanalytical Chemistry 2008, 612, 29–36.

235 Munoz, J.; Cespedes F.; Baeza, M. Modified multiwalled carbon nanotube/epoxy amperometric nanocomposite sensors with CuO nanoparticles for electrocatalytic detection of free chlorine. Microchemical Journal 2015, 122, 189–196.

236 Thiagarajan, S.; Wu, Z. Y.; Chen, S. M. Amperometric determination of sodium hypochlorite at poly MnTAPP-nano Au film modified electrode. Journal of Electroanalytical Chemistry 2011, 661, 322–328.

237 Gyan, I. O.; Wojcik P. M.; Aston D. E.; McIlroy D. N.; Cheng I. F. A Study of the Electrochemical Properties of a New Graphitic Material: GUITAR . ChemElectroChem 2015; 2; 700-706.

238 Cheng, I. F.; Xie, Y.; Gyan, I. O.; Nicholas, N. R. Highest Measured Anodic Stability in Aqueous Solutions: Graphenic Electrodes from the Thermolyzed Asphalt Reaction. RSC Adv. 2013, 3, 2379-2384.

239 Gyan, I. O.; Cheng, I. F. Electrochemical study of biologically relevant molecules at electrodes constructed from GUITAR, a new carbon allotrope. Microchem. J. 2015, 122, 39-44.

240 Kabir, H.; Zhu, H.; Lopez, R.; Nicholas, N. W. and Cheng, I. F. Electrochemical Determination of Chemical Oxygen Demand (COD) on Functionalized GUITAR Electrodes. Unpublished work.

241 Kabir, H.; Gyan, I. O.; Foutch, J. D.; Zhu, H.; Cheng, I. F. Application of GUITAR on the Negative Electrode of the Vanadium Redox Flow Battery: Improved V3+/2+

Heterogeneous Electron Transfer with Reduced Hydrogen Gassing. C--Open Access Carbon Res. J. 2016, 2, 13.

242 Gregory G. Wildgoose, Adam T. Masheter, Alison Crossley, John H. Jones, Richard G. Compton. Electrolysis of Ammonium Carbamate: A Voltammetric and Xray Photoelectron Spectroscopic Investigation into the Modification of Carbon Electrodes. Int. J. Electrochem. Sci., 2007, 2, 809 – 819.

243 Anisha N. Patel, Manon Guille Collignon, Michael A. O'Connell, Wendy O. Y. Hung, Kim McKelvey, Julie V. Macpherson, and Patrick R. Unwin. A New View of Electrochemistry at Highly Oriented Pyrolytic Graphite. J. Am. Chem. Soc. 2012, 134, 20117−20130.

244 Vasilios Georgakilas, Jason A. Perman, Jiri Tucek, and Radek Zboril. Broad Family of Carbon Nanoallotropes: Classification, Chemistry, and Applications of Fullerenes, Carbon Dots, Nanotubes, Graphene, Nanodiamonds, and Combined Superstructures. Chem. Rev. 2015, 115, 4744−4822.

245 Dimitrios Tasis, Nikos Tagmatarchis, Alberto Bianco, and Maurizio Prato. Chemistry of Carbon Nanotubes. Chem. Rev. 2006, 106, 1105-1136.

246 Da Chen, Hongbin Feng, and Jinghong Li. Graphene Oxide: Preparation, Functionalization, and Electrochemical Applications. Chem. Rev. 2012, 112, 6027−6053.

247 John H. T. Luong, Keith B. Male and Jeremy D. Glennon. Boron-doped diamond electrode: synthesis, characterization, functionalization and analytical applications. Analyst, 2009, 134, 1965–1979.

248 Jeffrey L. Bahr and James M. Tour. Highly Functionalized Carbon Nanotubes Using in Situ Generated Diazonium Compounds. Chem. Mater. 2001, 13, 3823-3824.

249 Christopher A. Dyke and James M. Tour. Unbundled and Highly Functionalized Carbon Nanotubes from Aqueous Reactions. Nano Letters 2003, 3, 1215-1218.

250 Jeffrey L. Bahr, Jiping Yang, Dmitry V. Kosynkin, Michael J. Bronikowski, Richard E. Smalley, and James M. Tour. Functionalization of Carbon Nanotubes by Electrochemical Reduction of Aryl Diazonium Salts: A Bucky Paper Electrode. J. Am. Chem. Soc. 2001, 123, 6536-6542.

251 Jackie Y. Cai, Jie Min, Jill McDonnell, Jeffrey S. Church, Christopher D. Easton, William Humphries, Stuart Lucas, Andrea L. Woodhead. An improved method for functionalisation of carbon nanotube spun yarns with aryldiazonium compounds. Carbon 2012, 50, 4655-4662.

252 Kevin Flavin, Manuel N. Chaur, Luis Echegoyen, and Silvia Giordani. Functionalization of Multilayer Fullerenes (Carbon Nano-Onions) using Diazonium Compounds and "Click" Chemistry. Org. Lett., 2010, 12, 840–843.

253 Sandip Niyogi, Elena Bekyarova, Mikhail E. Itkis, Hang Zhang, Kristin Shepperd, Jeremy Hicks, Michael Sprinkle, Claire Berger, Chun Ning Lau, Walt A. deHeer, Edward H. Conrad, and Robert C. Haddon. Spectroscopy of Covalently Functionalized Graphene. Nano Lett. 2010, 10, 4061–4066.

254 Ming Fang, Kaigang Wang, Hongbin Lu, Yuliang Yang and Steven Nutt. Covalent polymer functionalization of graphene nanosheets and mechanical properties of composites. J. Mater. Chem., 2009, 19, 7098–7105.

255 Jay R. Lomeda, Condell D. Doyle, Dmitry V. Kosynkin, Wen-Fang Hwang, and James M. Tour. Diazonium Functionalization of Surfactant-Wrapped Chemically Converted Graphene Sheets. J. Am. Chem. Soc. 2008, 130, 16201–16206.

256 Mildred Quintana, Konstantinos Spyrou, Marek Grzelczak, Wesley R. Browne, Petra Rudolf, and Maurizio Prato. Functionalization of Graphene via 1,3- Dipolar Cycloaddition. ACS Nano, 2010, 4, 3527–3533.

257 Konstantinos Kordatos, Tatiana Da Ros, Susanna Bosi, Ester Vázquez, Massimo Bergamin, Claudia Cusan, Federica Pellarini, Véronique Tomberli, Benedetta Baiti, Davide Pantarotto, Vasilios Georgakilas, Giampiero Spalluto, and Maurizio Prato. Novel Versatile Fullerene Synthons. J. Org. Chem. 2001, 66, 4915-4920.

258 Hirsch, A.; Brettreich, M. Fullerenes: Chemistry and Reactions; Wiley-VCH: Weinheim, Germany, 2005.

259 Vasilios Georgakilas, Athanasios B. Bourlinos, Radek Zboril, Theodore A. Steriotis, Panagiotis Dallas, Athanasios K. Stubos and Christos Trapalis. Organic functionalisation of graphenes. Chem. Commun., 2010, 46, 1766–1768.

260 Minhua Shao, Qiaowan Chang, Jean-Pol Dodelet, and Regis Chenitz. Recent Advances in Electrocatalysts for Oxygen Reduction Reaction. Chem. Rev., 2016, 116, 3594–3657; Andrew A. Gewirth, Jason A. Varnell, and Angela M. DiAscro. Nonprecious Metal Catalysts for Oxygen Reduction in Heterogeneous Aqueous Systems. Chem. Rev., 2018, 118, pp 2313–2339.

261 Gasidit Panomsuwan, Nagahiro Saito, and Takahiro Ishizaki. Nitrogen-Doped Carbon Nanoparticle−Carbon Nanofiber Composite as an Efficient Metal-Free Cathode Catalyst for Oxygen Reduction Reaction. ACS Appl. Mater. Interfaces 2016, 8, 6962−6971

262 Haihong Zhong, Shuwei Zhang, Jiawei Jiang, Dianqing Li, Pinggui Tang, Nicolas Alonso-Vante, and Yongjun Feng. Improved Electrocatalytic Performance of Tailored Metal-

Free Nitrogen-Doped Ordered Mesoporous Carbons for the Oxygen Reduction Reaction. ChemElectroChem 2018, 5, 1899–1904.

263 Mingkai Liu, Yanfang Song, Sixin He, Weng Weei Tjiu, Jisheng Pan, Yong-Yao Xia, and Tianxi Liu. Nitrogen-Doped Graphene Nanoribbons as Efficient Metal-Free Electrocatalysts for Oxygen Reduction. ACS Appl. Mater. Interfaces 2014, 6, 4214−4222.

264 Fan Yang, Mikel Abadia, Chaoqiu Chen, Weike Wang, Le Li, Lianbing Zhang, Celia Rogero, Andrey Chuvilin, and Mato Knez. Design of active and stable oxygen reduction reaction catalysts by embedding CoxOy nanoparticles into nitrogen-doped carbon. Nano Research 2017, 10, 97–107.

265 Wei Wei, Hongtao Ge, Linsong Huang, Min Kuang, Abdullah M. Al-Enizi, Lijuan Zhang and Gengfeng Zheng. Hierarchically tubular nitrogen-doped carbon structures for the oxygen reduction reaction. J. Mater. Chem. A, 2017, 5, 13634–13638.

266 Lei Qin, Yifei Yuan, Wei Wei, Wei Lv, Shuzhang Niu, Yan-Bing He, Dengyun Zhai, Feiyu Kang, Jang-Kyo Kim, Quan-Hong Yang, and Jun Lu. Graphene-Directed Formation of a Nitrogen-Doped Porous Carbon Sheet with High Catalytic Performance for the Oxygen Reduction Reaction. J. Phys. Chem. C 2018, 122, 13508−13514.

Appendix 1: Copyright Licenses

ELSEVIER LICENSE
TERMS AND CONDITIONS

Aug 03, 2018

This Agreement between Ms. Haoyu Zhu ("You") and Elsevier ("Elsevier") consists of your license details and the terms and conditions provided by Elsevier and Copyright Clearance Center.

License Number	4360280851912
License date	Jun 01, 2018
Licensed Content Publisher	Elsevier
Licensed Content Publication	International Journal of Coal Geology
Licensed Content Title	Pyrolytic carbon — Definition, classification and occurrence
Licensed Content Author	Barbara K. Kwiecińska,Sławomira Pusz
Licensed Content Date	Jun 1, 2016
Licensed Content Volume	163
Licensed Content Issue	n/a
Licensed Content Pages	7
Start Page	1
End Page	7
Type of Use	reuse in a thesis/dissertation
Portion	figures/tables/illustrations
Number of figures/tables/illustrations	3
Format	both print and electronic
Are you the author of this Elsevier article?	No
Will you be translating?	No
Original figure numbers	Figure 3
Title of your thesis/dissertation	GUITAR and its potential in electrochemical applications
Expected completion date	Aug 2018
Estimated size (number of pages)	120

Requestor Location	Ms. Haoyu Zhu 250 Baker St. Apt.08 MOSCOW, ID 83843 United States Attn: Ms. Haoyu Zhu
Publisher Tax ID	98-0397604
Total	0.00 USD

JOHN WILEY AND SONS LICENSE
TERMS AND CONDITIONS

Aug 03, 2018

This Agreement between Ms. Haoyu Zhu ("You") and John Wiley and Sons ("John Wiley and Sons") consists of your license details and the terms and conditions provided by John Wiley and Sons and Copyright Clearance Center.

License Number	4362870747275
License date	Jun 06, 2018
Licensed Content Publisher	John Wiley and Sons
Licensed Content Publication	ChemElectroChem
Licensed Content Title	A Study of the Electrochemical Properties of a New Graphitic Material: GUITAR
Licensed Content Author	Isaiah O. Gyan, Peter M. Wojcik, D. Eric Aston, et al
Licensed Content Date	Feb 12, 2015
Licensed Content Volume	2
Licensed Content Issue	5
Licensed Content Pages	7
Type of use	Dissertation/Thesis
Requestor type	University/Academic
Format	Print and electronic
Portion	Figure/table
Number of figures/tables	2
Original Wiley figure/table number(s)	2
Will you be translating?	No
Title of your thesis / dissertation	GUITAR and its potential in electrochemical applications
Expected completion date	Aug 2018
Expected size (number of pages)	120
Requestor Location	Ms. Haoyu Zhu 250 Baker St. Apt.08 MOSCOW, ID 83843

	United States Attn: Ms. Haoyu Zhu
Publisher Tax ID	EU826007151
Total	0.00 USD